Physik-Department

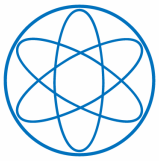

Characterization of a solid deuterium converter for ultra-cold neutrons (UCN) in the framework of the Mini-D_2 project at the FRM-II reactor in Munich

Dissertation

von

Daniele Tortorella

Technische Universität
München

Fakultät für Physik der Technischen Universität München
Physik Department E18

Characterization of a solid deuterium converter for ultra-cold neutrons (UCN) in the framework of the Mini-D_2 project at the FRM-II reactor in Munich

Daniele Tortorella

Vollständiger Abdruck der von der Fakultät für Physik der Technischen Universität München zur Erlangung des akademischen Grades eines

Doktors der Naturwissenschaften (Dr. rer. nat.)

genehmigten Dissertation.

Vorsitzender: Univ.-Prof. Dr. Andrzej Jerzy Buras

Prüfer der Dissertation:

1. Univ.-Prof. Dr. Stephan Paul
2. Univ.-Prof. Dr. Klaus Schreckenbach

Die Dissertation wurde am 25.01.2007 bei der Technischen Universität München eingreicht und durch die Fakultät für Physik am 07.02.2007 angenommen.

A mia moglie Susanne,

Mia "Lebenselixier".

Prova vivente di quanto

Straordinaria e Sorprendente

Possa essere Madre Natura.

Summary

Spontaneous breaking of fundamental symmetries is an attractive topic in modern particles physic. Understanding qualitative and quantitative the parameters involved in these kind of processes could help to explain the unbalanced presence in the universe of matter (baryons) with respect to antimatter (anti-baryons).
Due to their intrinsic properties, ultra cold neutrons (UCN) are excellent candidates in experiments measuring with high level of accuracy parameters like the electric dipole moment (EDM), the axial-vector coupling constant (g_A), the neutron lifetime (τ_n) or in search of quantum effect of gravity.
In this work are presented several contributions in the framework of the Mini-D_2 project, an innovative strong UCN source under construction at the FRM-II reactor in Munich. An important component of this facility, the solid deuterium UCN converter, is one subject of the thesis.

Zusammenfassung

Die spontane Brechung fundamentaler Symmetrien ist ein attraktives Kapitel der modernen Teilchenphysik. Das qualitative und quantitative Verständnis der Parameter, die in diese Art von Prozessen involviert sind, könnte dabei helfen, die völlig unausgegliche Balance zwischen Materie (Baryonen) und Antimaterie (Antibaryonen) zu erklären.
Bedingt durch ihre Eigenschaften sind ultrakalte Neutronen (UCN) bestens für Experimente geeignet, die mit höchster Genauigkeit das elektrische Dipolmoment des Neutrons (EDM), die Neutronenlebensdauer τ_{n}, die Axialvektorkopplungskonstante oder Quanteneffekte der Gravitation bestimmen.
In dieser Arbeit werden einige Beiträge im Rahmen des Mini-D_2-Projekts beschrieben, einer neuartigen, starken UCN-Quelle, die momentan an der Neutronenquelle FRM-II in Garching konzipiert und gebaut wird. Ein wichtiger Bestandteil dieser Einrichtung, der UCN-Konverter mit Festdeuterium, ist das Hauptthema dieser Doktorarbeit.

Contents

Chapter 1

Introduction and Motivations

Spontaneous breaking of fundamental symmetry is a fascinating topic in modern particles physic. Although remarkable steps forward, both in theoretical and experimental physics, are nowadays achieved, this phenomenon is not fully understood. Among all, exploring all kind of breaking mechanisms could help to explain the unbalanced presence in the universe of matter (baryons) with respect to antimatter (anti-baryon).

Affected by all types of interactions (gravitation, weak, lectro-magnetic and strong), neutrons are an excellent probe for the Standard Model (SM) of particles physics. For instance, important observable directly linked to SM are the electric dipole moment (EDM), the axial vector-coupling constant (g_A) and the lifetime (τ_n) of the neutron. Although, the values of these experimental quantities have been measured previously [1], the associated levels of accuracy are, from the theoretical point of view, unsatisfactory for univocal conclusions. New generations of experiments are proposed or under construction worldwide in order to improve the accuracy and the precision of those parameters [2, 3, 4, 5]. In these experiments, very low energy neutrons (Ultra-Cold Neutrons, UCN) are used.

It is common to define as UCN those neutrons suitable to be stored in material bottles or in magnetic trap [6]. The associated UCN kinetic energy is $E_{UCN}^{max} \simeq 250neV$.

In experiments performing precision measurements of observable like the EDM or the lifetime of the neutrons, the observation time is a crucial parameter. The longer this time is, the better the accuracy (uncertainly principle). Using UCN the statistical errors can be significantly reduced [7, 8]. At the time of writing, the only running UCN source is located at the ILL in Grenoble which distributes to the experimental area a relative low UCN density ($\rho_{UCN} \simeq 50n \cdot cm^{-3}$, [9]). A remarkable improvement in the UCN density could be achieved in the so-called UCN super-thermal sources.

Mini-D_2 is an innovative strong UCN super-thermal source [2] using solid deuterium as "converter material" under construction at the new high flux Heinz Maier-Leibnitz neutron source (FRM-II) in Munich [10]. In order to prove the concept and to optimize design parameter based on physics, a number of experimental investigations have been performed at the TRIGA reactor in Mainz [11], at the ILL in Grenoble and especially at the FRM-II reactor in Munich. In this work we present and discuss the results of several of those studies.

A short introduction is dedicated to present the Mini-D_2 facility, the basic UCN properties and the application of UCN to fundamental physic.

In chapter 3 the features of a multi-purpose device (called Cube-D_2) are presented which has been constructed for studies on a solid deuterium converter. Results on UCN production and storage at a cold neutron beam (Mephisto, [12]) at FRM-II are presented and discussed. These results are one subject of the thesis.

A relevant part of this work was dedicated to evaluate UCN guide properties. In chapter 4 we present an innovative approach to extract parameters such the UCN loss probability per wall collision (μ) or the probability for diffuse scattering (f) [13]. In this context, several experiments were performed at ILL in Grenoble.

In chapter 5 aspects associated with the so-called "para" and "ortho" deuterium species are explained. The influence of the ortho deuterium concentration (C_{ortho}) on the UCN production is discussed as well. The technique applied to extract C_{ortho} from deuterium gaseous samples is presented (Raman spectroscopy, [14]).

The last chapter refers to a secondary but important topic for the Mini-D_2 project: the radiation shield. Results of simulations performed using the Monte Carlo N-Particle code (MCNP, [15]) are presented.

Chapter 2

The Mini-D_2 source at FRM-II

2.1 The FRM-II reactor in Munich

The Heinz Maier-Leibnitz (FRM-II) research reactor is located at the university campus in Garching and had is first criticality on March 2004. The FRM-II was designed, constructed and put in operation following the most up-to-date technologies associated with research reactor science. Special effort was invested defining very strict safety and security criteria.

The concept is based on the use of a compact core containing a single cylindrical fuel element [10]. The basic material is an uranium silicide-aluminium dispersion with an enrichment factor in U^{235} of 93%. The duration of a typical cycle is about 52 days. The full thermal nominal power is $20MW$. The FRM-II offers a very high unperturbed peak flux ($8 \cdot 10^{14} n/cm^2 s$).

Almost half of all experiments at the reactor are performed using cold neutrons. The distribution of neutrons to the users is accomplished with 10 horizontal, 2 inclined and 1 vertical guide system. The diverse experimental facilities are located either in the reactor building, or in the so-called neutron guide hall which has a big experimental area ($50m$

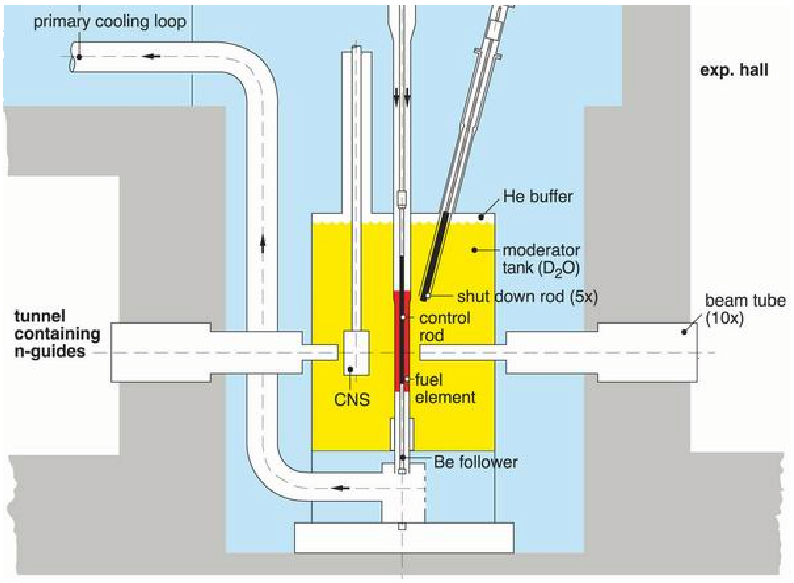

Figure 2.1: General layout of the FRM-II reactor core

long, $24m$ wide). The main secondary beam sources are the "cold" source (CNS), the "hot" source (HS), the positron source and the Mini-D_2 source for ultra cold neutrons (UCN), still in the planning phase. Figure 2.1 shows a schema of the FRM-II reactor core. The position of the "cold" source (CNS) is clearly evident.

2.2 Concept and basic ideas of the UCN source

The Mini-D_2 UCN source [2, 17] was originally proposed to be located at the so-called SR4 beam tube of the FRM-II reactor. Figure 2.2 depicts a cut-away view of the facility inside the biological shield of the reactor (in-pile cryostat) showing the main components of the system. At the level of the so-called "converter", an intense cold neutron flux is available ($\Phi_{CN}(40K) \sim 2.4 \cdot 10^{13} n/cm^2 s$). The converter material is placed close to the cold source [16].

The Mini-D_2 is a so-called super-thermal source (section 2.4.1) and uses solid deu-

terium as "converter material". UCN are produced by down-scattering of higher-energy neutrons (creation of phonon excitations in the moderator material, [36]). Solid deuterium is a proper converter material because has a high inelastic scattering cross section and a low absorption cross section. The up-scattering cross section can be reduced by reducing the temperature. At very low temperature ($\sim 5K$) the UCN losses in deuterium caused by up-scattering are smaller than those due to absorption. The UCN density is regulated by the relative small absorption in the converter.

In order to reach high UCN density up, the concept of the Mini-D_2 is based on the following ideas:

- The experimental volume is refilled with UCN periodically every few minutes. In the mean time UCN produced continuously are accumulated in the storage volume. Accumulation takes place as long as the losses in the storage tube are negligible as compared to losses in the converter. From the storage volume the UCN are re-directed to the different experiments using a special neutron valve.

- The storage tube is a neutron guide as well. The converter (small volume, $V_{D_2} \sim 200cm^3$) is placed in the storage tube. The UCN equilibrium in the tube is regulated by the losses in the converter (small), by the losses due to wall collisions, by holes eventually present in the system and by the β-decay of the neutrons.

The inner walls of the long storage tube ($\sim 8m$) are covered with an high Fermi potential material, preferentially beryllium or diamond-like carbon (DLC). According to calculations based on well-known theoretical models, a UCN density up to $10^4 n/cm^3$ could be achieved. This represents an improvement by several orders of magnitude with respect to existing running facilities.

As is illustrated in figure 2.2, to accomplish the UCN high density challenge, part of the Mini-D_2 facility (in-pile cryostat) has to be located inside the biological shield of the

FRM-II. As consequence, strict safety aspects have to be considered in the nuclear reactor environment.

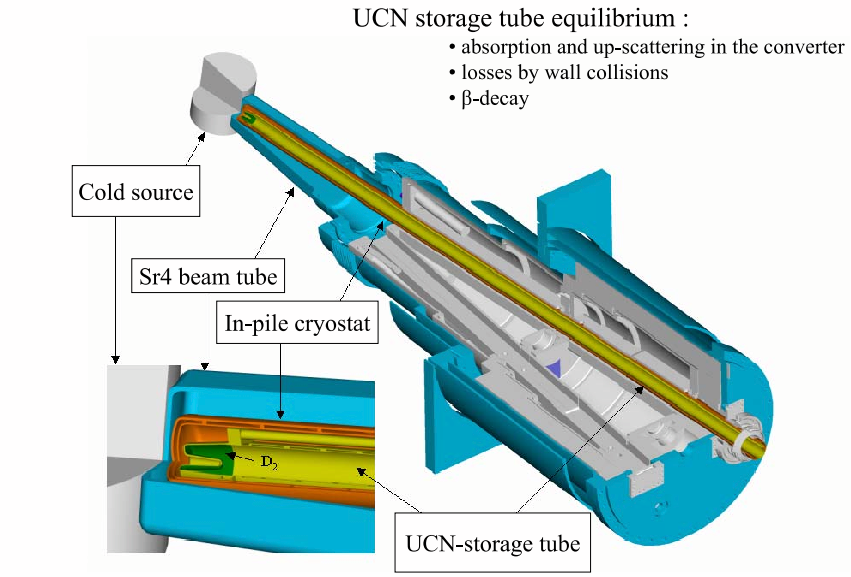

Figure 2.2: Cut-away view of the Mini-D_2 at the SR4 channel

2.3 Physics of ultra cold neutrons

It is common to define as UCN neutrons with energies such that they can be stored in material bottles or in magnetic traps [6, 8]. Referring only to wall interactions, UCN are neutrons that can be reflected at any incident angle by adequate material surfaces. In terms of energy and assuming only one kind of material, this corresponds to an upper limit for the kinetic energy:

$$E_{kin} \leq V_F = \frac{2\pi\hbar^2 N b}{m_n} \tag{2.1}$$

Here V_F is the effective Fermi potential of the material, N is the number density of nuclei, m_n is the neutron mass, b is the bound coherent scattering length. For example, the Fermi

potential for beryllium is $V_F = 252neV$. Moreover, neutrons are affected by gravitational, magnetic, weak (β-decay) and strong interactions (scattering, absorbtion, etc..). UCN can also be confined by means of:

- Magnetic field. Due to its non-zero magnetic moment ($\mu_n = -60.5neV$), a strong magnetic field ($\mathbf{B} \simeq 2T$) acts as storing potential ($V_{mag} = \mu_n \cdot \mathbf{B} \sim 120neV$).

- Gravitational field. At such low energies a neutron falling a distance $\Delta h = 1m$ in the earth's gravitational field gains $\Delta V_{grav} = m_n g \Delta h = 102neV$. Accordingly, UCN having energy of $E_{UCN} \sim 200neV$ can not escape from the top of a storage volume of $2m$ height.

A UCN storage experiment may thus make use of potentials to achieve storage times ideally limited only by the neutron β-decay ($\tau_\beta = 885.7 \pm 0.8s$, [1]).

Because of the low velocity ($v_{UCN}^{max} \sim 7m/s$) and the relative low density, UCN are generally treated as a gas. Therefore the important parameter is the neutron density (ρ_{UCN} in $[n/cm^3]$).

2.4 Production of UCN

Producing UCN means reducing the mean velocity of the neutrons to $0 - 7m/s$, corresponding to kinetic energies of up to $\sim 250neV$. This process generally involves inelastic scattering with energy loss of the neutrons. At thermal equilibrium with the moderator (for example heavy water at $T = 300K$) the neutrons spectrum is linked to the Maxwellian velocity distribution as:

$$\rho(v)dv = \frac{2\Phi_{th}}{v_{th}} \frac{v^2}{v_{th}^2} \exp(-\frac{v^2}{v_{th}^2}) \frac{dv}{v_{th}} \tag{2.2}$$

Where $\rho(v)dv$ is the neutron density in the interval $[v,v+dv]$, Φ_{th} is the integral thermal neutron flux and $v_{th} = \sqrt{\frac{2K_bT}{m_n}}$ is the corresponding neutron thermal velocity. In this case (so-called steady state moderation process, $T = T_n = T_{mod}$), the UCN density [6] is given

by

$$\rho_{UCN}^{equilibrium} = \int_0^{v_{lim}} \rho(v)dv = \frac{2}{3}\Phi_{th}\frac{v_{lim}^2}{v_{th}^4} \tag{2.3}$$

v_{lim} is given by the Fermi potential of the storage material $V_F = \frac{1}{2}m_n v_{lim}^2 \leq 250neV$. According with 2.3 the only effective way to increase the UCN density is to increase the neutron flux ($\rho_{UCN} \simeq 10^{-13}\Phi_{th}cm^{-3}$). In a high flux reactor (for instance FRM-II or ILL) this leads to a density at the experimental area of less than 100 UCN/cm^3.

2.4.1 Super-thermal UCN source

One possibility to enhance the UCN density is to drastically reduce the temperature of the moderator. For general scattering phenomena the principle of detailed balance of up and down scattering processes is:

$$E\exp(-\beta E)\sigma(E \to E^{'}) = E^{'}\exp(-\beta E^{'})\sigma(E^{'} \to E) \tag{2.4}$$

Where the E and $E^{'}$ are the neutron energy before and after a scattering process and $\beta^{-1} = \kappa_B T$. Assuming a moderator material with two well separated energy levels such that the energy gap is $\Delta = E^* - E^0 \gg \beta^{-1} \gg E_{UCN}$, the UCN up-scattering cross section is given by:

$$\sigma_{up}(E_{UCN} \to E_{UCN} + \Delta) = \frac{(E_{UCN} + \Delta)}{E_{UCN}}\exp(-\beta\Delta)\sigma_{up}(E_{UCN} + \Delta \to E_{UCN}) \tag{2.5}$$

and in principle could be made arbitrarily small by reducing the temperature of the moderator. In such systems no thermal equilibrium is reached ($T_n > T_{mod}$) and the term "UCN super-thermal source" is commonly used. In this case, the moderation is so effective that one could regard the phenomenon as a conversion process.

An equilibrium in the UCN density is reached when the production rate equals the global losses of the system [$\rho(E_{UCN}) = \tau P(E_{UCN})$]. Contributions to the loss rate factor τ^{-1} are

$$\frac{1}{\tau} = \frac{1}{\tau_{wall}} + \frac{1}{\tau_{up}} + \frac{1}{\tau_{\beta}} + \frac{1}{\tau_{abs}} \tag{2.6}$$

where τ_β is the natural lifetime of the neutrons, τ_{wall} corresponds to the losses due to the walls collisions, τ_{abs} is the absorption in the converter material and τ_{up} is the up-scattering rate in the moderator described by (detailed balance principle)

$$\frac{1}{\tau_{up} v_{UCN}} = \int N\sigma_{up}(E_{UCN} \to E) = \int \frac{E}{E_{UCN}} \exp(-\beta E) N\sigma_{up}(E \to E_{UCN}) dE \qquad (2.7)$$

Here N is the deuterium density. One should note that $\sigma_{up}(E_{UCN} \to E)$ is non-zero only in a narrow energy range around the excitable level E^*. Therefore the super-thermal UCN density [6] can be expressed

$$\rho_{UCN}^{super-thermal} = \frac{\sqrt{2}}{3} \Phi_{th} \frac{\sqrt{m_n}}{(k_B T_n)^2} V_F^{3/2} f_g = \rho_{UCN}^{equilibrium} f_g \qquad (2.8)$$

where $f_g = \exp((\beta_{conv} - \beta_{th}) E^*)$ quantifies the "gain" factor of the super-thermal source. Thereby $\beta_{conv}^{-1} = \kappa_B T_{conv}$ can be significantly increased by lowering the temperature of the converter.

2.4.2 Estimation of UCN density in a "film source"

A direct method to calculate the achievable UCN density for a given incoming neutron beam (thermal or "cold") was introduced by R.Golub [18]. The main idea is to consider a so-called UCN film-source model. A thin layer of a UCN converter (here deuterium) covers uniformly (Fig.2.3) part of the inner walls of a vessel (here stainless steel, SS). If the temperature of the film is low enough, the down scattering cross section can be treated using the Debye model for a one-phonon process in the incoherent approximation. The Debey model gives the density of the phonon states which can be populated by down-scattering process. The Debye model can be applied because the Debye temperature in deuterium is relative high $\Theta_D = 120K$, while a typical working temperature in an experiment using solid deuterium is $\sim 5K$.

We consider a Maxwell-Boltzmann distribution at a temperature (T_n) for an incoming beam (ϕ)

$$\phi(E_0) dE_0 = \phi \frac{E_0}{k_B T_n} e^{\frac{-E_0}{k_B T_n}} dE_0 \qquad (2.9)$$

According to this model a differential UCN production rate can be calculated as

$$P(E_{UCN})dE_{UCN} = \sigma_{bound}\frac{2\phi}{k_B^{3/2}}E_{UCN}^{1/2}\frac{m_n}{M_D}\frac{\Gamma(T_n,\Theta_D)}{\Theta_D^3 T_n^2}N_D dE_{UCN} \tag{2.10}$$

Where $\sigma_{bound} = 7.6 barns$ is the sum of the coherent and incoherent scattering cross section of the deuterium film material, $\Gamma(T_n, \Theta_D)$ is the UCN production rate (in n/s, [18]) and $M_D = 4$ is the atomic mass (deuterium). In an horizontal geometry (no additional gravitational "step" potential) the boundary conditions for equation 2.10 are $E_{UCN} = E_{max} - E_{min} = E_{SS} - E_{D_2} \simeq 200neV - 102neV$. Here E_{SS} is the Fermi potential for stainless steel (vessel material) and E_{D_2} is the UCN energy in the deuterium (Fig.2.3).

It is important to note that the UCN production rate depends only on the temperature of the incoming neutron beam (T_n) and on the deuterium Debye temperature Θ_D. More details can be found in reference [18] by Golub.

The model estimates the UCN production in the film material assuming UCN extraction from the film to the vacuum without additional losses. In chapter 3.13 we derive an expression which includes also losses in the film.

Once the UCN density is calculated, the UCN "transport" (for example in long tubes) can be derived using the theory of gas diffusion (see chapter 4).

2.5 Solid deuterium as converter material

Deuterium is a stable isotope of hydrogen, its natural abundance is 0.015%. At standard temperature and pressure (STP) the density is $0.180 Kg/m^3$, while in solid (melting point, $T_{melt}(D_2) = 18.7K$) is $\rho_{D_2} \sim 200 Kg/m^3$. The nuclide is called deuteron and is a boson ($S = 1$). Therefore in the D_2 molecules the total wave function must be symmetric under deuteron exchange. Special restrictions are needed for the coupling of the various spins, which results in species with different spin symmetry denoted as ortho-deuterium

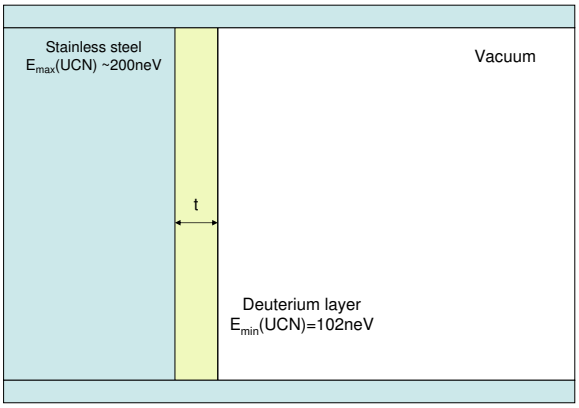

Figure 2.3: Model for a UCN film source (deuterium on stainless steel)

(ortho-D_2, $S_{tot} = 0, 2$) and para-deuterium (para-D_2, $S_{tot} = 1$). Within the two species, ortho-D_2 has the largest spin degeneracy (6 states, 2S+1 states, as S=0 and S=2). For para-D_3 the spin degeneracy is of 3 states (2S+1 states, as S=1).

Due to the total symmetry, even total molecular nuclear spins (ortho-D_2) require even J rotational quantum numbers. Accordingly, odd total molecular nuclear spin (para-D_2) are associated with odd J states. At normal temperature the ratio of the degeneracies is $\frac{J-even}{J-odd} = 6/3 = 2$. Hence the natural ortho deuterium concentration in a sample is $\rho_{ortho} = 66.6\%$. In solid deuterium only the lowest rotational quantum states are thermally populated ($J = 0$ in ortho-D_2 and $J = 1$ in para-D_2, see chapter 5.3). An extensive description of general deuterium properties can be found in the Silvera's review [34] or in Souers' book [35].

In the assembly of deuterium molecules (either ortho or para) it is possible to have significant interactions between the magnetic moments of the molecules. This leads to transitions between para and ortho deuterium (forbidden for an isolated molecule). A typical energy difference between two states is $\sim 7meV$ (J=1 to J=0). This transition

can also be induced in the interactions with neutrons. Therefore kinetic energy can be transferred to the interacting particles. In case of a UCN ($E_{UCN} \sim 200neV$) interaction with para-D_2, this energy is high enough that the interacting neutron is removed from the UCN regime and is "lost" in the next wall interaction. For this reason, deuterium used in super-thermal UCN sources (like the Mini-D_2), must be almost totally ortho-D_2.

One of the first experimental evidence of UCN production using solid deuterium was performed by Altarev et al. in Gatchina [37].

A method (Raman spectroscopy, [14, 34]) applied in order to discriminate the ortho-D_2 and para-D_2 species is described in chapter 5.

2.6 Experiments with UCN

We briefly present two key experiments which will take advantage of an available strong UCN source.

2.6.1 Electric Dipole Moment of the neutron

As the magnetic dipole moment μ_n, also an electric dipole moment (EDM) of the neutron d_n can contribute to the hamiltonian in an electromagnetic field

$$H = -(d_n \mathbf{E} + \mu_n \mathbf{B}) \cdot \frac{\mathbf{S}}{S} \tag{2.11}$$

Where $\mathbf{S}$ is the spin of the neutron. Evidently, as the electric field $\mathbf{E}$ is a polar vector, unlike $\mathbf{B}$, a non-vanishing EDM violates both parity and time reversal symmetry [20].

The standard model (SM) predicts only a very small value for an EDM of almost 5 orders of magnitude below the actual upper limit. Whereas others theories, for instance super-symmetry (SUSY) predict values of the EDM "only" 1-2 orders of magnitude smaller than the nowadays available limits for d_n [21]. Therefore, an improvement of the

sensitivity of the instruments measuring this important parameter could provide a unique constraint for physics beyond the standard model.

In a typical EDM experiment [22], a reference storage volume is filled with spin-polarized particles (UCN in this case). Strong electric and magnetic field are applied in parallel direction in the same volume. The electric field is frequently reversed and the Larmor precession of the spin inside this system (ω_L) is measured. A correlations found between ω_L and the direction of $\mathbf{E}$ gives a direct measurement of a permanent EDM

$$\Delta\omega_L = \omega_L(+E) - \omega_L(-E) = \frac{4d_n\mathbf{E}}{\hbar} \tag{2.12}$$

The statistical accuracy δd_n for an EDM is then given by

$$\delta d_n \propto \frac{1}{E \cdot t_{meas}\sqrt{N_n}} \tag{2.13}$$

where N_n is the number of polarized neutrons stored and t_{meas} is the measuring time. Following this approach [23] and using UCN as probe particles, different groups [24, 25, 26] improved over many years, this limit down to $|d_n| < 2.9 \cdot 10^{-26} e \cdot cm$. Beside others technological difficulties ($\mathbf{E}$ and $\mathbf{B}$ must be very constant and absolutely parallel) the main limitation is N_n. Many of the experiments using UCN were performed at the ILL in Grenoble ($\sim 50 n/cm^3$). It's evident that a new generation of UCN sources like the Mini-D_2 ($10^4 n/cm^3$) can improve the sensitivity down to the SUSY expectations.

2.6.2 Precise neutron lifetime measurement

In the standard model, the neutron lifetime τ_n is related to other measurable quantities by

$$\tau_n \propto \frac{1}{|G_V|^2(1+3|\lambda|^2)} \cdot |V_{ud}| \tag{2.14}$$

Where $\lambda = \frac{G_A}{G_V}$ is the ratio of the axial vector and vector coupling strengths [27] and $|V_{ud}|$ is the first element of the so-called CKM matrix, which describes the transition amplitude between the "u-quark" and the "d-quark". The average value of the neutron

lifetime from various experiments is 885.7 ± 0.8 [28]. Very recently a new value was published ($\tau_n = 878.5 \pm 0.8$, [29]) deviating by about six standard deviations from this average.

Due to their magnetic moment ($\mu_n = -60.5 neV/T$), UCN can be stored in a magnetic trap with $B > 2T$. Following this idea, an innovative life time experiment [30, 31] is planned to be installed at the Mini-D_2 source at the FRM-II. The main feature of this experiment is the online detection of the decay protons coming from the β-decay in the storage volume complemented by the more standard counting of neutrons remaining after a preset storage time τ. The main components of the facility are 19 super-conducting coils working in cryo-environments (down to $5K$). If the experiment is placed in a UCN source with $\rho_{UCN} \sim 10^4 n/cm^3$, according to extensive simulations [32, 33], the statistical error of the neutron lifetime could be reduced to $\delta\tau_n \sim 0.1s$.

Using UCN one can also study quasi-elastic scattering with very low momentum transfer [17]. An attractive emerging field is the use of UCN in searching of quantum effect of gravity [38].

2.7 Other components of Mini-D_2 facility

Beside the deuterium converter, important components associated with the Mini-D_2 source are:

- the UCN extraction system
- the so-called oxisorb para/ortho converter unit
- the neutron detection chain
- the radiation shield

These specific "auxiliaries" are also subject of this work and are described in specific chapters or sections. Others main components are the deuterium gas system (DGS) and

the global cooling system [39, 40].

Chapter 3

Cube-D2 experiment at the FRM-II

Essential component of the Mini-D_2 "super-thermal" source is the UCN deuterium converter. A preliminary systematic investigation of this element is mandatory. Motivated by this aim, a multipurpose test device called Cube-D_2 [41] was projected, assembled and put in operation at the Mephisto "cold beam" of the FRM-II reactor [12].

In this chapter we describe the hardware components of the set-up, the features and the outcomes of the experiment. The complete scientific program includes: measuring of the UCN production as a function of the temperature in solid, liquid and gas deuterium, influence of the freezing procedure and of the ortho-D_2 concentration on the UCN production; evaluation of the properties of electro-polished stainless steel as material for extraction and storing of UCN; estimation of the thickness of the "active layer" for UCN extraction. A summary of the results are presented and discussed. Relevant implications for the Mini-D_2 project are also considered.

3.1 Description of the Set-up

The apparatus is composed of different but integrated sections. The cooling stage which allows to reach the cryogenic temperature needed. The gas handling system which permits

the proper allocation of deuterium in the different areas. The ortho-deuterium converter unit which allows in a reasonably short time a high concentration of ortho-deuterium to be reached. The data acquisition system (DAQ) which includes the UCN detector. The fundamental component of the Cube-D_2 is the small converter cubic cell and the UCN extraction system.

3.2 Converter cells and UCN extraction system

Deuterium is mainly frozen in a cubic chamber made of aluminium (AlMg3, $46mm$ external side-length). The bottom face of the cell is in contact with a cold-head (Fig.3.1). Two diode sensors monitor constantly the temperature. One sensor is mounted directly on the cold-head (T2), the other on the deuterium cell (T1). On two lateral opposite surfaces of the cube are mounted two sapphire windows (indium sealed, view diameter $\emptyset = 14mm$) for optical investigation. Two lateral sides are in the direction of the neutron beam and are used as neutron portholes. One (cold neutron entrance window) is directly machined from the aluminium block (0.5mm thickness). UCN eventually produced are extracted on the opposite side via a very thin ($100\mu m$) aluminum foil glued on the chamber with Stycast^{TM} and pressed with a special shaped stainless steel flange. In the schema 3.1 are presented the main elements of this stage of the extraction system.

As will be better described in more details, three cells are used. They differ mainly by the useable volume for deuterium freezing and by the fact that only one cell (described above) has mounted, the sapphire optical windows. The diverse volumes sizes are obtained by a different dept in the machining of the cold neutron windows inside the aluminium block (3cm, 2cm, 1cm, 0.5cm). The others dimensions are similar. Particular care has to be taken on the preparation and on the assembling of the extraction foil. Definitely this is the critical element for the safety concept of the full system. The foil has to withstand, in cryogenic environment, either high vacuum ($LR \simeq 10^{-10} mbar \cdot l/s$) or a relative high pressure (up to 3.5bar). Indeed, a breaking (or even a small leaking)

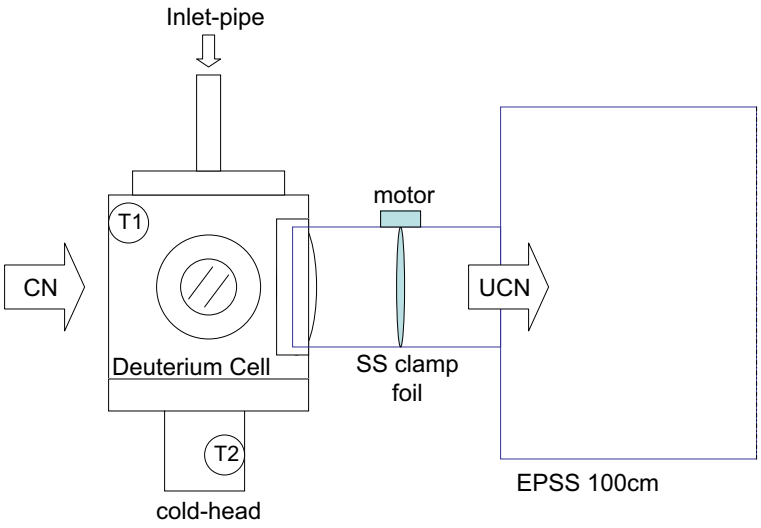

Figure 3.1: First stage of the extraction system

at this level produces a flow of deuterium in the so-called isolation-vacuum system with possible creation of an intolerable and potentially explosive air/deuterium mixture. After the mounting of the aluminium foil, each cell was first vacuum tested, then pressurized with air (at a rate of 0.5bar/10min), and finally maintaining keeping at 3.5bar for 1h. This technique permits a plastic deformation of the foil with a stable bulge ($R_b = 2cm$, outside) also when the pressure is released. Hence a standard and well-definite geometry coupling of every cell with the so-called extraction system is possible. A further bath in liquid nitrogen ($\sim 77K$) and a global leak-test was performed at the end.

The first stage of the UCN extraction system (Fig.3.1) is composed by a small cylinder (stainless steel, 50mm, $\emptyset = 30mm$). One end-part matches (eventually without touching) the foil flange of the aluminium cell. A special clamp-foil of stainless steel is mounted on the inner cross section of the cylinder. The foil is driven by a small magnetic motor and allows selection (to block) of the UCN from the relative high-velocity neutrons (very cold neutrons, VCN) present in the neutron spectra. The other side of the cylinder is connected with an electro-polished stainless steel tube (EPSS, 100mm, $\emptyset = 70mm$) which transports, and partially stores, the UCN to the experimental area. To favour the guiding of the UCN to the next section, and therefore reducing the losses by wall-collisions, a mirror-like additional stainless steel foil (elliptical shape, at 45°) is placed inside the very end of the electro-polished guide. The material of the cell and the geometry of the guiding system were selected in order to avoid high activation in the very intense irradiation regime of the Mephisto beam. Indeed, focusing on the stainless steel components, only the mirror-like thin foil (easily removable afterward) is located in the direct neutron beam.

After the mirror, the UCN are guided in a small vertical piece tube (EPSS, h=25cm). The main function of this element, which also works as "gravitational step", is to direct the UCN away from the direct cold beam. The UCN are afterward channeled in a long EPSS tube (200cm, tilted by $\sim 30\circ$) which works either as neutron guide (through mode),

or as a storage volume (when the UCN valves are installed). The final component of the extraction system is a vertical section (125cm) which couples directly into the detector flange. Traveling the vertical section the UCN gain a sufficient energy to pass almost without absorption (or reflection) the detector entrance window. At this level is also installed a special flange for pumping.

All the EPSS tubes, a part from the length, have the same characteristics (H5-type, outer $\emptyset = 70mm$, roughness $\sim 0.25\mu m$) and are provided by the Nocado GmbH company.

3.3 Cooling stage

The cooling power for deuterium freezing is provided by a liquid helium closed system integrated with an active cooling surface (cold-head) and with an external air cooled compressor (1.6kW). The machine (Sumitomo^{TM}, SHI-RDK-serie) has a relatively strong cooling capacity (0.25W at 4.5K). The temperature sensors (Lakeshore^{TM}, DT-670) have a total accuracy at 4.2K of $\pm 31mK$ and an excitation current of only $10\mu A$. In order to fix the temperature of the sample cell, a variable heating power is needed. This feature is performed with the help of a heater resistor (R=25Ohm) mounted on one of the cold-head flanges. The excitation current and the read-out of the temperature is remote controlled by a temperature controller (Lakeshore^{TM}, TC-331). An automatic "loop-regulation" of the resistor excitation current allows to release at the cell level up to 25W with relative low impendence (few seconds to reach stable condition at a definite temperature). In pictures 3.2-left are shown details of the 3cm cell already mounted on the cold-head.

The coldest temperature recorded ones all components (aluminium cell, extraction system, etc..) were correctly assembled was about $5.7 \pm 0.3K$ for the cold-head sensor and $7.2 \pm 0.12K$ for the cell one, where "$\pm$" are the intrinsical periodical oscillation ($\sim 2Hz$) linked with the helium compression/expansion cycles and are very much attenuated at higher temperature.

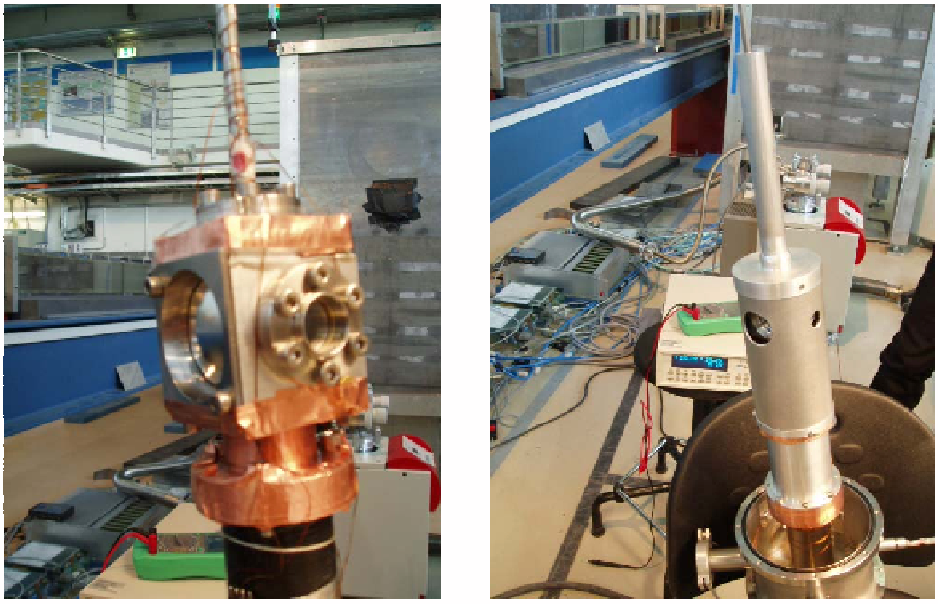

Figure 3.2: Deuterium freezing chamber mounted on the cold-head

As already mentioned the Mephisto-NL3a position at FRM-II has an intense neutron beam. In operational regime the level of the radiation (mainly scattered neutrons) outside the experimental area has to be lower than the legal limit ($5\mu Sv/h$). This goal is basically reached by applying at the cooling stage level a cage of high neutron absorber material (borated aluminium), modeled like the first active shield of the cold-head (Fig.3.2-right).

3.4 Gas handling system

Particular care has to be taken when deuterium is involved, especially in nuclear reactor environment. Despite the small amount of material used in the Cube-D_2 experiment (maximum 3mol), relative big effort was invested to build a deuterium gas system (DGS) which allows to safely handle such potentially explosive substance. In Fig.3.3 is presented the flow schema and the main components.

Generally, pure gaseous deuterium is introduced and stored in a reservoir vessel and successively distributed, via proper sequences of metering valves or to the aluminium cell, either to the converter unit (to be described next). On a metallic support front-panel are mounted the valves and the pressure gauges active during the normal operation (filling, freezing, etc..). Others valves or elements which are directly supported by the stainless steel pipes lines, are used only in particular procedures (first filling, evacuation, etc..). All the valves and the connections assembled are provided by the highly reliable company Swagelok^{TM}. A short description of the functionality of each elements is presented. Focusing on the front-panel, four bellows sealed valves (V1,V2,V3 and V4) are used for preliminary pumping and are normally closed afterward. Additional bellows sealed valves (D1, D2, D3) are active components of the deuterium-line connecting (or disconnecting) respectively the deuterium reservoir, the Raman's cell and freezing Cube-D_2 cell. All the bellows sealed valves (SS-6M-MM series) operate in a completely opened (or completely closed) mode and are manufactured in stainless steel (type 316). Two poppet check valves (C1 and C2) operated in one direction only when the relative pressure exceeds a define

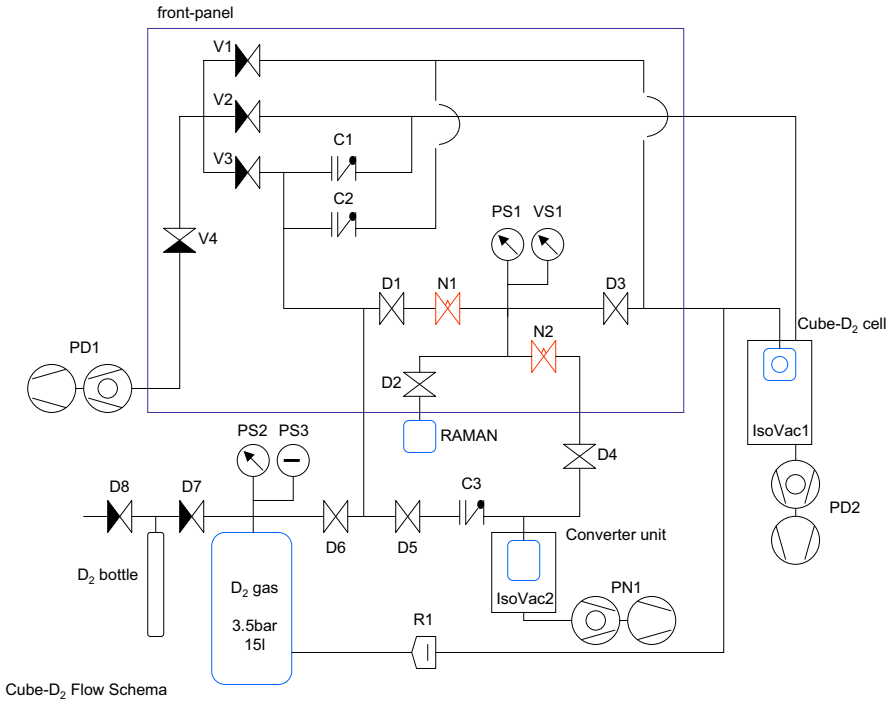

Figure 3.3: Gas handling system and auxiliary components

value (cracking pressures 3.5bar and 1.5bar). The idea is to protect (especially with C2) the thin aluminium extraction foil of the freezing cell against high overpressure conditions eventually generated by rapid evaporation of the deuterium due to sudden loosing of cooling power. The high pressure is therefore released in the big reservoir. Two bellows sealed metering valves (N1 and N2, small flow coefficient) are used to regulate the deuterium flow through the different volumes. For example, with N2 is possible to feed either the deuterium freezing cell (D1, D2 closed and D3 opened) or the reservoir (D2, D3 closed and D1 opened). One pressure gauge (PS1, calibrated for deuterium) and one vacuum gauge (Leybold^{TM}) are also mounted on the front-panel. The sensors are continuously measuring and sending the data to computers and, working in parallel, are able to cover a wide range of pressure (from high vacuum up to 10bar). The lower part of the flow-scheme (Fig.3.3), which reflects the real dislocation of the components of the DGS, is related with the deuterium reservoir (15l), with three pumping stages and with the converter unit. The pumps active on the deuterium-line (PD1, PD2) are special "dry" pumps in order to avoid oil contamination. The pump stage PN1 (turbo and primary pump) guarantee high "isolation-vacuum" in the converter unit. Two pressure sensors (PS2 and PS3 with display) are mounted at the reservoir level. The high pressure deuterium bottle (up to 100bar) is removed for safety reason from the reactor after the first filling of the reservoir. The bellows sealed valves D7 and D8 are used during this procedure. Another overpressure valve (C3, cracking pressure at 3.5bar) is active on the line between the converter unit and the reservoir. D5 and D6 (also bellows sealed valves) are used at the beginning for searching for leak in the different volumes of the DGS. Thereafter, because they are in series with the overpressure valves, they are blocked to be always in open position. An important element for the global safety concept of the Cube-D_2 is the rupture disk (R1, breaking pressure 2.5bar) placed on a special direct line between the deuterium freezing cell and the reservoir. Particularly, this device gives a fast reaction in case of an intense shock wave that is the most dangerous event for the aluminium extraction foil. Almost all the components of the DGS (including a spare nitrogen bottle) are arranged on a portable rack.

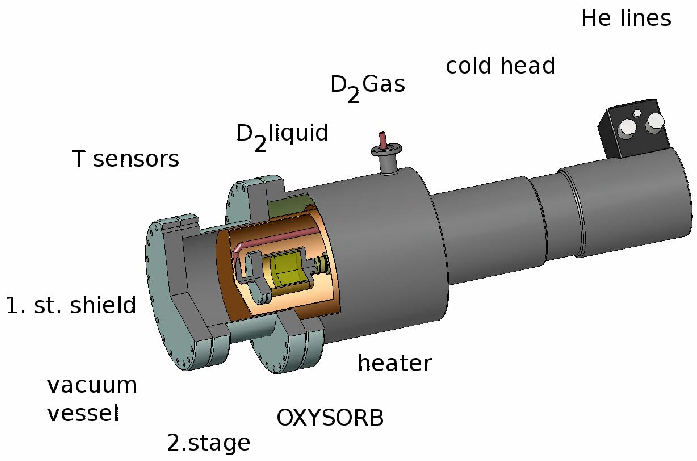

Figure 3.4: Para-to-Ortho deuterium "Oxisorb" converter unit

3.5 High "Ortho deuterium" converter unit

For efficient UCN production high concentration of ortho-D_2 is required [6]. To accelerate the "para-to-ortho" natural conversion rate [34], liquid deuterium is placed in contact with a catalyst ferromagnetic material ([42], Oxisorb^{TM}) in the so-called converter unit. In Fig.3.4 is presented a sketch of the inner cryostat. Like for the deuterium freezing cell, the cooling power is provided by a liquid helium closed system (Leybold^{TM}) integrated with an external water cooled compressor. Deuterium is introduced in a chamber containing the catalyst embedded in a special porous membrane. The chamber is mechanically in contact with the active cooling surface of the cold-head which allows to reach temperatures down to 10K. Two sensors (Lakeshore^{TM}, Cernox-serie, PT-serie) monitor the temperature and are connected with a read-out system that includes a temperature monitor (Lakeshore^{TM}, TM-218). An heater resistor wire is mounted on the cryostat and is connected with an external power supply (VoltKraft^{TM}). The converter unit is connected with the other part of the DGS according with the schema in Fig.3.3. A preliminary test of the functionality of the converter was performed. As is better explained in chapter

5, the ortho-D_2 concentration is determined using a Raman spectroscopy technique [34]. The general outcome gives a conversion rate in the order of a few hours with an associated ortho-D_2 concentration of about 97%. Therefore, a standard deuterium "freezing" procedure includes a preliminary filling of the converter unit (gas from the reservoir) and storing (liquid at $\sim 20K$) for an adequate time (at least 15h). Only afterwards, is the high-ortho deuterium introduced into the freezing chamber.

3.6 Remote control system, detector and DAQ

The Cube-D_2, as the majority of the experiment is performed with components under irradiation, has to be adequately shielded. Hence, a considerable part of the set-up is located inside a closed bunker made of blocks of heavy concrete, lead and borated plastic properly assembled. As a consequence, an efficient remote control system (RCS) which allows operation inside the bunker is required. Three computers are used. One is dedicated, via a Labview^{TM} based interface program, to read-out and to store in a ".txt" format the data of the various sensors (temperatures mounted on the freezing cell and pressures of all the system). With another computer are controlled (via a special electronic interface box) the UCN valves used in the storage experiment. On the same unit a program (also Labview^{TM}) which operates remotely the parameters of the converter unit (heating power, temperatures) is installed. Additionally, the computer is used for a visualization of the outputs of two digital cameras focused on the sapphire windows of the deuterium freezing cell (in opposite directions). Those cameras, located inside the dark bunker, are illuminated with "low-heat" lights. One computer is completely dedicated to data acquisition (DAQ) of the neutron detector. The computer receive the digital output signal from a standard Camac-CC32 interface. The data is treated and partially analyzed "on-line" with a ROOT based routine. Beside the CC32, the DAQ electronic hardware consists of a standard amplifier (Ortec-440A) and a digital converter (Silena ADC-4418). A special module (ALC-8806) performers the interface (conversion) between those components. The original signal from the detector is also partially treated (shaping

time $\tau \sim 4\mu s$) in order to reduce the general electronic noise.

The most efficient way to measure a neutral particles like a neutrons is to convert them into a detectable charge via nuclear reactions. For UCN, the detector is an He-3 gas proportional counter [43]. The particular reaction involved is expressed by the following equation

$$^3He + n \rightarrow ^3 H + p \tag{3.1}$$

With a very high cross section ($5330 barns$) for "thermal" neutron. The associated Q-value is $0.765 MeV$. The amount of helium in the reaction chamber is relatively small ($30 mbar$). In this way, due to the "1/v" behavior of absorbtion cross section, the detector is practically transparent to high energy neutron but very sensitive in the UCN energy region. The quenching gases are methane (CH_4) and argon (Ar). A thin aluminium foil ($50\mu m$) is used as neutrons entrance window. The amplification of the generated charge is provided by a set of multi-wires connected with an external high-voltage supply which operate at about $1.1 KV$. The detector is also integrated with a pre-amplifier. Unfortunately it was not possible to re-fill the active gas (He-3) before the measurements. According with the specifications [44], at the time of use, a reduction in the relative efficiency of about 60% is expected. Indeed this was the value successively extrapolated at the ILL UCN source in Grenoble from comparison with another "new filled" detector of the same kind. During the operation, the external case of the detector was adequately shielded with layers of borated plastic (against neutrons) and blocks of lead (against γ-rays). The level of the background was reduced down to a negligible value ($BG \simeq 10^{-4} s^{-1}$).

An important element of the DAQ is an additional neutron "monitor". This detector, a fission chamber with a small active cross section ($\emptyset = 2mm$), is located in the direction of the beam just before the "beam-stopper". Hence, it is also aligned with the middle of the UCN extraction window. Therefore it is possible to extract information related with the transmitted neutron beam.

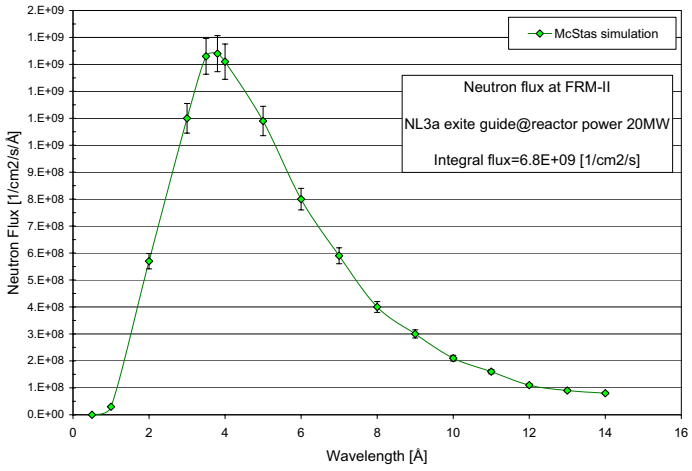

Figure 3.5: Simulated neutron spectra at NL3a position

3.7 Operation at FRM-II and related safety aspects

The Cube-D_2 apparatus is used to test basic ideas associated with the Mini-D_2 project. For instance the efficiency of the deuterium solid converter, the UCN extraction (or storage) system, the ortho deuterium converter unit and the DAQ. To explore these features a set of measurements are performed at the FRM-II reactor. The location is one of the beam lines (NL3a) of the Mephisto instrument where an intense cold neutron beam is available. In Fig. 3.5 is shows the simulated spectra at the NL3a exit guide position.

The maximum equivalent neutron wavelength is ~ 4 angstrom which corresponds to $\sim 5meV$ (60K). As comparison, the best value for UCN production is $\sim 2.6meV$ (30K). In order to optimized the irradiation of the deuterium freezing cell, a special intermediate collimator (cross section selector) was assembled between the exit guide flange and the Cube-D_2 experiment. Because of the introduced geometry modification, the integral neutron flux was measured again. This information was extracted with the technique of

the activation foil. A very thin gold foil ($37.5\mu gr$) was placed at the level of the converter cell. With an adequate irradiation time (in this case 31s), the measured gamma activity of the foil is proportional to the flux. An associated neutron integrated flux of $\Phi_n = 1.56 \cdot 10^9 n/cm^2 s$ was measured. To operate at the FRM-II additional aspects has to be considered. Very conservative criteria have to be achieved especially in defining detailed post-accident procedures (for example in case of evacuation of the deuterium for replacing small components). Several emergency procedures related with possible accidents were presented. The FRM-II authorities (technical, electrical and for radioprotection) released an agreement to safely open the NL3a neutron shutter and hence to start to irradiate the cell. During the long operation (about 50 days) a periodical monitoring of the radioactivity (including tritium) was accomplish.

In the pictures 3.6 and 3.7 are presented a global views of the Cube-D_2 experiment already assembled (a part the external concrete shield) at the Mephisto position of the FRMM-II. Beside the others components, it's easy to distinguish the storage long tube (tilted by 30°) and the UCN valves.

3.8 First UCN production at FRM-II with a 3cm thickness cell

A systematic irradiation of a 3cm thickness cell was done. Measurements in solid, liquid and gas phases were investigated. The first set of measurements was performed in the so-called flow through-mode. UCN continuously produced at the converter cell pass through the full extraction system ($L \sim 5m$) and arrive at the detector after a typical transfer time ($\sim 4sec$). Hence, an equilibrium is reached inside the system between production and losses. The definitive evidence that the particles detected are neutrons in the UCN energy region comes from the following experimental fact. The counting rate with and without the "clamp" stainless steel foil (described above) differs by a factor of 3.

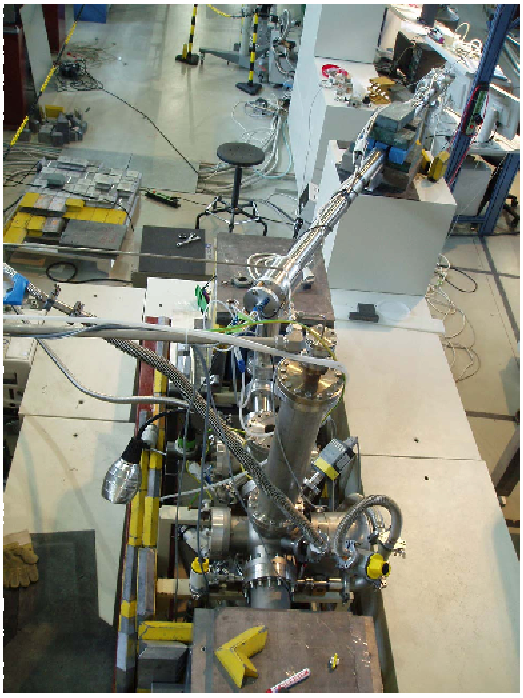

Figure 3.6: Set-up at the Mephisto position of the FRM-II, top view

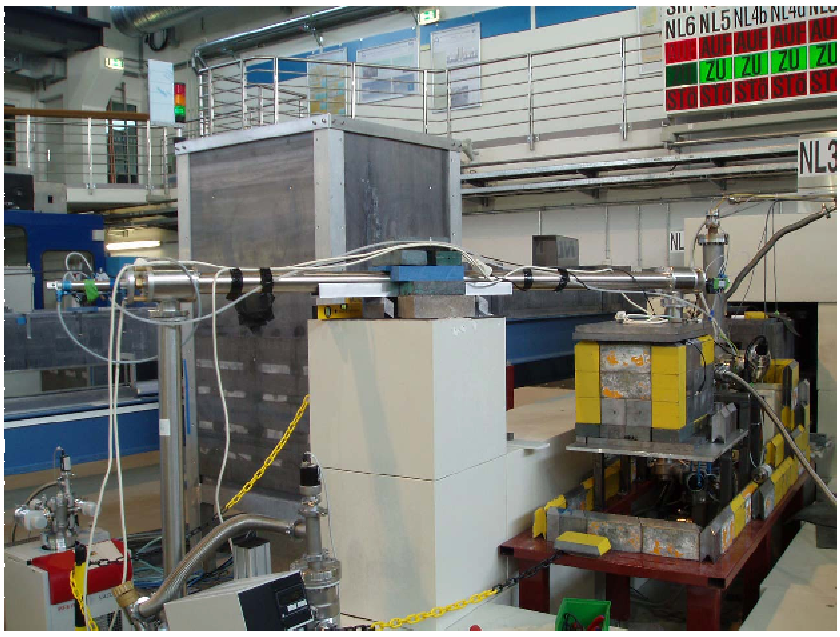

Figure 3.7: Set-up at the Mephisto position of the FRM-II, side view

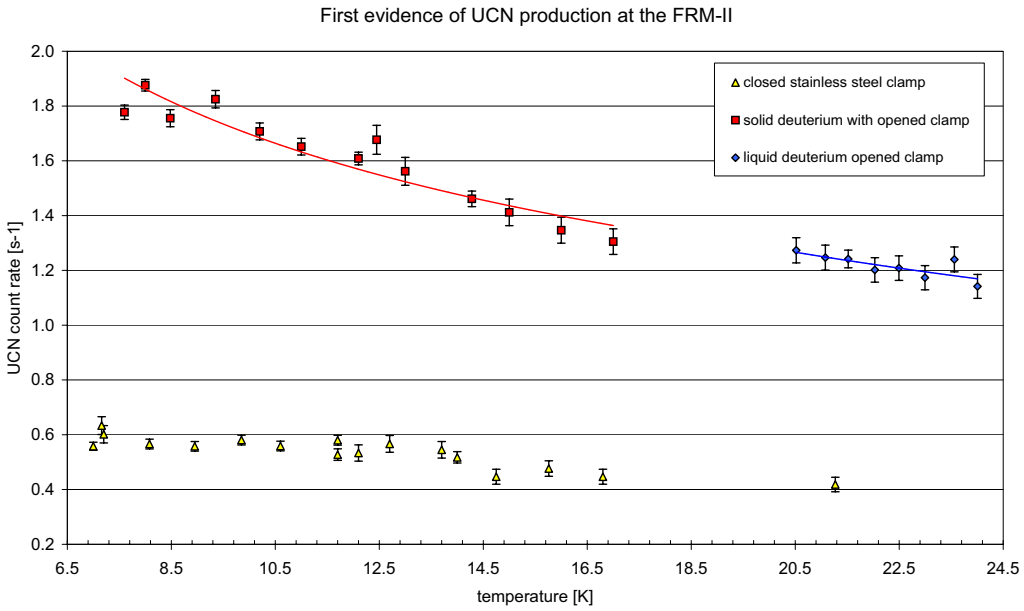

Figure 3.8: UCN production in solid and liquid deuterium

Moreover, by a simple geometrical argumentation, the probability that a "high-energy" neutron performs just multi-scattering inside the extraction system and afterward reaches the detector is almost zero. An additional "storage" experiment with valves was also done and will be explained in details in the next section. In Fig.3.8 are presented results from one of the first deuterium freezing experiences.

Primarily, it is possible to observe that the gain UCN factor between liquid and coldest reachable temperature of the solid deuterium ($\simeq 8K$) is not more than 2. This crucial unexpected result, which is reiterated in all the successive measurements, will be considered and explained in another section. As expected, the UCN production in liquid is

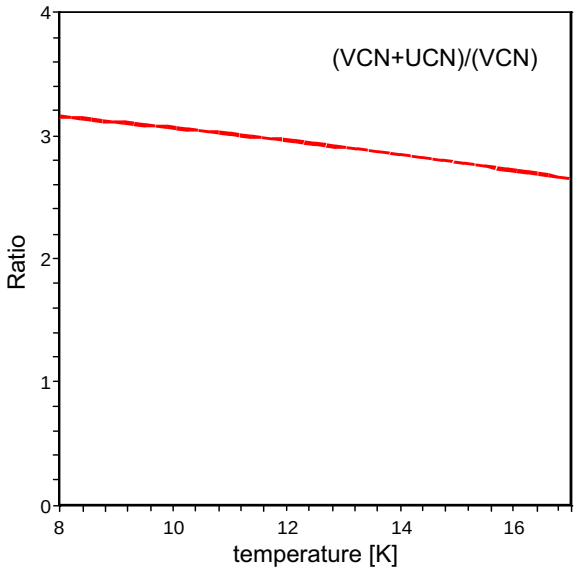

Figure 3.9: Ratio between the "opened" and the "closed" clamp

almost constant in a wide temperature range with a small reduction due to the different deuterium density. For different freezing procedures (from gas, from liquid, annealing, thermal cycling, etc..) a variation in the UCN counting rate within 15% was registered.

It is important to note that the ratio between the total neutrons detected with the open stainless clamp (red-squared series, Fig.3.8) and the ones detected with the clamp in closed position (yellow-triangle series, Fig.3.8) is almost constant over the range of the temperatures investigated (Fig.3.9). That is reasonable considering that in first approximation both series are ultimately related at each temperature to the absolute intensity of the incoming cold neutrons flux and to the deuterium density. According with this idea (confirmed in different set of measurements), it was decided to acquire the successive data sets only with the clamp in the open position and to use the measured ratio as correction function. Indeed the VCN (very cold neutrons) fraction should be always conserved.

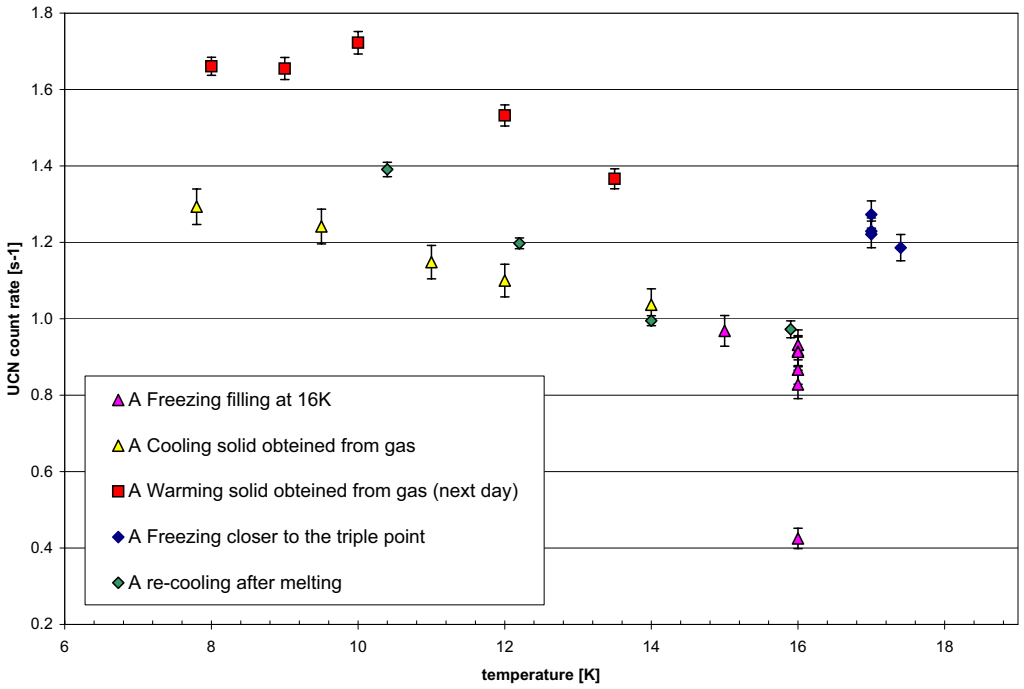

Figure 3.10: UCN typical acquiring cycle in solid and liquid deuterium: Filling A

3.8.1 UCN production in solid and liquid deuterium

In order to quantify the influence of the different parameters involved, several filling cycles with the 3cm cell were done. According with the theory, high UCN count rate is expected to be measured in liquid and especially in very cold solid deuterium. Therefore, particular effort was concentrated at those thermodynamical phases. A description of a typical acquiring cycle is presented in Fig.3.10 and Fig.3.11.

In the series denoted "Filling A", deuterium is freezing out directly from the gas phase

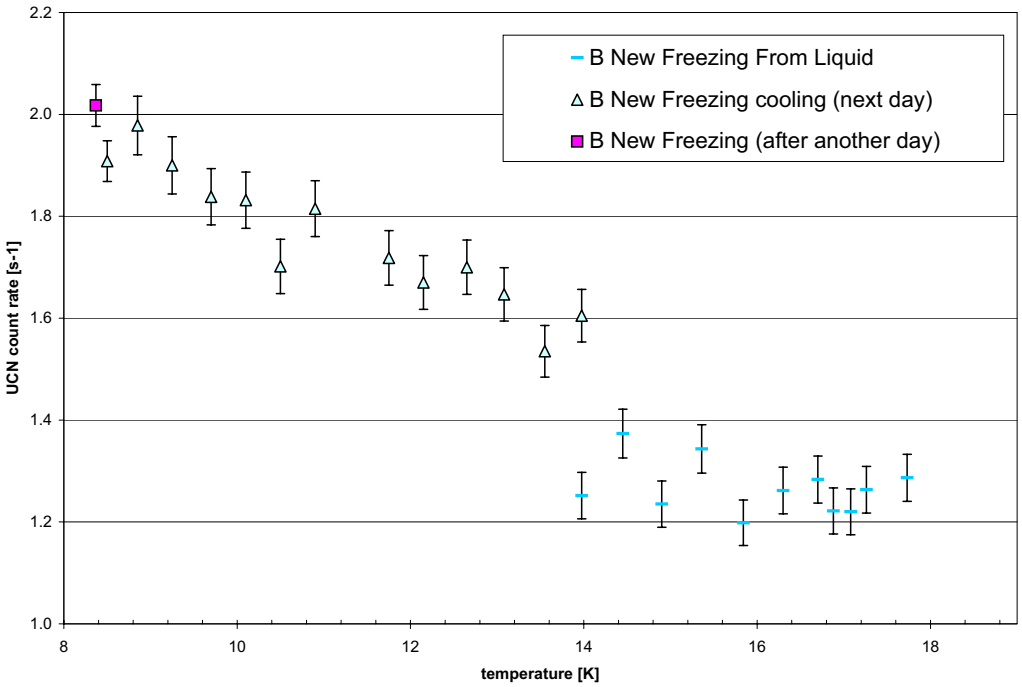

Figure 3.11: UCN typical acquiring cycle in solid and liquid deuterium: Filling B

(sublimation) at around 16K. According with the phase diagram, this process requires a pressure below 100mbar. This condition is guaranteed by properly setting the inlet metering valve (N2, Fig.3.3). Data (accumulation time, 600s) was acquired during the filling of the cell (pink-triangle series). Very quickly saturation in the UCN counting rate was registered. The deuterium block obtained was relative transparent. At this moment, the inlet connection was closed. Then, a slow cooling was performed (yellow-triangle). As expected, the UCN count rate increased almost linearly with the temperature decreasing. At the coldest temperature ($\sim 7K$), a UCN rate of $1.3s^{-1}$ was detected.

During this cooling process, although the solid was optically unchanged (almost transparent), the value of the transmitted cold neutrons registered with the "monitor" detector was unstable over the time. A clear indication that the deuterium crystal was rearranging the structure to reach "equilibrium" conditions. Indeed, after one night of keeping the solid at the coldest temperature, an improvement in the UCN count rate of about 27% was registered (squared-red series). After a slow warming-up process, the deuterium block was melted ($\sim 20K$) and slowly frozen again closer to the triple point (blue-rhombus series). During this procedure it was realized by optical inspection of the level of the liquid that only 2/3 of the cell was filled. The following very slow cooling (data were acquired over three days) are presented in the green-rhombus series. It is possible to note that, although the slope is almost conserved (with respect to the squared-red series), the absolute UCN count rate is reduced by $\sim$ 25%. This is a characteristic behavior for a sublimation-melting-freezing cycle (corroborated in another freezing experience at $13K$) and could be explained using the following argument. When gaseous deuterium is introduced in the cold aluminium chamber ($16K$) the freezing process initiates preferentially at the bottom (coldest surface). Therefore, layers of solid are created and accumulate. But the middle-top area of the cell is also at a temperature below the triple point ($\sim 18.7K$). As the thermal conductivity of the solid deuterium is small compared with aluminium ($\lambda_{D2} = 0.4W/mK$, $\lambda_{Al} = 27W/mK$), freezing on the vertical inner walls is also possible or even favoured. Therefore, additional thin layers of solid deuterium are created in the

freezing chamber and also on the whole UCN extraction window. As will be explained, there are consistent indications that UCN are influenced, at least with respect to the extraction process, only by a relative thin "active layer". Under this assumption, it is evident that an additional deuterium layer (described above) could significantly enhance the global UCN count rate. Once the deuterium is liquified and frozen again from the liquid phase, it is not possible to recover anymore this layer. Furthermore, because the cell is not completely filled, the reduction of the deuterium density associated with the phase transition liquid-solid (15%), introduces an additional diminution (shrinking) of the deuterium amount available at the level of the extraction window. Both those phenomena contribute to the results of the green-rhombus series. A "turbo" freezing cycle was also investigated. The procedure involved a rapid cooling (3min from $19K$ to $8K$) with an associated fast liquid-solid phase transition. The UCN count rate dropped down by a factor of 2. By optical inspection one could note that the deuterium block obtained was completely black. In the figure 3.11, measurements from a "Filling B" data set are shown. In this case a solid block was obtained by continuous slow cooling of liquid (from T=21K to about T=14K). As expected, due to the rearrangement of the crystal, relatively broad oscillations in the UCN counting rate are registered in this range (cyan-line series). Thus, the solid was kept at T=14K for one night. The results are displayed in the aquamarine-triangle series. Again, a significant improvement in the UCN count rate (28%) was measured. During the following cooling of the deuterium, data points were acquired every 0.5K. At the coldest temperature (T=8.5K) a UCN rate at about $2s^{-1}$ was detected. The solid was kept at those temperature for another day. This time, no significant increase in the UCN count rate was found (squared-purple point). In fact, the "monitor" value of the transmitted neutrons through the cell remained unchanged ($20KHz$).

3.8.2 UCN production in gaseous deuterium

Although the Cube-D_2 was projected mainly to investigate the UCN production in a solid converter, an important part of the experimental program was dedicated to explore the deuterium gas phase. Actually, the motivations came up during the beginning of the measurements at the FRM-II. Indeed the absolute UCN count rate in gas was registered to be relatively high (in some cases comparable with liquid) and definitely higher than the background. Therefore, preliminary conditions to start a systematic investigation concerning the UCN production in deuterium gas phase were achieved.

The advantage of performing measurements in the gas phase are, of course, related with the fact that the parameters involved are only two, for instance pressure and temperature (volume is fixed). Moreover, when the chamber is filled with gas (or vapor), the whole available volume ($40cm^3$ for the 3cm thickness cell) is isotropically filled with deuterium. Especially for comparison within the results obtained with cells having different sizes (as will be better explained in the specific section), ideal conditions are realized. A set of measurements in so-called isobaric conditions were performed at 300mbar, 1000mbar and 3000mbar. The overview of the results are presented in Fig.3.12.

To keep the pressure in the cell constant over a relatively wide range of temperature ($20 \div 150K$) a special procedure was used. Starting from gas (or vapor) at fixed pressure conditions (for example 3000mbar at 29.5K, yellow-triangles series) the chamber was warmed up typically in 2K steps. The extra pressure generated by the thermodynamical "Boltzmann-factor" was released in the converter unit. Similar results were obtained by cooling the cell starting from relative high temperature (150K). In this case, to maintain isobaric conditions, additional cold deuterium material was introduced from the converter unit. The limitations concerning the coldest measurable temperatures are due to the associated condensation process. For example for the 300mbar series, deuterium starts to liquify at around 20K. The upper value for the pressure is limited, for safety reasons, by

the thin aluminium extraction foil (tested for not more than 3.5bar).

Each data series (300mbar, 1000mbar and 3000mbar, Fig.3.12) was fitted with a variable power function ($y(T) = a * T^n$, where a and n are parameters extracted from the measurements). As expected, the higher the pressure, the higher is the UCN count rate. In fact, at a certain temperature, in a closed system, the pressure is directly proportional to the number of deuterium molecules. Thus the probability that an incoming cold neutron interacts with deuterium molecules producing more neutrons in the UCN energy region, should increase proportionately. Within the same series the UCN count rate reduced as the temperature increases. This result reflects the fact that the deuterium gas density decreases as the temperature increases ($\rho_{D_2} * T$= constant, ideal gas law). Indeed, these are the outcomes obtained for the isobaric series performed at relative low pressure (300mbar and 1000mbar, Fig.3.12) the extracted exponent $n \simeq -1$.

The ratio of the UCN count rates of different series is also relative constant ($R_{1000/300} \simeq 2.4$) over the temperature but is less than predicted ($P_{1000}/P_{300} = 3.33$). This unexpected phenomena is even more prominent in the 3000mbar series ($R_{3000/300} \simeq 3$, should be 10) and could be justified by the following argument. For the deuterium cell we have to distinguish two processes: production and extraction of UCN. At every specific temperature, the UCN production depends mainly on the amount of deuterium in the cell (isotropically distributed in the volume). Hence, also the UCN production density (in UCN/cm^3 units) is conserved. For the extraction characteristic, instead, the process is different. Let's assume that a UCN is produced in whatever unit volume inside the cell. The more this unit volume is away from the extraction windows, the grater is the chance for the UCN to interact again with other deuterium molecules, performing for example an "upscattering" process. Consequentially, some of the UCN produced are lost on the way to the extraction windows. This effect is proportional to the amount of deuterium inside the cell and therefore, in the conditions described above, to the pressure. Even at relatively low pressure (300mbar, 1000mbar) this process contributes significantly ($\sim 38\%$) and, as

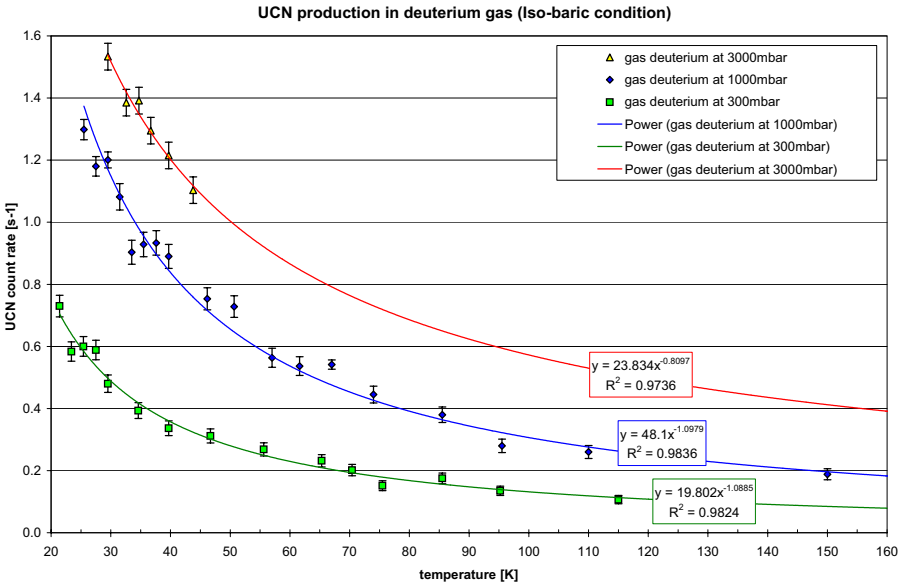

Figure 3.12: Gas deuterium at different pressures, x is the temperature

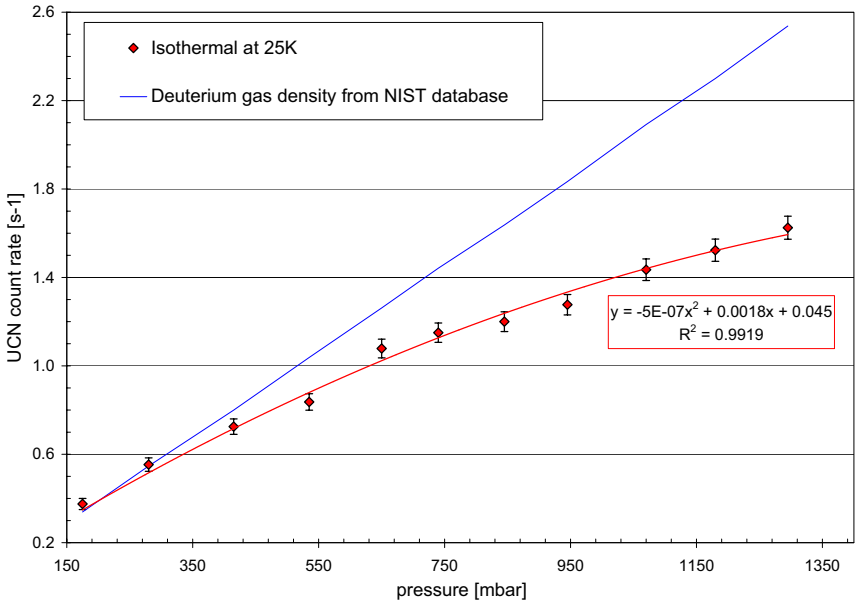

Figure 3.13: UCN production in gaseous deuterium at 25K

clearly shown in Fig.3.12, becomes dominant already at 3000mbar. For the same reason, focusing on the temperature dependence, the fit to the experimental data in the same series does not follow anymore the "1/T" behavior ($n \simeq -0.8$).

This explanation is confirmed by successive measurements performed in isothermal conditions. The outcome are presented in Fig.3.13. Data was acquired keeping the temperature of the deuterium chamber constant at $\sim 25K$. The pressure covers a range from 150mbar to 1300mbar. The upper limit is again due to the condensation of the deuterium. The deviation from the linearity (red-rhombus series) is evident by comparison with the best experimental values available (blu-line, NIST database) and is in perfect accord with the results extracted in isobaric conditions.

The main conclusion from the experimental results obtained from the set of measurements performed in deuterium gas phase, for instance UCN production/extraction

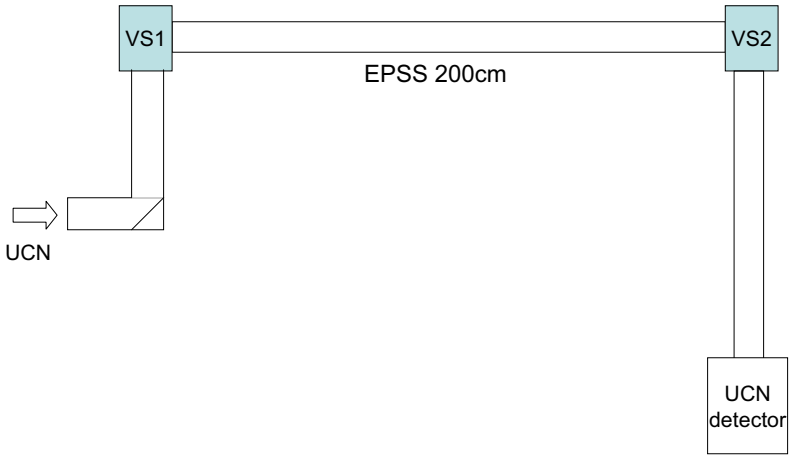

Figure 3.14: UCN extraction system for the storage experiment, side view

as function of pressure and temperature, could be expressed in this way: in gas phase, a saturation in the UCN count rate mainly due to a bad extraction characteristic (high up-scattering) is registered. Therefore, besides the technical difficulty to find a suitable extraction foil withstanding a relatively high pressure, gas-phase converters (deuterium, oxygen, heavy methane, etc..) are not adequate for efficient UCN production.

3.9 Storage experiment in a electro-polished stainless steel bottle

The uncontestable proof that the neutrons detected are UCN is accomplished with a real storage experiment. For this specific set of measurements, the UCN extraction system is modified (Fig.3.14). The two EPSS bends are replaced by two stainless steel valves (VS1, VS2). Therefore, it is possible to store the neutron in the long horizontal part of the

system (200cm, Fig.3.6). The promising properties of this guide (transmission coefficient $\tau_{SS} = 0.96m^{-1}$ and wall loss probability per bounce $\mu \sim 2 \cdot 10^{-4}$) were already investigated at ILL in Grenoble [45]. The method used to extract this information is described in more details in chapter 4.

The neutron valves (also electro-polished) were specially designed to operate efficiently in closed position (metal sealed) and are driven by a fast (1sec) pneumatic device (pressurized air at 6 bar) and are controlled remotely via computer. In this new configuration of the extraction system, when VS1 and VS2 were fixed in opened position, a reduction in the UCN count rate by a factor ~ 3 was registered. The experiment was performed at the highest UCN count rate, therefore with solid deuterium at the coldest temperature obtained ($\sim 10K$).

Generally, the main outcome of a "UCN storage experiment" is the value of the so-called lifetime of the storage bottle (τ_{stor}). This parameter, which estimates the losses in the volume mainly due to wall collisions ("β-dacay" is neglected), allows comparison of bottles made out of different materials. For a storage experiment in a cylindrical geometry (long tube like in the Cube-D_2), applying the kinetic theory of rarefied gas [6], τ_{stor} is directly related to μ_{wall} and in a first approximation can be expressed by

$$\mu_{wall} = \frac{2R}{< v_{UCN} > \tau_{stor}} \tag{3.2}$$

Where $< v_{UCN} > (5 \div 6)m/s$ is the mean velocity of the UCN at the entrance of the EPSS tube tested and R=3.3cm is the inner tube radius. In a closed system the starting UCN number drops down in time according to the following decay law.

$$N_{UCN}(t) = N_{UCN}(t = 0) \cdot e^{-t/\tau_{stor}} \tag{3.3}$$

A typical measuring procedure consists of different steps in time which define a UCN storage cycle. At the beginning, VS1 is opened and VS2 is closed. Therefore, the UCN

continuously produced in the solid deuterium cell create an equilibrium density inside the whole system (production versus global losses).

A preliminary set of measurements were done to find an "optimum" filling time (τ_{fill}) for the bottle, which characterizes the maximum reachable UCN density. Although τ_{fill} doesn't affect the storage lifetime, it is used to reduce the influence of the background. The value extracted was $\tau_{fill} = 12s$. After filling also VS1 is closed. Now, the neutrons are located inside a closed volume ($V_{bottle} = 6842cm^3$) and perform collisions with the walls. After a certain time (τ_{keep}), VS2 is opened and the UCN are counted by the detector within $\tau_{meas} = 20s$. Between two cycles, a sufficient "cleaning" time ($\tau_{wait} = 7s$) is also considered. Using data sets with different τ_{keep} it is possible to extract τ_{stor} from equation 3.3.

In order to accumulate statistics, several cycles were measured for each value of τ_{keep}. The result, background corrected, is shown in Fig.3.15 using a logarithmic scale, which allows an elegant graphical solution of equation 3.3. The lifetime of the electro-polished stainless steel bottle is $b^{-1} = \tau_{stor} = \sim 40s$.

Using equation 3.2 it is possible to estimate the wall loss probability per bounce in the tube. The value obtained was $\mu_{wall} \sim 2.8 \cdot 10^{-4}$. It is very close to the value obtained at ILL (see chapter 4.3.6) using the same sample but a different approach [45].

3.10 Influence of the irradiation on the ortho deuterium equilibrium

The paramount condition for experiments on UCN production is a high ortho-deuterium concentration. In section 3.5 we illustrated the technique to reach such performances (C_{ortho} closer to 1). But once the deuterium is placed under irradiation the value of C_{ortho} may change. Only a little is known on this subject [46]. Therefore, in the Cube-D_2 experiment, measurements to explore this open question were also done.

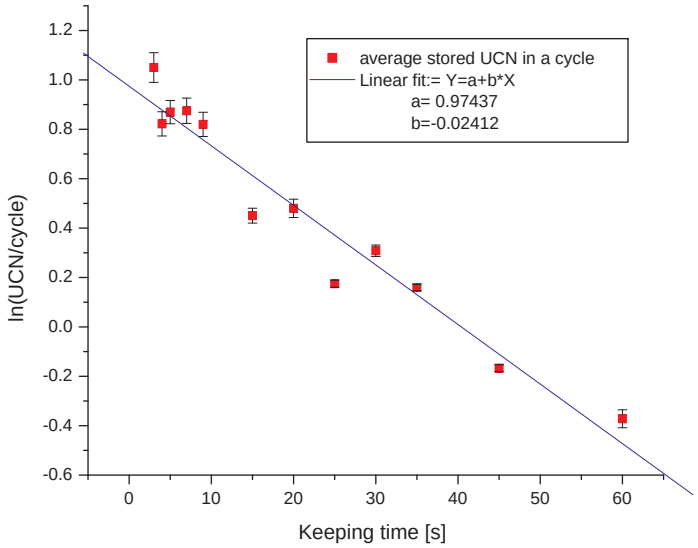

Figure 3.15: UCN lifetime in a EPSS bottle

A gaseous deuterium sample was taken shortly before starting the irradiation. As expected, the outcome (see chapter 5) was an ortho-deuterium concentration of $C_{ortho} = 0.970 \pm 0.004$. After relative long irradiation (more than three days), another sample was taken out showing a value very similar ($C_{ortho} = 0.968 \pm 0.005$). The associated integral dose in the irradiated deuterium was $\Psi_{CN} \sim 5 \cdot 10^{15} n$. Hence, in the irradiation conditions of the Cube-D_2 experiment at the Mephisto-NL3a beam of the FRM-II, no significant evidence of changes of the ortho-deuterium concentration was registered.

3.11 Additional experiments performed with similar cells having different thickness

In the previous sections an overview of the main results obtained with the 3cm thickness deuterium cell was presented. Measurements performed in solid and gas phase demonstrated, at least qualitatively, that the deuterium "active layer" is smaller than expected

(ideally in solid $\lambda_{mfp} \sim 15cm$). To explore systematically this phenomena, a set of measurements was performed with deuterium cells having different freezing volumes and particularly different thickness in the direction of the cold beam. For instance, freezing experiments were performed with 2cm, 1cm and 0.5cm thick cells. Unfortunately, due to limited space, it was not possible to mount optical windows. Therefore the amount of deuterium frozen out in the cell it was not know with high precision. A general unexpected behavior was found: the smaller the cell thickness (less deuterium), the higher the absolute UCN count rate. Specific data sets for each cell are illustrated in the next sections.

3.11.1 Measurements in a 2cm thickness cell

The 1cm cell was replaced by the 2cm thick cell. The procedure involved several steps and, because was the same for all the other cells, is shortly described. At first, the deuterium was safely stored in the converter unit (liquid at $\sim 20K$). The small residual gas in the pipes was pumped out. Then, the whole system was warmed up (300K) with a consequent breaking of the isolation vacuum. According with the FRM-II authorities of radioprotection, the concrete bunker was partially dismounted. Due to the extremely high radioactivity detected at the cold-head area, a relative long waiting time was respected (almost 2 days). The EPSS bends were remounted again instead of the UCN valves. Finally, the previous cell was removed and replaced by the 2cm one. The bunker was again reassembled and, after a new general check (including monitoring of tritium) the authorities gave the permission to open safely the NL3a neutron shutter. In this new configuration, the transmitted cold neutron beam measured for an "empty cell" was slightly higher than before ($38.5KHz$). Once the freezing chamber was cold enough ($\sim 19K$), vapor deuterium from the converter unit ($\sim 21K$) was introduced. The difference in the temperatures ($\sim 2K$) guaranteed, due to the differential vapor pressure, the flow of material from the converter unit to the cell. In these conditions, therefore, deuterium started to liquefy in the chamber (for example at τ_0). The "monitor" detector aligned with the

middle of the UCN extraction windows ($h_{1/2}$) was used to verify the level of the liquid in the cell. Indeed, due to the small active size of the fission chamber ($r = 1mm$), the transmitted cold neutron count rate starts to drop down linearly only when the level of the liquid deuterium is closer to the half-height of the cell (from $h_{1/2} - r$, at $\tau_{1/2}$) and after a short time ($\tau_\epsilon \ll \tau_{1/2}$), when the level of the deuterium reaches the height $h_{1/2} + r$ (at $\tau_{1/2} + \tau_\epsilon$), is almost stable because the full geometrical acceptance of the "monitor" ($A = \pi * r^2$) is already covered. Therefore, in approximately the time $2 * \tau_{1/2}$ the cell is completely filled. A first freezing series down to $T \sim 10K$ was acquired.

During the warming up of the cell an accident occurred. Probably due to a shock wave, the rupture disk (R1, Fig.3.3) bursts, releasing overpressure into the reservoir. It's important to note that the integrity of the extraction windows was preserved. According with the FRM-II authorities, before replacing this component, almost all the deuterium was pumped out from the DGS (via D2) into a big external bottle and then safely removed from the reactor. New deuterium gas was introduced into the reservoir (3.5bar) from a standard pressurized bottle. Obviously, this deuterium was never in contact with the oxisorb catalyzer. Therefore the ortho concentration corresponds to the equilibrium value at room temperature ($C_{ortho} = 0.666$). This condition gave the opportunity to perform a cross-check measurement of UCN production in solid at a relative low ortho deuterium concentration. The outcome, already corrected by the total background, is presented in figure 3.16. The difference in the UCN count rate for the two sets of measurements is evident.

3.11.2 A method to extract a temperature dependent cross section

From the experimental data presented in figure 3.16, other useful information was extracted. In general the UCN count rate (CR_{UCN}) is inversely proportional to the total

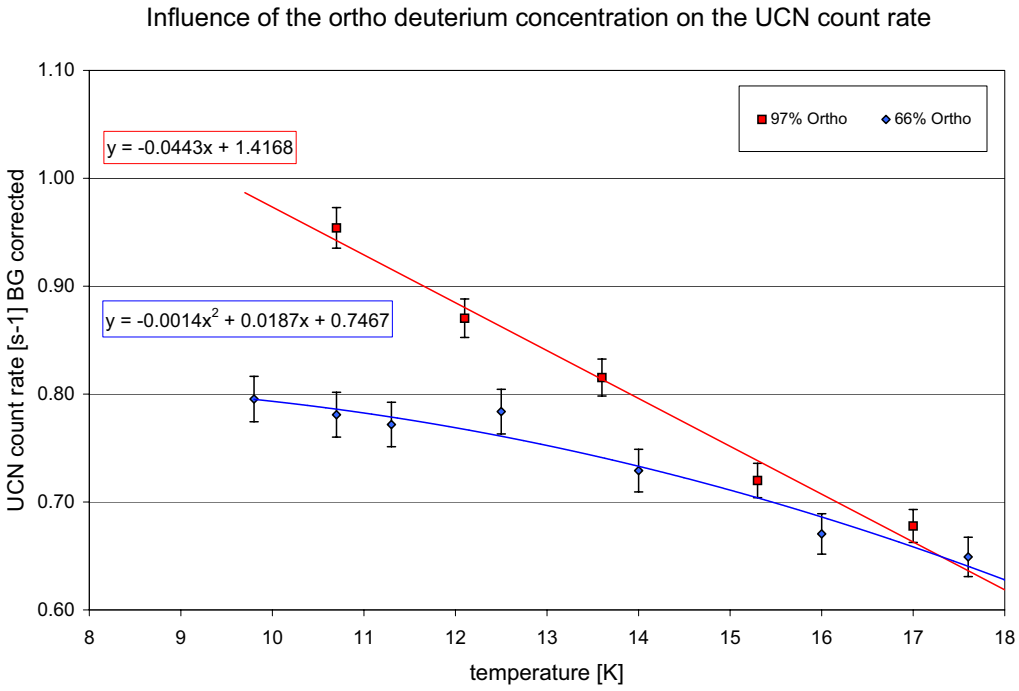

Figure 3.16: UCN production with different ortho-deuterium concentration

absorption cross section in the solid deuterium:

$$CR_{UCN} \propto \frac{1}{\sigma_{tot}} \tag{3.4}$$

where σ_{tot} includes all cross sections which involve UCN losses. Thus, for deuterium with a para-D_2 concentration $C_{para} = \gamma$,

$$\sigma_{tot} = \gamma[\sigma_{paraJ1\to0} + \sigma_{para}(T)] + \sigma_{absD2} + [1-\gamma]\sigma_{ortho}(T) + \sigma_X(T) \tag{3.5}$$

Here we consider possible unknown quantity $\sigma_X(T)$. For the known cross sections in 3.5, theoretical predictions are available. For example the para-D_2 temperature independent cross section associated with a pure relaxation process is $\sigma_{paraJ1\to0} = 31barn$. Also well known is the small contribution due to the absorption on the deuterons ($\sigma_{absD2} = 0.157barn$). Furthermore, calculations for the remaining temperature dependent cross sections ($\sigma_{para}(T)$, $\sigma_{ortho}(T)$) with a model based on one-phonon process were done by Liu et al. in [47]. Using the two measurements with different para-D_2 concentration ($\gamma_A = 0.03$, $\gamma_B = 0.333$), assuming the various efficiencies (extraction system, detector, etc..) to be the same for both we can write the ratio of counting rate as:

$$\frac{CR_A}{CR_B}(T) = \frac{0.333[\sigma_{paraJ1\to0} + \sigma_{para}(T)] + \sigma_{absD2} + 0.666\sigma_{ortho}(T) + \sigma_X(T)}{0.03[\sigma_{paraJ1\to0} + \sigma_{para}(T)] + \sigma_{absD2} + 0.97\sigma_{ortho}(T) + \sigma_X(T)} \tag{3.6}$$

For each measured temperature (T_i, $i = 9 \div 18K$), the only unknown parameter is $\sigma_X(T_i)$. Therefore it is possible to cross check the theoretical model. If the absolute values of those predictions were correct, the additional cross section contribution should be very small ($\sigma_X \simeq 0$). Extracted results following this approach are presented in figure 3.17. Here we also included the different theoretical contributions to σ_{tot} for the two series of measurements (CR97, deuterium from the oxisorb converter unit and CR66, deuterium from a standard room temperature bottle). The absolute values extracted for σ_X are large ($\sigma_X(9K) \sim 36barn$) if compared to the calculated values and exhibit a strong temperature dependence. The best fit on the data is obtained using an exponential function

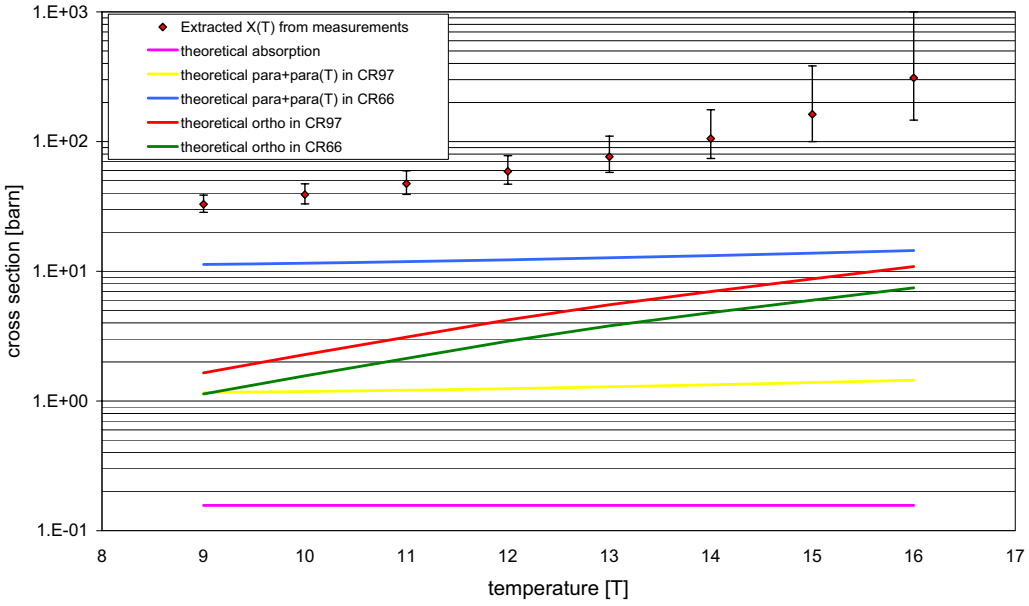

Figure 3.17: Extracted temperature dependent total cross section

dependance on T.

In the analysis presented above we assumed $\sigma_X(T)$ to be independent of the para content. Actually, this is an assumption that "a priori" is not physically justified. Therefore, additional cross-checks are required. An intuitive approach is to assume the unknown cross section to be simple proportional to the theoretical and temperature dependent cross sections $\sigma_{para}(T,\gamma)$, $\sigma_{ortho}(T,\gamma)$ or both:

$$\sigma_X(T,\gamma_{exp}) = f1 * [\sigma_{ortho}(T,\gamma_{exp}) + \sigma_{para}(T,\gamma_{exp})] \tag{3.7}$$

or,

$$\sigma_X(T,\gamma_{exp}) = f2 * \sigma_{ortho}(T,\gamma_{exp}) \tag{3.8}$$

In figure 3.18 we present the values (f1, f2) extracted from the measurements according to the equation 3.6. If equations 3.7 and 3.8 were numerically exact for each temperature, the expectations over the full range would be flat (f1 and f2 constant). It is evident that this is not the case. Focusing on the second assumption (3.8), which is the physically more plausible as this cross section should be the dominant one, we note a strong temperature dependence of the proportionality factor, especially at low temperatures where the errors are smaller. It is possible therefore to conclude that the function describing the extracted cross section σ_X is uncorrelated with the theoretical para-D_2 cross sections. In the scenario (3.7), the associated errors bars are quite big especially at higher temperature, where the measured ratio in the equation 3.6 is closer to 1.

Figure 3.19 shows the total extracted cross section together with the theoretical prediction for the high ortho concentration series (CR97). The discrepancy is large. A realistic explanation is that the solid deuterium, despite the excellent transparency, never was a "perfect" crystal. Indeed, it is well known [48, 49] that the best way to produce a deuterium mono-crystal is to perform a slow sublimation (from gas phase) at very low temperature (less than 6K). Unfortunately, this was not possible with the cooling power

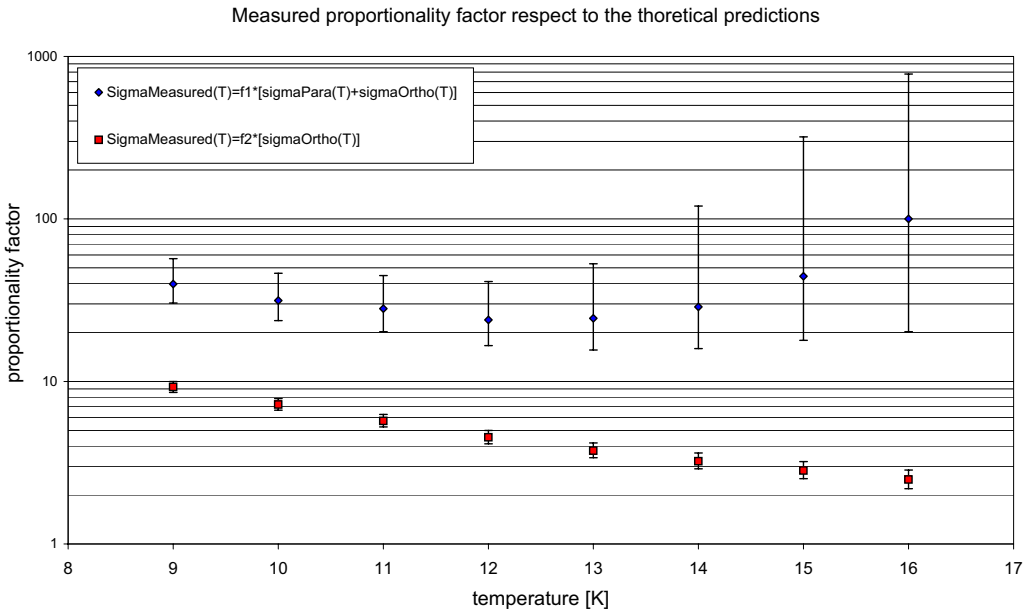

Figure 3.18: Extracted f1 and f2 for two different hypothesis, equation 3.7 and 3.8

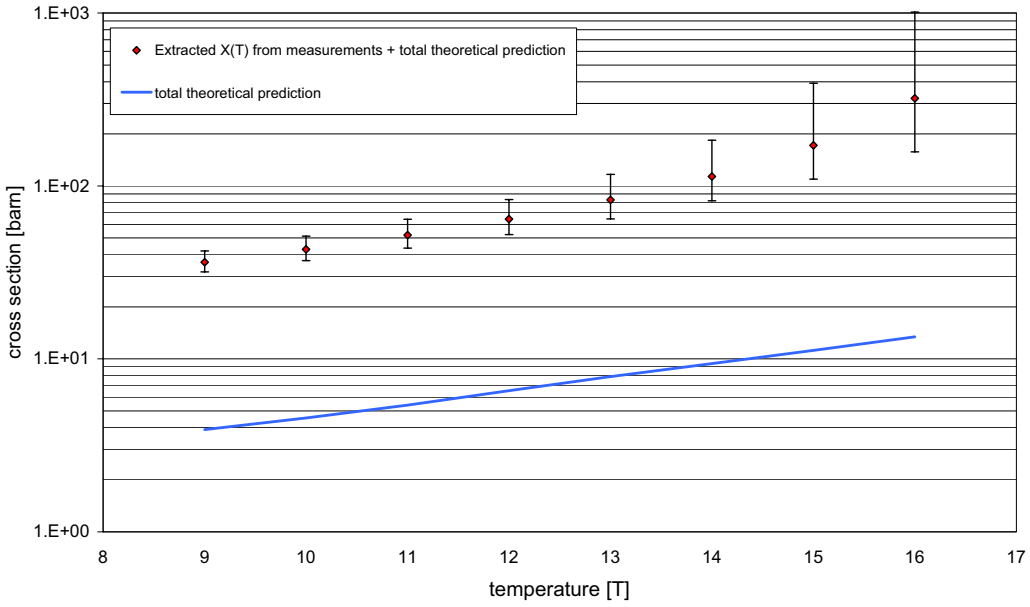

Figure 3.19: Comparison between the extracted total cross section and the theoretical predictions

available in the Cube-D_2.

All previous considerations are done under the assumption that the deuterium used was not contaminated by others high neutron absorber materials (oxygen, nitrogen, etc..). For this reason an accurate chemical analysis of the deuterium used was successively performed at the Mainz university (Institut für Kernchemie). The outcome showed that the deuterium was indeed almost pure (others compounds in the ppm region).

In summary, a large temperature dependent UCN "loss" cross section was observed. This additional component, if not related to the specific geometry of the experiment or to the quality of the deuterium crystal, could significantly reduce the UCN density expectations for standard super-thermal sources.

3.11.3 Measurements in a 1cm thickness cell

Another set of measurements was performed with a 1cm thickness cell. The total inner volume, including the bulge of the UCN extraction foil, was measured as $V_{cell}(1cm) = 13cm^3$. The maximum amount of solid deuterium in the $1cm$ thickness cell is therefore about $D_2 = 0.64mol$. The transmitted cold neutron beam rate detected for an "empty" cell was 39.5KHz. In this new geometry, measurements on UCN production in solid, liquid and gas deuterium were performed. Deuterium was frozen out in the chamber from the liquid phase. The filling of the cell was done using the standard liquifying technique already described ($T_{conv.unit} > T_{cell}$). In this special case, particular care was used in order to completely fill the cell (very long filling time). Results for two different filling procedures are presented in figure 3.20. Especially at low temperature, it was observed an unexpected relative high UCN count rate ($CR_{1cm} \sim 3.2s^{-1}$). However, the improvement due to the reduction of the temperature (from liquid to cold solid) is also in this case, relative small ($G_{temp} \sim 1.6$). Taking into account the efficiency of the detector ($eff_{det} = 60\%$), the maximum UCN count rate is about $5s^{-1}$.

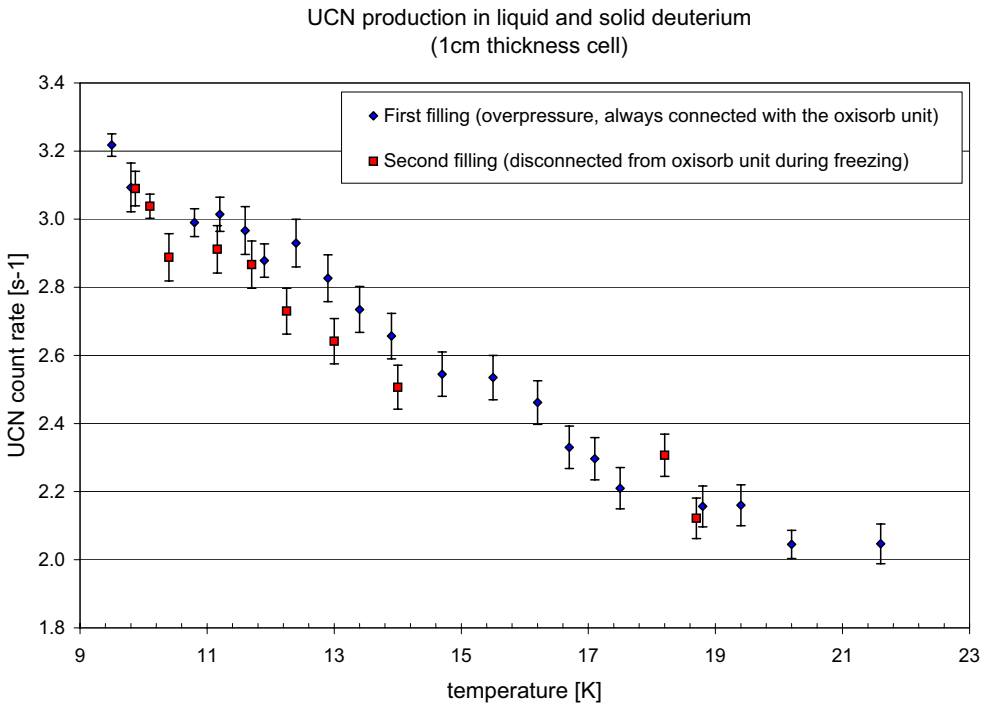

Figure 3.20: UCN production in solid and liquid in a 1cm thickness cell

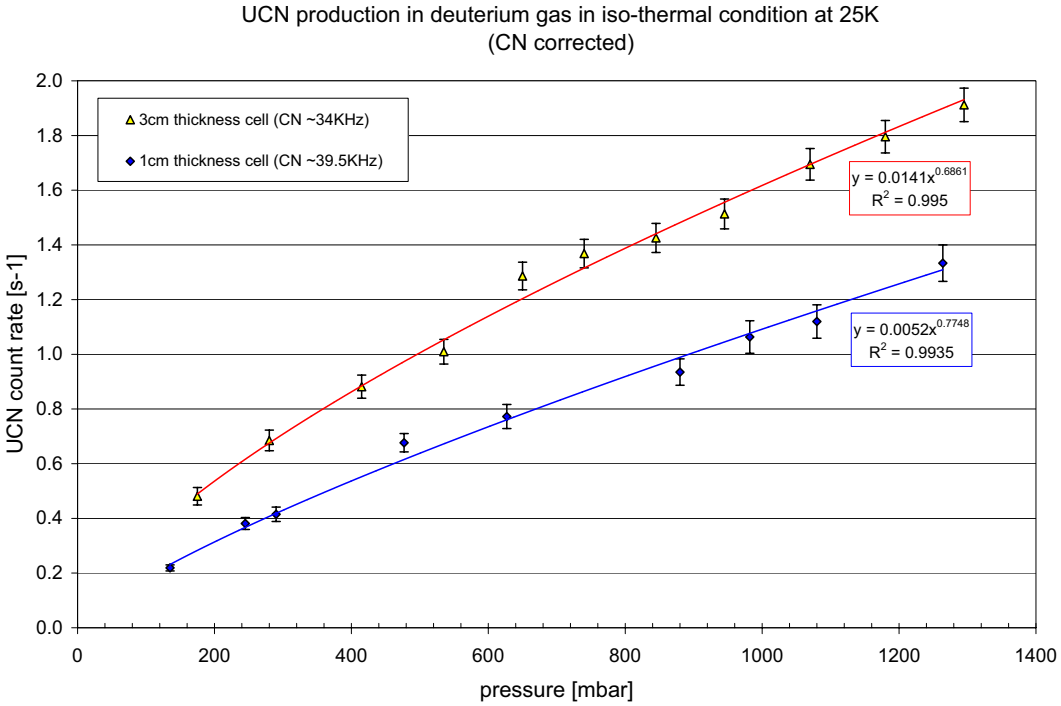

Figure 3.21: UCN production in gas deuterium

Using again gaseous deuterium, the UCN count rate in isothermal condition (T=25K) confirmed the "saturation" behavior registered with the 3cm thickness cell. The results are shown in figure 3.21. For quantitative comparisons we need to apply a small correction which is due to the difference of the transmitted cold neutron beam in the two cells. The ratio of functions fit to the data at very low pressure is $R_{3/1} \sim 2.5$. This is the ratio between the measured volumes of the chambers (including the "swell" volume due to the bulge of the extraction foil).

3.11.4 Measurements in a 0.5cm thickness cell

During the first part of the Cube-D_2 experiment at the FRM-II it was decided to construct (and to measure) an additional cell with a 0.5cm thickness. The idea was to verify the magnitude of the so-called UCN active layer which, after a preliminary analysis of the results obtained with the others cells, turned out to be very small. Deuterium at high ortho concentration was frozen in the small chamber ($V \simeq 8.5cm^3$). The gain factor between liquid and the coldest solid was consistent with the previous measurements. The maximum absolute UCN count rate registered was $CR_{0.5cm}(T = 10K) \sim 2.8s^{-1}$.

3.12 Comparison between the measurements obtained in the different cells

In this section we discuss the results of the experiments performed with similar cells having different sizes in the direction of the incoming beam, as well the main aspects of the data analysis.

3.12.1 Attenuation of the cold beam

Figure 3.22 shows the measurements of the transmitted cold neutron flux using the fission chamber "monitor" detector. Two series are presented, for liquid (T=20K) and cold solid (T=10K). Due to the different amounts of deuterium in the direction of the beam (3cm, 2cm, 1cm, 0.5cm), the intensity of the incoming beam is attenuated to:

$$\Phi_{CN}(x) = \Phi_{CN}(0)e^{-\overline{f}_{CN}x} \tag{3.9}$$

Where $\overline{f}_{CN}$ is the cold neutron attenuation factor and x is the deuterium layer thickness. Within the errors, the extracted value of $\overline{f}_{CN} \simeq 0.16cm^{-1}$ for solid deuterium is in accord with results extracted in similar experiment [50]. The equivalent total cross section for the Mephisto beam (5meV) is $\sim 5barns$.

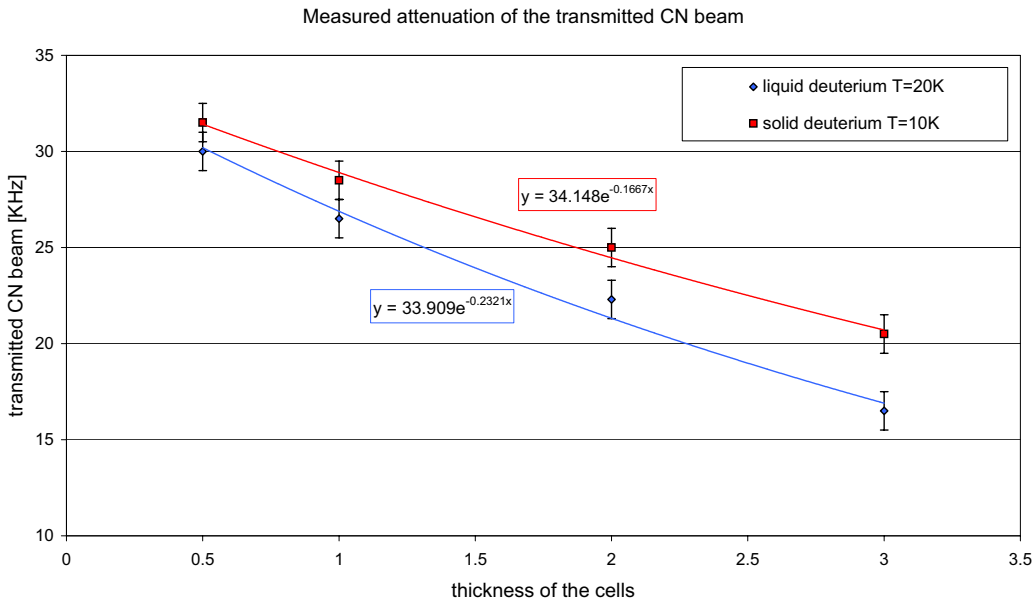

Figure 3.22: Attenuation of the incoming cold beam

3.12.2 Production and extraction of UCN to the detector

In the previous sections we introduced the evidence for the UCN active layer to be very small. By definition, the "active" layer is the thickness of a specific material (in this case deuterium) in which the extractable UCN yield drops by a factor of "e". This parameter is directly linked to the effective diffusion length of UCN in solid deuterium. A theoretical value for a "perfect" deuterium crystal given in the literature is $\lambda_{UCN} = 14cm$ [17]. In the "Cube-D_2" experiment, the maximum cell length is only 3cm. The UCN extraction process should not be affected by the different thickness, while the UCN production should be directly proportional to the amount of the solid deuterium in the cells. Therefore, in this specific geometry, the expectation is at least a linear increase of the UCN count rate with the thickness of the measured cells. All the results of the Cube-D_2 experiment performed at the FRM-II are in contradictions to those predictions.

Figure 3.23 presents the absolute UCN count rate for the different cells. Both the contribution due to the VCN (relative high energy neutrons, $\sim$ 30%), and the small background detected with an "empty" cell ($BG = 0.045s^{-1}$), are already subtracted. We note the interesting phenomenon that the UCN count rate is varying inversely to the thickness. The temperature dependence for all the series is very similar (gain factor liquid-cold solid $\sim$ 2). A realistic assumption in order to explain this unexpected behavior is that not all UCN produced in the cell are able to be detected because they are lost "in the deuterium" on the way to the extraction window. Within the geometry of the Cube-D_2, it has become evident that UCN "effective" diffusion length ($\overline{\lambda_{UCN}}$) in deuterium is certainly less than $1cm$ and even smaller. Under this condition, the attenuation of the incoming cold beam in the cell plays a fundamental role, as the production rate (P_{UCN}) is proportional to the cold neutron flux:

$$\frac{dP_{UCN}}{dx} \propto \Phi_{CN}(x) \tag{3.10}$$

For a comparison with the measured UCN count rate, due to the low UCN extraction efficiency, the integration of the equation 3.10 cannot be extended to the full range of

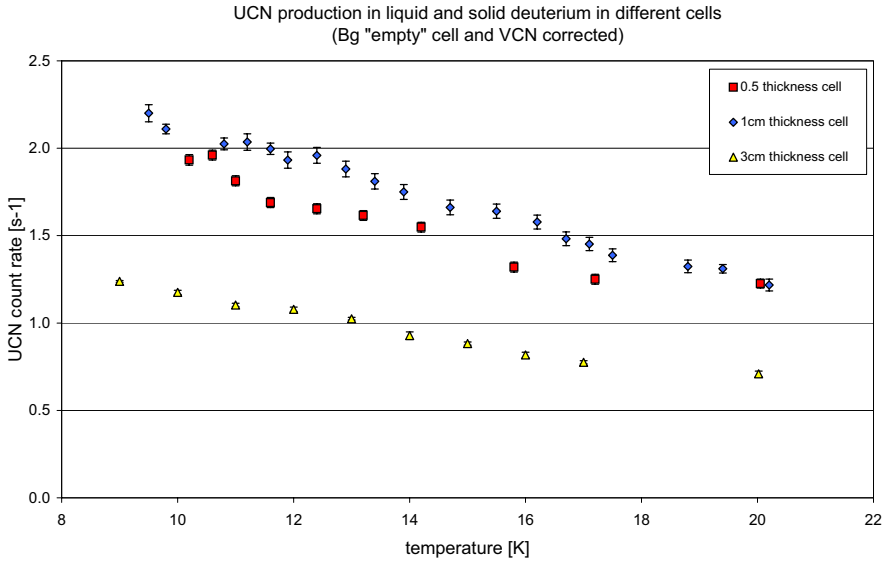

Figure 3.23: UCN absolute count rate in liquid and solid deuterium

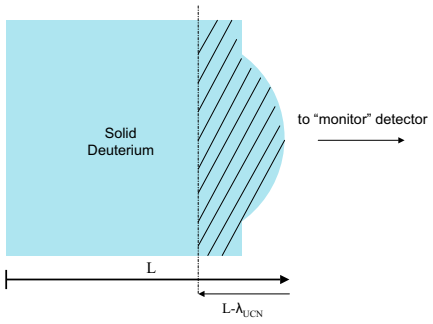

Figure 3.24: Schema of the relative distances in the deuterium cell

the deuterium thickness. The UCN produced in a unit volume away from the extraction windows (for example the first centimeter in the 3cm cell) are certainly not detected. We thus take the mean free path of the UCN into account:

$$Extracted(UCN) \propto P_{UCN} = \int_{L-\overline{\lambda_{UCN}}}^{L} (\frac{dP_{UCN}}{dx})dx \tag{3.11}$$

Where L is the position of the UCN extraction window (thickness+bulge, Fig.3.24). Therefore, according with 3.10 and 3.9, the measurements in the different cells can only properly be compared, if they are "weighted" by the attenuated intensity of the cold beam in the zone compatible for the UCN extraction. If the "active" layer at the extraction window is very thin we may assume the cold beam to be constant within this layer ($\overline{\lambda_{UCN}} \ll \overline{\lambda_{CN}^{att}}$). The UCN extraction system is identical in all measurements (windows to monitor detector). Thus we can write:

$$\Phi_{CN}(L) \simeq \Phi_{CN}(L - \overline{\lambda_{UCN}}) \simeq k\Phi_{CN}(det) \tag{3.12}$$

Where $\Phi_{CN}(det)$ is the transmitted cold neutron beam detected with the fission chamber and in k are included the additional attenuation of the cold beam from the UCN extraction window to the "monitor", as well as the efficiency of the detector itself. Evidently, this factor is the same for all the cells and therefore cancels out. Using 3.12 we can write for each temperature (T)

$$\frac{CR_{UCN}(T, L_i)}{\Phi_{CN}(L_i)} \simeq const \tag{3.13}$$

where CR_{UCN} is the measured UCN count rate and $L_i, i = 0.5cm, 1cm, 2cm, 3cm$ are associated with the measurements performed with the different thicknesses. In figure 3.25 we present the same data as Fig. 3.23 corrected for the effective flux (Φ_{CN}/L) according with the equation 3.13. The good experiment shows that the effective thickness in the deuterium usable for UCN production $\overline{\lambda_{UCN}}$ is equal for all the cells and $L_i^{min} \geq \overline{\lambda_{UCN}}$. It's evident that the hypothesis "small active layer" is compatible with the experimental data.

The different measurements in Fig.3.25 were also corrected by the level of the deuterium in each cell, which was not always the same. The criteria applied for this "scaling"

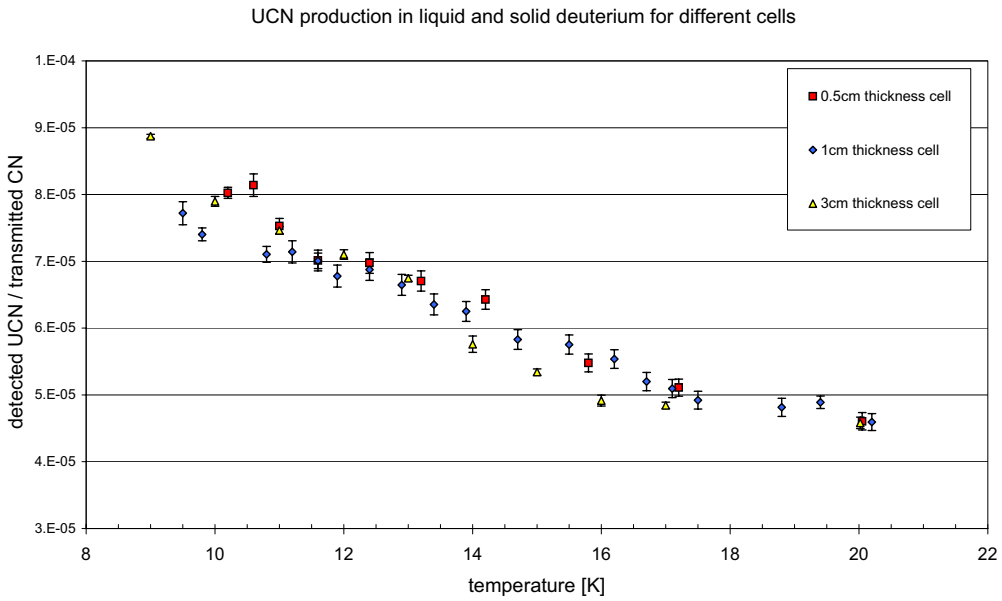

Figure 3.25: Comparison between the different cells

was based on the assumption that the UCN production in liquid (for a specific temperature and for a specific intensity of the cold beam) must always be the same. If not, the discrepancy is due to a different amount (level) of deuterium in the cell. As reference we use the measurements obtained with the "1cm" cell (blue-rhombus series) which was certainly completely filled (sect.3.11.3). The effect of the "shrinking" due to the phase transition liquid-solid was also considered.

Moreover, in figure 3.26 we present measurements performed during the freezing/filling of the "3cm" cell in "sublimation" condition (16K). In this particular procedure, as already mentioned (sect.3.8.1), the temperature inside the chamber was everywhere cold enough to favour the creation of layers of deuterium at the inner walls and therefore also at the

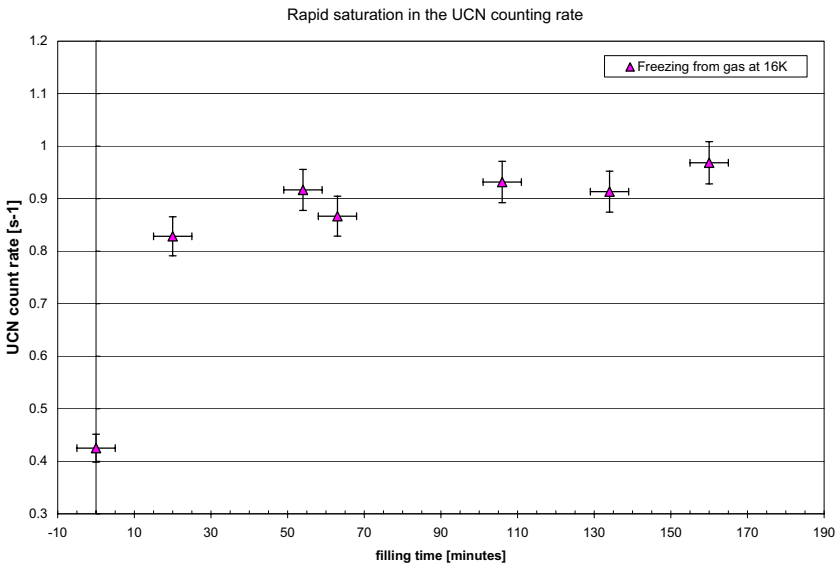

Figure 3.26: UCN data acquired during a "sublimation" series

UCN extraction window. Data was acquired regularly over the time. During these measurements, the transmitted cold neutron beam drop down linearly from $36KHz$ (starting, opening N2 valve) to $22KHz$ (after about $2hs$). The rapid saturation in the UCN count rate in figure 3.26 corroborate once again that the hypothesis of the very small "active" layer is realistic.

The results performed with "2cm" thickness cell have similar behavior but are not included in Fig.3.25 because the thin UCN extraction windows was not stable as the other cells (irregular bulge, almost flat). For all the other cells (3cm, 1cm and 0.5cm) the extraction window has the same bulge ($R_{bulge} = 2cm$). This pure geometrical factor could influence the UCN extraction especially in the measurements performed in liquid phase. Indeed in liquid deuterium the theoretical UCN active layer is almost zero [6]. Therefore, an irregular shaping of the extraction window could enhance the UCN extraction aptitude (better solid angles with respect to the guiding system) with a consequent overestimation of the UCN count rate in liquid. Indeed this is what is measured in all the series performed with the "2cm" cell. Figure 3.27 presents the simple "normalized" UCN count rate (not corrected by the level of the liquid) for those cells that were not completely full but with more or less the same level of deuterium (3cm, 0.5cm and 2cm). It is evident the overestimation of the UCN count rate in liquid deuterium.

3.13 Comparison of the experimental results with theoretical predictions

In the introduction different mathematical models were introduced in order to estimate the UCN density (or flux) expected in standard UCN sources. A particular model was presented for the so-called "film UCN source" [18].

As extensively discussed in the previous sections the UCN "active layer" in the Cube-

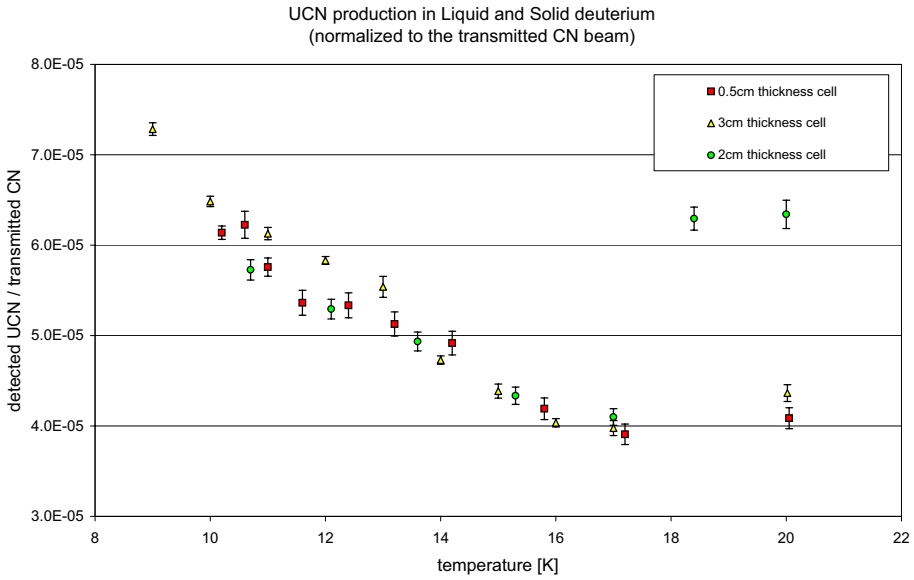

Figure 3.27: Normalized UCN in the different cells

D_2 turned out to be very small (less than 1cm). Therefore, in order to compare the measurements with theoretical predictions, the "film UCN model" (especially with the thinner cell 0.5cm), seems the most adequate. The model was upgraded introducing the influence of the attenuation of the incoming could beam, as well as the various efficiencies associated with the detection-extraction chain of the UCN to the detector area. The general temperature dependent equation which allows direct estimation of the UCN count rate at the level of the detector is

$$Rate_{UCN} = A \int_0^{LD} \epsilon_{det} \cdot \epsilon_{ext} \cdot \epsilon_{geo} \cdot P \cdot [e^{-\lambda_{CN} x}][e^{\frac{-(LD-x)}{v_{UCN} \tau_{UCN}(T)}}]dx \tag{3.14}$$

Where P is the expected UCN production rate for a standard film-source (sec.2.4.3), $A = 9cm^2$ is the extraction area and v_{UCN} is the mean UCN velocity at the level of the extraction window. The measured detector efficiency is $\epsilon_{det} = 0.6$ (ILL UCN source in Grenoble, France). According with previous tests [53], the extraction contribution of the long stainless steel section was estimated as $\epsilon_{ext} = 0.8$. A solid angle contribution associated with the geometry of the UCN extraction foil was also considered ($\epsilon_{geo} = 0.56$).

The first exponential factor in the equation 3.14 takes into account the attenuation of the incoming cold beam due to the presence of the deuterium ($\lambda_{CN} = 0.17cm^{-1}$, Fig.3.22). The second exponential factor is related with the escaping ability of the UCN inside the deuterium block and is linked with the UCN life-time parameter τ_{UCN} defined as

$$\tau_{UCN} = \frac{1}{\sigma_{tot}(T) N v_{UCN}} \tag{3.15}$$

Where $N = 3 \cdot 10^{22} cm^{-3}$ is the solid deuterium density and $\sigma_{tot}(T)$ is the total "loss" cross section defined in the equation 3.5 and extracted from the measurements as

$$\sigma_{tot}(T)\ [barn] = 5.53 e^{0.206T} \tag{3.16}$$

In figure 3.28 we present the outcome for LD=0.5cm. The relatively big errors associated with the fit of the extracted function (which enters in the equation 3.14) are also included. It is important to note that, beside the absolute numbers of the UCN count rate (effi-

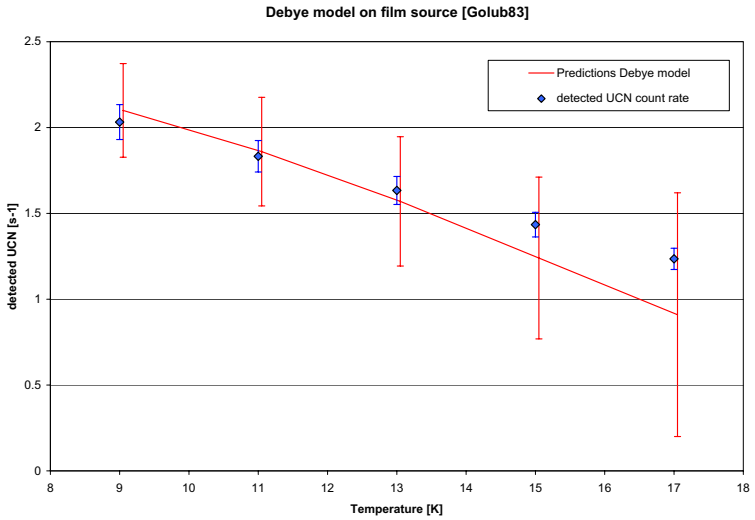

Figure 3.28: Comparison between the measurements and the "film-source" model

ciencies not exactly known), the "film-model" predicts the same small temperature gain factor as measured.

3.14 Summary and outlook of the Cube-D_2 experiment

In this section, a synthesis of the results of the Cube-D_2 experiment is presented. For the first time UCN produced in solid deuterium were detected at the FRM-II rector in Munich. A maximum UCN count rate close to $5s^{-1}$ was measured. The gain factor between the deuterium liquid phase and the solid at the coldest temperature obtained (8K) was unexpectedly small (G$\leq$ 2) but compatible with results obtained in similar recent experiments [51].

A real UCN storage experiment was performed. The storage bottle was a long electropolished stainless steel tube ($\sim 200cm$). The UCN valves used for this purpose were made of the same material. The extracted lifetime for the bottle is $\tau_{stor} \sim 40s$. The estimated wall loss probability per bounce is $\mu_{wall} \sim 2.8 \cdot 10^{-4}$.

The influence of irradiation on the ortho-deuterium concentration was also investigated. No significative changes were found before and after the irradiation of the sample (high "ortho" solid deuterium, $C_{ortho} \simeq 97\%$).

Experiments with similar freezing chamber having different thickness (3cm, 2cm, 1cm, 0.5cm) in the direction of the incoming beam were performed. After a systematic comparison of the results, different indications were found that the UCN "active" layer, with the freezing procedure performed in the Cube-D_2 (and same geometry) is small (less than 1cm) compared to the theoretical value. Indeed the best model that could explain the measured data is based on UCN production in film source. Different scenarios are expected in experiment [49] performing deuterium freezing at very low temperature ($T < 6K$).

By comparing measurements performed with different ortho-deuterium concentrations, an additional temperature dependent UCN "loss" cross section was extracted (σ_X). The absolute value of this quantity is high (at 9K, $\sigma_X \simeq 30barn$). This new information could reduce the UCN density expectation in experiments having similar geometry by an order of magnitude.

During the whole experiment a remarkable synergy between the Cube-D_2 at the FRM-II and a "Test" experiment at the TRIGA reactor in Mainz running in parallel, was realized. This experiment is the subject of another work in the framework of the Mini-D_2 project [52]. The feedback of available new information sometimes involved a rearrangement of the scheduled scientific program of both experiments (for example the deuterium

freezing procedure). In this way, basic ideas associated with the Mini-D_2 project were successfully tested (converter, extraction system, detection chain, para-to-ortho unit, etc..).

The Cube-D_2 experiment was initially projected to acquire experiences in freezing procedures in material suitable for UCN production (D_2, CD_4, etc). Then, the scientific program was extended in order to produce UCN at the FRM-II and to test components of the Mini-D_2. Although this was accomplished, during the experiment new open questions (mainly related with the crystal quality of the solid deuterium converter) rose up. Indeed, a better understanding of the freezing process (especially at very low temperature) seems essential. For this reason the Cube-D_2 facility is planned to be up-graded in the near future (higher cooling power, stereo-camera system, neutron scattering investigation of the crystal, etc..). In this way it will be possible to complete a systematic characterization of the solid deuterium converter for an optimum UCN production in the Mini-D_2 source.

Last but not least, the Cube-D_2 operated for more than one reactor cycle ($\sim 70 days$) continuously and safely at the FRM-II. As standard procedure, at the end of the experiment a global radioactive checks of all the Cube-D_2 components was performed. No activation (including tritium in the deuterium) was found. Therefore the set-up was removed from the reactor experimental hall.

Chapter 4

Extraction of UCN from the production zone to the experiments

4.1 Introduction

In this chapter are presented results of a series of experiments performed at the ILL UCN source in Grenoble. The measurements mainly refer to studies of ultra-cold neutrons guides. For this specific issue, a method for evaluation of the guide properties has been developed and tested. An extensive description of the method could also be found in a recent paper [13].

In the first part we introduce the technique applied, the associated theoretical background and the general results. The last part of the chapter we present specific results obtained in UCN guides made of different materials (or different coatings). In this set of measurements, the temperature dependence behavior was also investigated [53].

4.2 Motivation and scientific program

Efficient guiding of ultra-cold neutrons (UCN) from their source to the experimental set-up is crucial to all experiments using UCN. The transport of UCN through any guide depends mainly on two of its physical properties: the loss probability per wall collision (μ) and the probability for diffuse scattering from the wall (f).

Normally, when no particular constrains associated with high radioactivation are present, stainless steel is an excellent candidate for UCN guides. Indeed, stainless steel tubes are commercially available and rather easily adaptable to the experimental requirements. Furthermore, such tubes have good transport properties for UCN when their inner surface is of fine quality, i.e. the diffuse scattering probability f is small. Nowadays, high performances could be easily achieved by standard treatments (mechanically or electro-polished).

A direct way to improve the efficiency of a typical UCN source (and therefore the UCN density available for the experiment) is, of course, to locate the UCN production section of the facility in a high intense neutron flux environment (closer to the reactor core). To accomplish this goal it is unavoidable to introduce additional restrictions on the usable materials. For example, due to the high and long "post-irradiation" activation, stainless steel tube could not be used. Therefore, at least in the first "extraction" section of a UCN source designed like the Mini-D_2, different structural materials have to be considered (zircalloy, aluminium alloy, etc..). An improvement could be achieved by coating the inner surfaces of the first guiding section with low neutron absorbing materials as beryllium, nickel, diamond-like carbon (DLC) or stainless steel.

An optimized UCN extraction system should be composed by two distinct sections. The first part, which also partially store the UCN produced, should be made of aluminium (or zircalloy) coated with a low absorber material having high Fermi pseudo-potential. Then, the extraction-distribution of the UCN to the experiments, which are generally located away from the reactor core, could be achieved by assembling stainless steel tubes. We present results on a 3.4 meter aluminum tube coated with a double layer of stainless

steel (500 nm) and beryllium (250 nm) and results on electro-polished stainless steel tube (provided by Nocado company). Both options are proposed for the UCN guide system for the Mini-D_2 UCN source at the FRM-II reactor in Munich.

In order to investigate different coating possibilities, a dedicated and unique sputtering facility has been developed. This apparatus permits the inside coating of tubes of up to 9 meter length and 5-10 cm diameter. Not only single layers of beryllium or stainless steel can be produced but also double and multi-layers of these materials are feasible. By means of this facility various tubes made of aluminum or stainless steel for comparison and with different surface roughness will be inside coated with beryllium or stainless steel or beryllium on stainless steel. A correct comparison of specially coated tubes each other should involve an estimation of the both essential parameters: the loss probability μ and the probability of diffuse scattering from the wall f which is especially important for the long and non-polished aluminum tubes. Obtaining f is a challenge of this work as, unlike wall losses, it cannot be measured in storage experiments. The next section will be dedicated to illustrate the method developed to estimate those parameters.

4.3 Description of the method applied to evaluate the UCN guides properties

In this section we present our first attempt to extend the so-called "Two Holes" technique or "Constant Flow" method [55] for the evaluation of transmission of the UCN through the tubes. The set-up was built up at the so-called "Test" beam position of the PF2 UCN facility in ILL. At this level a relative intense and constant UCN flux is available. The data acquisition system (DAQ) includes commercial "He-3" detectors, standard electronics and computer. The specific features of the DAQ will be described in a specific chapter.

4.3.1 General aspects and set-up

The "Two holes" technique is commonly used for measuring the effective "black" (absorbing UCN) area of the sample, which is contained between two diaphragms **A** and **B** with small and well-known openings as it is shown at figure 4.1.

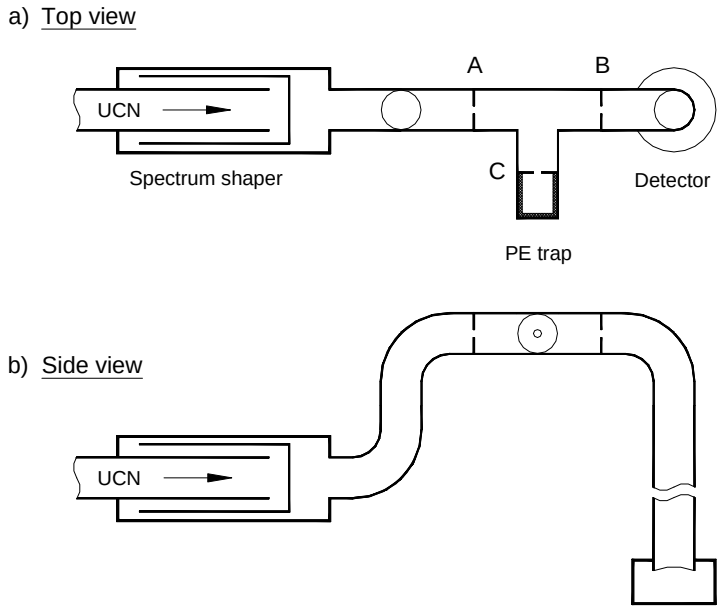

Figure 4.1: The principal scheme of the common "Two Holes" method

We used spectrum shaper made from stainless steel and stainless steel guiding tubes so that to cut off the energy spectrum of the UCN above the stainless steel wall fermi-potential. A sample under investigation is attached at position **C**. It was placed 24 cm higher than the spectrum shaper in order to guarantee an absence of the overbarrier neutrons filling the sample. Thus, the energy range is limited to 165 neV. In figure 4.1 the sample is replaced with the equivalent "black hole" formed by the diaphragm **C** followed by a polyethylene cavity (PE trap). If J_0 denotes the neutron flux through diaphragm **A** into the volume and J is the flux counted by the detector, then the following flux balance

equation takes place.

$$J_0 = \frac{J}{a}(2a + b_0 + b) \tag{4.1}$$

Here a is a cross section of the opening of the diaphragm **A** and **B**, b is an effective black area of the attached sample and b_0 is the blackness of the tee joint.

The experimental procedure includes several steps depicted as configurations a), b), c) and d) in the figure 4.2. At first the value J_0 is measured. For this (a) the tee joint h

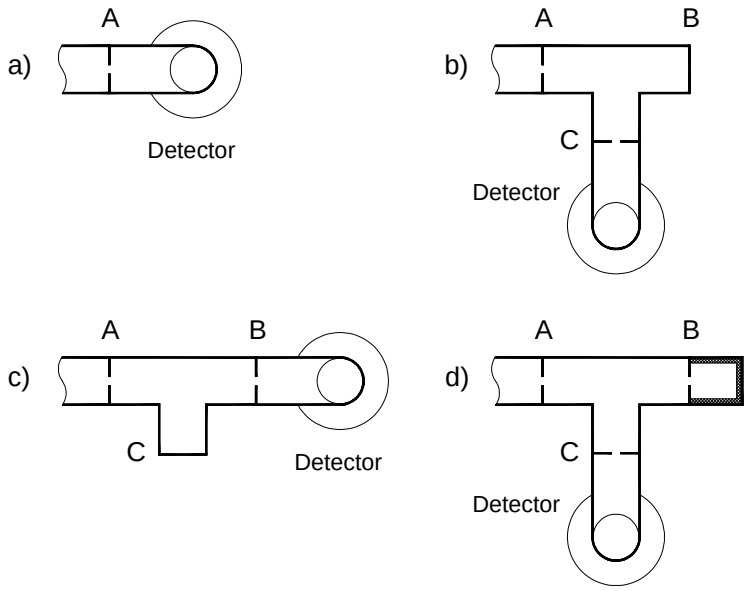

Figure 4.2: Experimental procedure and calibration

is removed and detector is moved from position **B** to position **A**. Then J is measured in configuration (b) or (c). We have observed to a high degree equivalent each other results for these configurations that proves an assumption about an isotropic angular distribution of the neutron flux inside the tee joint. With this measurement the value b_0 can be obtained from equation 4.1 since $b = 0$ in this configuration. Measurement of J with the sample attached to the position **B** (d) gives the value of interest b. Finally, a replacement of the sample with the equivalent opening of the diaphragm **B** has to be performed to verify the result or calibrate the measurements.

Indeed, there are at least two reasons for calibration. The first one is a possible presence of the over-barrier neutrons in the incoming neutron spectrum. They are increasing the measured value of J_0 making no contribution to J since their life time in the tee joint is much less than the life time of the underbarier ones. The second reason is an anisotropic angular distribution of the incoming flux that results to a higher detector counting rate compared with the isotropic angular distribution at the same density of UCN. In both cases the value of J_0 can be corrected by a coefficient k as $J_{0(\text{uncorrected})} = kJ_0$. For this an additional measurement with the PE trap has to be performed. If opening of the PE trap is taken equal to the opening of other diaphragms, then the following flux balance conditions are valid for the configurations (b) and (d), figure 4.2.

$$\frac{J_{0(\text{uncorrected})}}{k} = \frac{J_{(\text{b})}}{a}(2a + b_0) \tag{4.2}$$

$$\frac{J_{0(\text{uncorrected})}}{k} = \frac{J_{(\text{d})}}{a}(3a + b_0) \tag{4.3}$$

Hence k and b_0 is easy obtained.

The cross section of the diaphragm opening a has to be relatively small. Typically in the order or less of the measured blackness depending on the available beam intensity and the background conditions. In our measurements we used diaphragms with the round hole of 12 mm diameter (a=1.13 cm^2). The correction coefficient was found to be k=1.12. The measured blackness was of the order of several square centimeters.

4.3.2 Theoretical background and application of the method to long tubes

The "Two Holes" method can be applied to the long tube sample as it is shown at the figure 4.3 (a) and (b). The difference from the technique described above is that the concept of effective blackness exploited by the method cannot be directly interpreted in this case since the UCN density changes along the tube. In case (a) the flux balance eq.

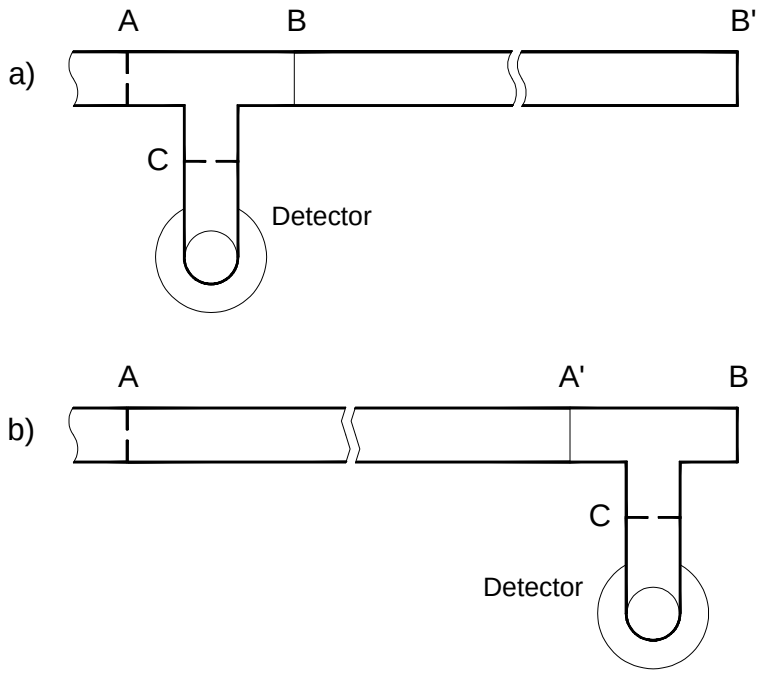

Figure 4.3: Long tube transmission measurement

(4.1) remains correct if the effective blackness b is related to the inlet of the tube at the position **B**. In case (b) the eq. (4.1) has to be modified taking into account the UCN density variation from the beginning to the end of the tube. That requires modelling of the UCN flow in the tube.

A UCN transport through tubes is well understood theoretically [8, 6]. As was already mentioned, the transmission of UCN is under the influence of two factors of different nature: the loss probability per wall collision μ and the probability of diffuse scattering from the wall f. When f is relatively large one can assume an isotropic angular distribution everywhere in the tube and consider UCN in the tube as an ideal gas. This approach is well described by a one-dimensional diffusion equation. If specular reflections are dominating, then an anisotropy is naturally developing as neutrons transported along the tube.

Whichever theoretical approach is performed it includes μ and f as two unknown parameters to be fit to the measurements. Therefore both experiments in the configuration (a) and in the configuration (b) should be done in order to resolve these two parameters. We have tested this idea with the 3.4 meter aluminum tube coated with a double layer of stainless steel (500 nm) and beryllium (250 nm) proposed as a prototype of UCN guide for the Mini-D_2 UCN source at the FRM-II reactor in Munich.

4.3.3 Constant flow approach and concept of "blackness"

As already mentioned, a one way net constant flow of UCN through the tube could be considered. At this condition a distribution of the UCN density along a tube $\rho(x)$ is described by one-dimensional stationary diffusion equation

$$D\frac{d^2\rho}{dx^2} - \frac{\rho}{\tau} = 0, \tag{4.4}$$

with diffusion coefficient D and life time of UCN in the tube τ. The combination $L = \sqrt{\tau D}$ represents the diffusion length. Further we will use an inverse of diffusion length $\gamma = L^{-1}$. For the tube of diameter R and length X the boundary conditions at the inlet ($x = 0$) and at the outlet ($x = X$) of the tube are defined by the incoming $J_{\rm in}$ and outcoming $J_{\rm out}$ net flux as

$$\frac{J_{\rm in}}{\pi R^2} = -D\left[\frac{d\rho}{dx}\right]_{x=0} \tag{4.5}$$

$$\frac{J_{\rm out}}{\pi R^2} = -D\left[\frac{d\rho}{dx}\right]_{x=X} \tag{4.6}$$

The solution with the given boundary conditions is

$$\rho\,(x) = -J_{in}\frac{1}{\pi R^2 D\gamma}\sinh\gamma x + J_{in}\frac{1}{\pi R^2 D\gamma}\frac{\cosh\gamma X - \beta}{\sinh\gamma X}\cosh\gamma x, \tag{4.7}$$

where $\beta = J_{\rm out}/J_{\rm in}$.

Though the UCN energy spectrum can be rather wide, UCN density, as well as UCN loss coefficient, depends on energy very strongly, we suggest a use of the mono-energetic

approach as sufficient for a rough estimation of specific for the given spectrum average values. Indeed, due to the stainless steel spectrum shaper and due to the gravitational step, this hypothesis is realistic.

In assumption of a full isotropy of angular distribution an aperture flux density is given as $(1/4)v\rho$ for neutrons with velocity v. A concept of effective blackness allows to connect the net flux $J_{\rm in}$ and $J_{\rm out}$ with corresponding aperture fluxes as

$$\frac{1}{4}v\rho(0) = \frac{J_{\rm in}}{b_{\rm in}} = J_{\rm in}\frac{v}{4\pi R^2 D\gamma}\frac{\cosh\gamma X-\beta}{\sinh\gamma X} \tag{4.8}$$

$$\frac{1}{4}v\rho(X) = \frac{J_{\rm out}}{b_{\rm out}} = J_{\rm in}\frac{v}{4\pi R^2 D\gamma}\frac{1-\beta\cosh\gamma X}{\sinh\gamma X} \tag{4.9}$$

Since a mean path between two successive wall collision is equal to the tube diameter we have

$$\mu = \frac{2R}{v\tau} \tag{4.10}$$

Using this expression the formulas (4.8, 4.9) can be transformed as

$$\mu = b_{\rm in}\frac{\gamma}{2\pi R}\frac{\cosh\gamma X-\beta}{\sinh\gamma X} \tag{4.11}$$

$$\mu = b_{\rm out}\frac{\gamma}{2\pi R}\frac{1-\beta\cosh\gamma X}{\beta\sinh\gamma X} \tag{4.12}$$

Equating the right hand parts of (4.11) and (4.12) results in a quadratic equation

$$\beta\frac{b_{\rm in}}{b_{\rm out}} = \frac{1-\beta\cosh\gamma X}{\cosh\gamma X-\beta}, \tag{4.13}$$

from which β is determined as function of γ with parameters $b_{\rm in}$ and $b_{\rm out}$. We have to pick out one of two possible solutions. One is trivial. It amounts $\beta = 1$ if $\gamma = 0$, that corresponds to an ideal tube without absorbtion and diffusion. The another gives a right physical result $\beta = b_{\rm out}/b_{\rm in}$ when $\gamma = 0$. The solution is

$$\beta = \cosh\gamma X + \frac{b_{\rm out}}{2b_{\rm in}}\cosh\gamma X - \frac{\sqrt{b_{\rm in}^2\cosh^2\gamma X + 2b_{\rm in}b_{\rm out}\cosh^2\gamma X + b_{\rm out}^2\cosh^2\gamma X - 4b_{\rm in}b_{\rm out}}}{2b_{\rm in}} \tag{4.14}$$

Thus, formulas (4.8, 4.9) define μ as function of γ with parameters b_{in} and b_{out}, which have to be delivered by the experiment. The independent measurements at both ends of the tube depicted as (a) and (b) in figure 4.3 have to be performed to resolve μ and γ. Then the diffusion coefficient is calculated as $D = \mu v/(2R\gamma^2)$. The probability of diffuse reflection can be found as

$$f = \frac{2D_0}{D_0 + D}, \tag{4.15}$$

where $D_0 = (2/3)Rv$ is an ideal (all reflections are diffusive) diffusion coefficient. Specific applications of the considered approach to the experiment is described in the next section.

4.3.4 Detector before tube inlet

Analysis of the measurements in the configuration (a) of figure 4.3 is straightforward. From equation 4.1 b_{in}, denoted there as b, is plainly calculated. The incoming flux J_0 has to be corrected, the correction coefficient and b_0 measured in advance as it was described in the previous section. Since the end of tube (position $\mathbf{B}'$) is closed with the reflecting wall, $b_{\text{out}} = 0$ and $\beta = 0$. We made an additional measurement with PE trap attached to the tube end. In this case $b_{\text{out}} = a$ and β is defined by formula (4.14). Expression (4.11) represents the value of interest μ as function of γ in both cases.

4.3.5 Detector behind tube end

This configuration is shown at figure 4.3 (b). Losses in the tee joint determine b_{out} as $b_{\text{out}} = a + b_0$. For the aperture flux density in the tee joint we have

$$\frac{1}{4}v\rho(X) = \frac{J_{\text{out}}}{b_{\text{out}}} = \frac{J}{a} = J_{\text{in}}\frac{v}{4\pi R^2 D\gamma}\frac{1 - \beta\cosh\gamma X}{\sinh\gamma X} \tag{4.16}$$

that defines J_{out} as J is measured. An aperture flux density at the beginning of tube is given by $J_{\text{in}}/b_{\text{in}}$. A flux balance condition can be written as

$$J_0 = J_{\text{in}} + a\frac{J_{\text{in}}}{b_{\text{in}}} \tag{4.17}$$

and therefore the aperture flux density

$$\frac{1}{4}v\rho(0) = \frac{J_{\rm in}}{b_{\rm in}} = \frac{J_0 - J_{\rm in}}{a} = J_{\rm in}\frac{v}{4\pi R^2 D\gamma}\frac{\cosh\gamma X - \beta}{\sinh\gamma X} \tag{4.18}$$

Using expressions (4.16, 4.18) we obtain a quadratic equation for β which does not contain unknown $b_{\rm in}$ and $J_{\rm in}$ as

$$\frac{J_0}{J} - \frac{b_{\rm out}}{a\beta} = \frac{\cosh\gamma X - \beta}{1 - \beta\cosh\gamma X} \tag{4.19}$$

As in case of eq. (4.13), one possible solution of eq. (4.19) leads to $\beta = 1$ when $\gamma = 0$, that corresponds to an ideal tube without absorbtion and diffusion. We have to choose another one, which we do not present here just because it is rather long expression. Formula (4.12), which contains defined above β, expresses μ as function of γ.

One more measurement has been done in this configuration and with PE trap attached to the tee joint at the position **B**. This case differs from the considered basic one by the value $b_{\rm out} = 2a + b_0$ only.

4.3.6 Experimental results on the 3.4m tube

The specific results of the analysis applied on the 3.4m aluminium Be-coated sample are shown in figure 4.4 as μ–γ plot. For every one of four measurements the hatched area represents a region of possible values of μ and γ with 90% confidence which was defined according to eq. (4.11) or (4.12). The area of overlap delivers the following results

$$\mu = (1.10 \pm 0.10) \cdot 10^{-3}$$

$$\gamma = 0.310 \pm 0.033$$

$$f = 0.180 \pm 0.037$$

The errors include statistical uncertainties obtained in 1000 second integration time for every measurement and systematical error of calibration. The UCN detector used was the same for each measurement step. Therefore, in the comparing of the data, the absolute efficiency plays no rule.

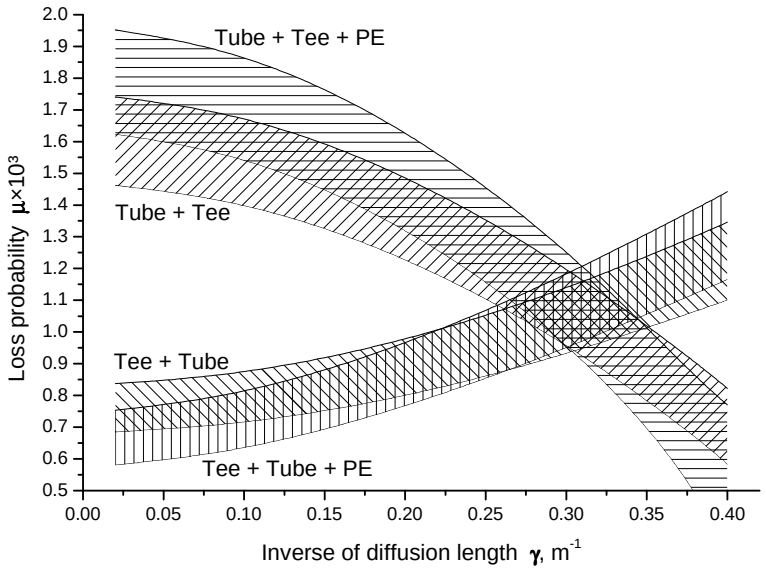

Figure 4.4: Experimental results

The measured value of wall losses corresponds well to what was observed in [55] for untempered beryllium foil and also in [56] for beryllium coated tubes tested before the glow discharge cleaning procedure was applied. The probability of diffuse reflection shows a reasonable value for that rough aluminum tube.

4.4 Further improvement of the method

In the previous section, we have shown the experimental technique and the analysis that can be used for evaluating transmission properties of neutron guides for UCN. The results prove the feasibility of the method that delivers the loss probability per wall collision (μ) and, that is mostly wanted and significant for our goals, the probability for diffuse scattering from the wall (f).

For more precise evaluation of the UCN guides properties we improved the previous

apparatus (fig.4.1). A simple sketch is presented in figure (4.5). The set-up offers si-

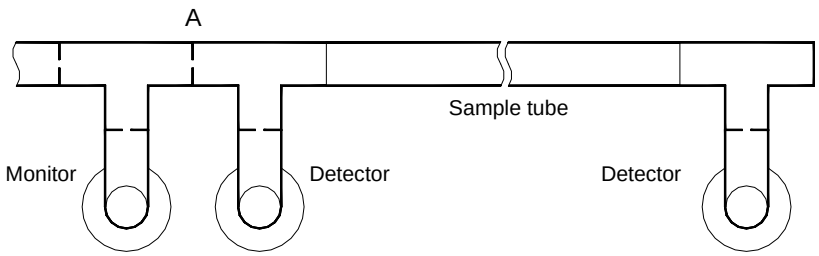

Figure 4.5: Configuration for precise transmission measurement

multaneous measurements before and behind the sample tube. It includes an additional tee joint placed right before the entrance diaphragm **A**. Though the tee reduces available UCN intensity, it creates a well isotropic angular distribution of the incoming through the diaphragm **A** flux and allows an additional detector to be used as a monitor of J_0. All the detectors are of the same kind (He-3). Moreover in this up-dated version is included the possibility to variate the temperature of the sample tube. For this issue we implemented a nitrogen cryostat which surround the sample and allows to cool the sample by radiation, reaching temperature down to $180K$. In the picture 4.6 is presented one side view of the facility. In the left photo, the shaper, the gravitational step and the tees joint are evident. The right photo emphasize the nitrogen cryostat vessel ($\sim 2.5m$). A sensor mounted on the sample tube (PT-100 Lakeshore^{TM}) monitor continuously the temperature.

4.4.1 Results at room temperature

Two samples ($L = 2m$) where tested. An electro-polished stainless steel tube and an aluminium tube of the same size but coated respectively with beryllium ($250nm$) on stainless steel ($500nm$). Respect to the method explained in the previous section the analysis is simplified. Indeed, the simultaneous presence of three detectors ($det1$, $det2$, $det3$) allows to resolve $\beta = f(b_{in}, b_{out})$ (4.14) in the same acquiring procedure. On the other hand,

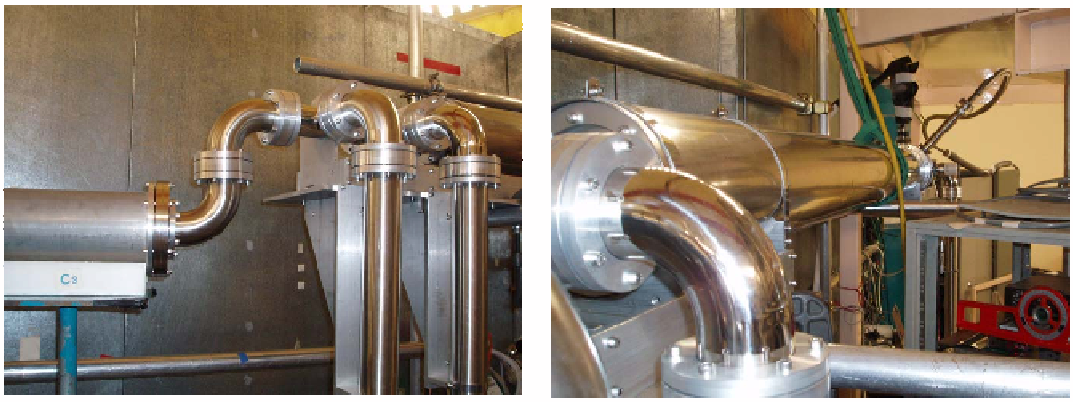

Figure 4.6: Set-up at the ILL

in order to properly apply the method, additional cross-checks had to be performed to quantify the relative efficiency of the detectors used ($\epsilon_{det1}, \epsilon_{det2}, \epsilon_{det3}$). A "detector-unit" is mainly composed by the detector itself and by a $1m$ long "UCN acceleration stage" made of stainless steel. Those components, which evidently are not exactly the same for each detector, could theoretically reduce the detection efficiency. Also this contribution was resolved and turned out to be very small (less than 2%). After this cross check, a specific detector was associated with a specific guide. A global efficiency parameter was extracted replacing each detector at a fix location with the other ones (permutation). Two auxiliary transitory connections (stainless steel) were used to match the length size of the sample tube (2m) and the cryostat vessel ($\sim 2.5m$). The associated small contributions ($\sim 2cm^2$) to the total "blackness" was also included in the analysis.

The extracted value of the wall loss probability per bounce at "room" temperature ($300K$) for the 2m beryllium coated aluminium sample tube was $\mu_{Be} = (7.3 \pm 1.5) \cdot 10^{-4}$. The associated probability of diffuse scattering was $f_{Be} = 0.27 \pm 0.04$. The results on the 2m long sample are very similar to the previous measurements performed with the 3.4m tube. The slight differences might be caused by a better pre-cleaning of the surface before the coating or by a better UCN isotropy due to the additional tee joint.

For the 2m electro-polished stainless steel tube provided by Nocado^{TM} the performances were surprising relative good. The wall loss probability found was only $\mu_{SS} = (1.6 \pm 0.3) \cdot 10^{-4}$, the diffuse scattering coefficient extracted was $f_{SS} = 0.07 \pm 0.01$. The pure transmission coefficient measured was $\tau_{SS} = 0.96m^{-1}$.

4.4.2 Temperature dependence of the parameters

According with theoretical prediction, the up-scattering cross section (UCN losses) of typical guides materials could be reduce by reducing the walls temperature [6, 57]. Therefore, in order to improve the performances, specific cryostat are usually integrated in the UCN guide system. As already mentioned, a set of measurements at different temperatures were performed to explore this phenomena.

The same samples presented in the previous section (beryllium coating on stainless steel) were cooled from "room" temperature down to $180K$. The nitrogen cryostat was optimized for a rapid exchange of the samples. Indeed, in this case reduced surfaces contact (less friction) between the cryostat and the tested tube is preferable. Therefore, the cooling technique adopted was based on the radiation effect. As consequence, also the cleanness of the external surface of the samples was preserved. A synthesis of the results are presented in figures 4.7 and 4.8. It's possible to note that the value of the wall loss probability per bounce is not appreciably reduced over the range of the temperature

investigated (especially for the beryllium coated sample). A realistic explanation for this unexpected behavior could be found in the fact that during the measurements the vacuum conditions were not excellent ($1.5 \cdot 10^{-5} mbar$ at 300K, $6 \cdot 10^{-6} mbar$ at 180K). Indeed is well known that the presence of high absorber elements (H_2, O_2, N_2, etc..) allocated on the inner surface of the guide could compensate the gains in the performances due to the reduction of the up-scattering. For example in the stainless steel tube this seems to happen at around 240K (Fig.4.7). Moreover, the coldest temperature reached with this set-up was "only" 180K. As expected, the diffuse scattering coefficient stays almost constant over the full temperature range. Indeed this is a property related with the roughness of each specific neutron guide.

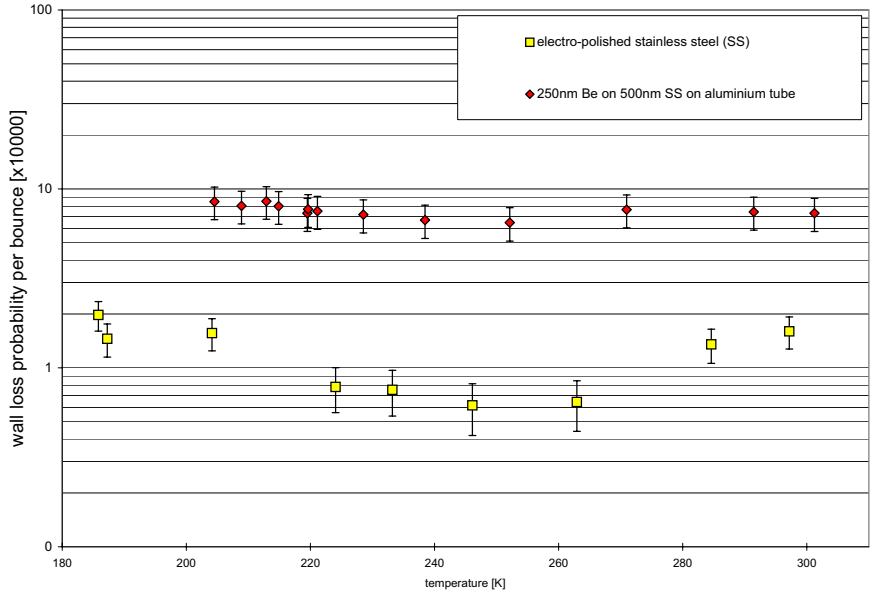

Figure 4.7: Temperature dependence of the wall loss probability

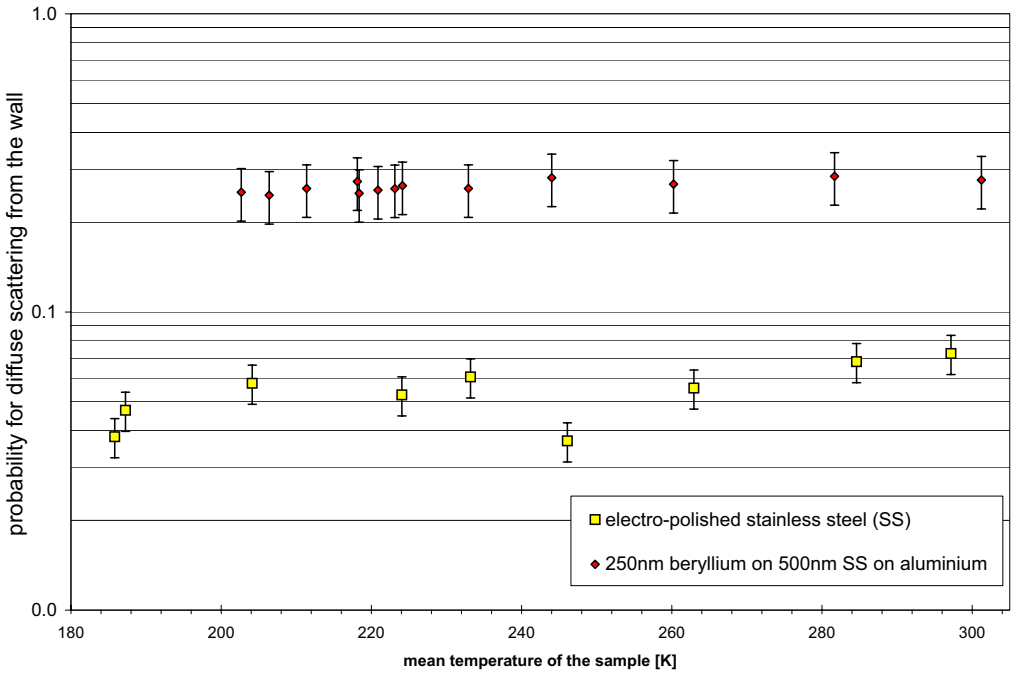

Figure 4.8: Temperature dependence of the diffuse scattering

4.5 Conclusions and outlook

A method for evaluating the properties of UCN guides has been developed and tested at the ILL UCN source in Grenoble. This new technique was applied on measurements performed with several samples (Al, SS) with different coating layers (Be and SS) or different size (1m, 2m, 3.4m). The results obtained at room temperature for the beryllium coated aluminium sample are compatible with the data found in the literature in experiments performed in the same conditions (for instance before glow discharge cleaning). For the 2m electro-polished stainless steel tubes provided by Nocado^{TM}, the results

showed very good performances (either μ, either f). This suggested to use the same guide in another UCN test experiment at the FRM-II reactor in Munich (see Cube-D_2 chapter).

Unfortunately, with the nitrogen cryostat was not possible to fully investigate the temperature dependance of the UCN up-scattering cross section (bad vacuum and relative high temperature).

A further improvement could be done integrating the cryostat with another pump-stage and with a better cooling system (cold-head or helium).

Chapter 5

Influence of the Para-Ortho deuterium on the UCN production

5.1 Para-Ortho deuterium species in the UCN context

The Mini-D_2 facility is a powerful source of ultra cold neutrons (UCN) at the FRM-II reactor in Munich [2]. One way to produce UCN is to shift down in energy the maximum of the Maxwellian spectra of an available neutron source (cold neutrons, En$\sim 4meV$). This can be realized by using a "converter material" that is able to produce down-scattering of the incoming higher-energy neutrons. Unfortunately, down-scattering (creation of UCN), is not the only probable process involved. Is also possible to have up-scattering or absorption in the converter (in both cases losing of UCN). A good converter material should minimize these negative phenomena. The converter selected for the Mini-D_2 source is solid deuterium (relative low absorption cross section).

Natural deuterium is a mixture of two possible compounds, the so-called ortho-D_2 and para-D_2, having different nuclear spin and orbital angular momentum states. This makes influence in the UCN production because after a neutron collision in para-D_2 (S=1; J=1) a

de-excitation to the ortho-D_2 ground state can occur (S=0,2; J=0). Due to the transition energy, the effect is a $7meV$ transfer as kinetic energy to the neutron, which consequently loose the UCN properties. An ideal deuterium converter should have only ortho-D_2 states. At standard conditions the ortho-D_2 fraction is relative low ($C_{ortho}/C_{para} = 2$, at $293K$).

There are several techniques to improve the standard ortho-deuterium concentration. A direct way is to store the deuterium at low temperature (liquid phase). Indeed, a specific ortho-deuterium concentration is related with the thermodynamical equilibrium of the available states at a specific temperature. In deuterium a reduction of the temperature involves an enhancement of the ortho-deuterium populations. Of course, the process is regulated by the time constant needed to approach the equilibrium. Unfortunately, in case of deuterium this "natural" conversion constant is in the order of the months [58, 59].

The approach to thermodynamical equilibrium (at a specific temperature) could be accelerate by using ferromagnetic catalyst like oxisorb^{TM} [42]. An optimization of the conversion phenomena could be performed storing deuterium at low temperature ($\sim 20K$) in contact with a catalyst. In this case, ortho-deuterium concentration closer to $C_{ortho} \simeq 1$ could be reached in relative short time (few hours). For the Mini-D_2 project a special "converter unit" based on this concept was designed, assembled and tested. The testing phase was performed in the framework of the Cube-D_2 experiment. Details on features and functionality of this important unit will be presented in that specific chapter.

Whatever technique is applied, for an optimization of the UCN production is important to evaluate with relative high accuracy the ortho-D_2 concentration in the deuterium used. In the next sections is presented an introduction on the method applied (Raman scattering effect) to measured the ortho-D_2 content and results obtained on deuterium gas samples.

5.2 General aspects on Raman spectroscopy

When electromagnetic radiation is scattered by a molecule or by a crystal, one photon ($h\nu_0$) annihilates and simultaneously one photon is created. The scattering mechanisms can be classified on the basis of the energies difference (or frequencies) of the incident photon and scattered ones. If the scattered photon has the same frequency as the incident radiation ($h\nu_0$) the process is called Rayleigh scattering. If the energy of the incident photon is different ($h\nu_i$) the process is called Raman scattering. Plotting the scattered photons intensity as function of the frequency shifts, one can identify a typical spectrum characteristic for each molecule or compound. In fact, it is possible to distinguish a series of well definite peaks (lines). A very intense line (Rayleigh scattering, ($h\nu_0$)) and several lines symmetrically distributed around (Raman scattering, ($h\nu_i$)). The lines with frequencies less than the exciting lines are called Stokes, the others anti-Stokes. The technique that uses as a discriminator the Raman shift effect is called Raman spectroscopy.

Raman effect is connected with polarization (α) property of the matter. A strength applied electric field (ξ), produces a proportional distortion of the molecule. The result is a dipole moment ($\mu = \alpha\xi$) that has to be added to the dipole moment possibly already present. If a diatomic molecule is rotating at frequency ω_0, its polarisability oscillates, because of symmetry, with frequency $2\omega_1$. Therefore

$$\mu = \alpha\xi = [\alpha_0 + \beta \sin(4\pi\omega_1 t)] \cdot \xi_0 \sin(2\pi\omega_1 t) \tag{5.1}$$

Where β is connected with the anisotropy polarisability of the molecule. As consequence the dipole moment oscillates with frequencies components

$$\omega_0, \quad \omega_0 - 2\omega_1, \quad \omega_0 + 2\omega_1 \tag{5.2}$$

These three terms are the parameters of the scattered radiation and are specific for each substance present in nature. One can note that if β=0 then the dipole oscillates only with frequency ω_0. Hence in order to have Raman effect the molecule must have an anisotropy

polarization. Raman shift doesn't depend of the frequency of the incident radiation. This allows comparing measurements on the same sample obtained with different laser source.

5.3 Application to resolve the ortho-deuterium content

Inelastic photon scattering on molecules can involve transitions between rotational and vibrational states. In deuterium, the energy magnitude to have rotational transitions (quantum number J) is in the "meV" scale. With the normal laser source, mostly excitation at the J-states level occurs. A general estimation of the rotational Raman shift [34] for a known vibrational state (ν) is

$$F_\nu(J) = B_\nu J(J+1) - D_\nu J^2(J+1)^2 + H_\nu J^3(J+1)^3 \tag{5.3}$$

Where B_ν, D_ν and H_ν are constant for each vibrational state. With photons as incident radiation, according to the selection rules, only ΔJ=$\pm$2 transitions are allowed (S-branch). The thermodynamical equilibrium distribution for even and odd rotational states are

$$\rho_{even} = \frac{g_I^e}{Z} \sum_{J=0,2,..} (2J+1)\exp(-E_J/\kappa T) \tag{5.4}$$

$$\rho_{odd} = \frac{g_I^o}{Z} \sum_{J=1,3,..} (2J+1)\exp(-E_J/\kappa T) \tag{5.5}$$

Where g_I are the nuclear weights (degeneracies), with

$$Z = g_I^e \sum_{J=even} + g_I^o \sum_{J=odd} \tag{5.6}$$

as normalization factor and E_J are the rotational energy that can be approximated by the first term in 5.3. In a deuterium sample (mixture of para-D_2 and ortho-D_2), knowing the distribution of the J-shifts, exists a well-defined ratio between the intensity for each Raman lines. For example, considering the first allowed transition in ortho-D_2 (S-branch 0$\rightarrow$2) and in para-D_2 (S-branch 1$\rightarrow$3), it is easy to derived a direct expression for the

ortho-D_2 concentration as

$$C_{even} = \frac{(S0 \rightarrow 2)/(S1 \rightarrow 3)}{(S0 \rightarrow 2)/(S1 \rightarrow 3) + \frac{5}{3}\tau[(\omega - \omega_{02})/(\omega - \omega_{13})]^3} \tag{5.7}$$

Where τ is an integral sum on the probability of the initial states (at $T = 293K$, $\tau_{deut} = 0.447$), ω is the frequency of the incident photon, ω_{02} and ω_{13} are the associated Raman shifts. Assuming the efficiency of the Raman spectroscope constant in the channels, $S0 \rightarrow 2$ and $S1 \rightarrow 3$ are proportional to the peaks intensity. Therefore one can replace S_{ij} simple with the integral area ("gaussian distribution" fit within 3σ C.L.) under the particular Raman peak in the general spectra.

The approach to the equilibrium concentration (for example ortho-D_2 at $18.7K$, $\rho_{eq} = 0.985$) could be expressed [34] by a first order differential equation as

$$\frac{dC_{ortho}}{dt} = -K\frac{(C_{ortho} - \rho_{eq})}{1 - \rho_{eq}} \tag{5.8}$$

Where C_{ortho} is the changing concentration of the even rotational species and K is the rate constant $[h^{-1}]$. As already mentioned, without presence of catalyst, typical values for the associated time constant are in the range $\tau_{liq.}$=3100hs.

5.4 Raman facility at Walther-Meissner Institute

The Raman facility utilized for the measurements is located at the Walther-Meissner Institute in Garching [14]. Figure 5.1 shows a scheme of the experimental setup. The deuterium sample is placed at the "gas chamber" level. The laser source is Krypton (18837 cm^{-1}) with an associated power of 40mW. In order to reduce "cosmic ray sparks" on the CCD camera pixels, data series relatively short (typically 30s) were acquired. The deuterium sample (gaseous form) was placed in an aluminium cell (box 4x4x4cm with quartz suprasil windows).

Two typical output spectra, already normalized in counting rate per second (bps), are displayed in figure 5.2 and 5.3 as examples. The first plot is the raman's outcome of normal gas deuterium at room temperature. The second spectra refers to a deuterium gas sample (relative pure and with a relative high ortho-concentration) taken from the so-called TRIGA test experiment located at the TRIGA reactor in Mainz which is another test device in the framework of the Mini-D_2 project [52].

Is possible to clearly distinguish the first 3 even (J_{D2}=0 at 179.1cm^{-1}, J_{D2}=2 at 414.6cm^{-1}, J_{D2}=4 at 642.4cm^{-1}) and the first 2 odd (J_{D2}=1 at 297.5cm^{-1}, J_{D2}=3 at 529.7cm^{-1}) rotational states of the deuterium. In the first spectra, additional peak referring to HD content are evident (J_{HD}=0 at 267.1cm^{-1}, J_{HD}=1 at 443.2cm^{-1} and J_{HD}=2 at 616.2cm^{-1}). As expected, the relative ratio between the even and the odd peaks changes according with the formula 5.7. It's remarkable to note that the raman's technique could also be used to recognize the presence in the deuterium of specific "high UCN absorbers" impurities like HD or H_2. In all the measurements, a very low and stable background is achieved. A so-called signal to noise ratio (SNR) better than 100 is generally obtained.

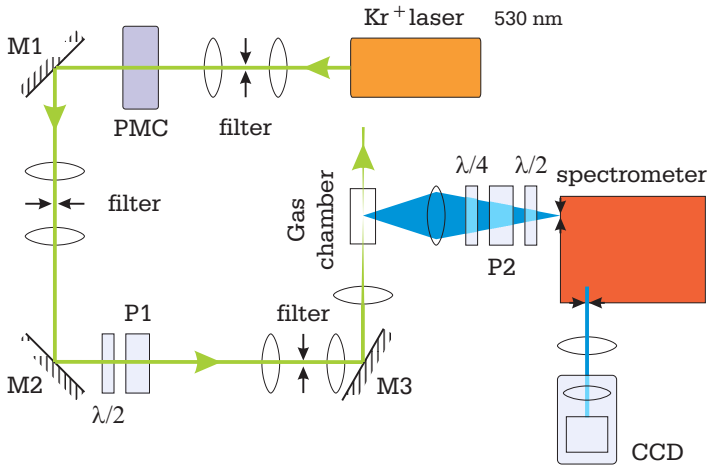

Figure 5.1: Raman set-up at Walther-Meissner Institute

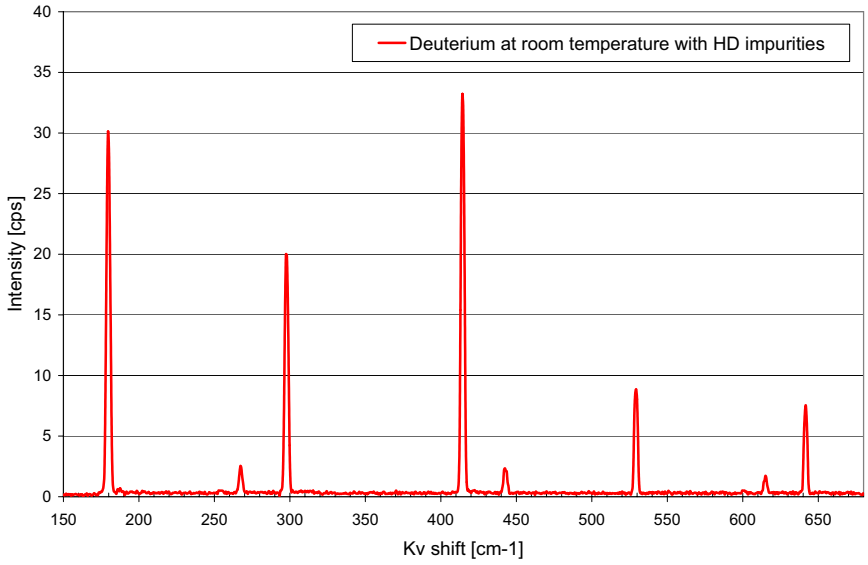

Figure 5.2: Raman spectra for normal deuterium at room temperature

5.5 Measurements on deuterium samples for the Cube-D_2 experiment

As is described in a specific chapter, several ideas (or components) associated with the Mini-D_2 project are tested in the Cube-D_2 experiment. The oxisorb^{TM} converter unit is one of those. By using the Raman spectroscopy technique we measured the associated performances.

5.5.1 Extrapolation of the para-to-ortho conversion rate

As already mentioned, the main goal of the converter unit is to produce high ortho-deuterium concentration in relatively short time. A set of measurements was performed

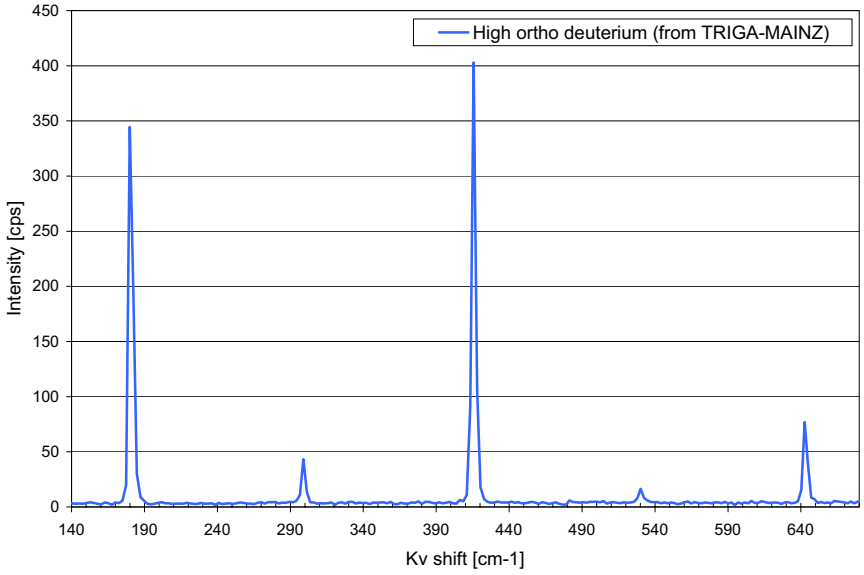

Figure 5.3: Raman spectra for a high ortho and relative "pure" deuterium

to evaluate the para-to-ortho conversion rate when oxisorb^{TM} is used. First a deuterium sample was extracted and measured. This probe ($\sim 300K$) was never in contact with the catalyst. As expected, the ortho-D_2 concentration evaluated according with the equation 5.7 was closer to the natural equilibrium ($C_{ortho} \simeq 0.66$). Then, the liquid deuterium ($\sim 20K$) was placed in contact with the catalyst. After a certain time ($\sim 3hs$), another deuterium gas sample was extracted. Others probes with the same time interval were taken and almost immediately measured (10min) at WMI. In the picture 5.4 are presented data of the full series. It is clearly evident an exponential "conversion curve" according with equation 5.8.

An ortho deuterium concentration closer to the saturation value at $\sim 20K$ is al-

ready obtained after few hours ($\sim 12hs$). Comparing with the natural conversion rate ($\sim 3000hs$) the improvement is remarkable.

The vertical errors bars ($\sim 4\%$) are in this case relative high because during the measurements, the raman's apparatus was relatively busy with parallel works. Therefore, relative short time was dedicated at each sample in order to optimized the signal response of the spectrometer (exact alignment sample-laser).

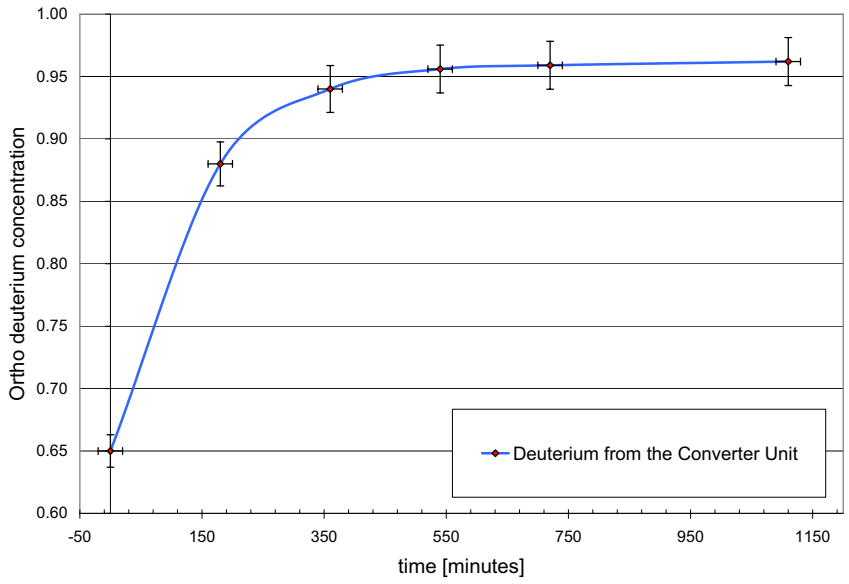

Figure 5.4: Para-to-ortho conversion rate in presence of catalyzer

5.5.2 High accuracy measurements

In the previous section were presented data in which the accuracy was not a critical parameter. Indeed, we were interested to find a roughly upper limit of the "storage" time

needed to reach high ortho deuterium concentration. When relative high accuracy is a sever requirement, for instance in very high ortho conditions like in the Cube-D_2 experiment, a relative more elaborate procedure is performed. Let's assume that a deuterium gas sample is acquired at a time τ_0 and is measured in a raman's spectrometer at a time τ_{mes0} (room temperature). If the sample is untouched for sufficient time and no others mechanisms are present (magnetic or electric field), the theoretical expectation is to have a "re-conversion" ortho-to-para deuterium due to the approach to the new (300K) thermodynamical equilibrium. Several measurements on the same sample were acquired over a relative long period (τ_{mes1}, τ_{mes2}, τ_{mes3}). The outcome are presented in figure 5.5. An exponential fit allows to extract the value of the ortho concentration at the exact τ_0. Statistical errors less that 0.5% were obtained.

The re-conversion (ortho-to-para) phenomena should be regulated by the same time constant for a conversion (para-to-ortho) because the process is perfectly bi-directional and is only function of the equilibrium temperature. Indeed, in our measurements a value in excellent accord with the theory was extracted ($0.056\%/hs$, [59]).

This specific series in figure 5.5 refers to measurements on a deuterium sample taken from the converter unit shortly before the irradiation at the FRM-II reactor. The upper limit reachable with the oxisorb^{TM} of $C_{ortho} \simeq 0.97$ is corroborated. Another sample was extracted from deuterium after a relative long irradiation. The calibration procedure was the same and, within the errors, a similar ortho-deuterium concentration was found.

5.6 Conclusions

The performance of the so-called oxisorb converter unit planned to be used in the Mini-D_2 source was investigated. The associated deuterium "para-to-ortho" conversion constant extracted was $\sim 12hs$. Comparing with the natural conversion rate ($\sim 3000hs$) the improvement due to the catalyst is remarkable.

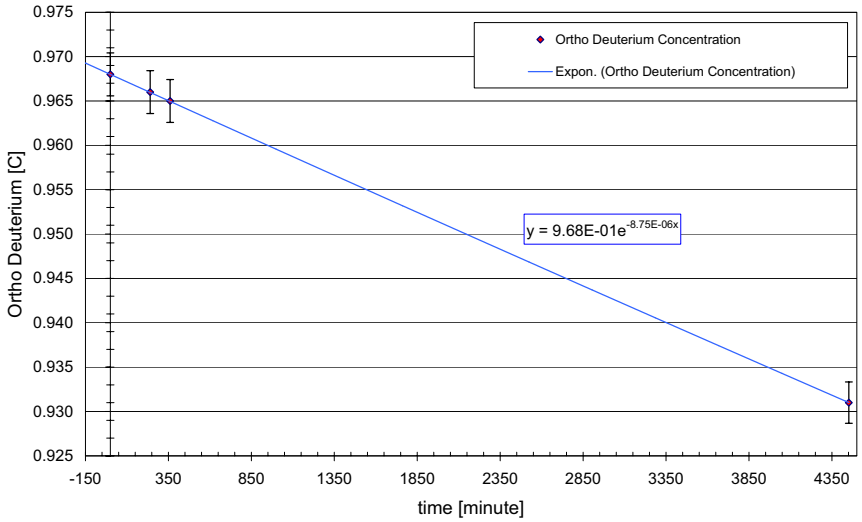

Figure 5.5: Procedure for an high accuracy measurement

Raman's spectroscopy is a powerful technique to resolve the ortho deuterium concentration in gas samples. Using particular caution or special procedure, a small relative error in the estimation could be achieved (0.5%).

For all the measurements with deuterium used in experiment associated with the Mini-D_2 project (TRIGA-test in Mainz and Cube-D_2 at FRM-II) we collaborate (L.Tassini and Dr.R.Hackl) with the Walther-Meissner Institute in Garching where a high performance Raman spectrometer is located. The strategic position of this facility (closer to the FRM-II reactor), suggests to use the same device also when the Mini-D_2 facility will be definitively installed at the FRM-II.

Chapter 6

Project of the Mini-D_2 radiation shield

Project and technical design of the Mini-D_2 take in account all safety requirements to be expected for nuclear installation such as the FRM-II. At the time of writing, because of the existence of the liquid deuterium "cold-source", the so-called SR4 beam channel of the reactor was selected. The SR4 also provides neutrons for the tomography facility [60].

In this chapter, will be considered the influence of the external shielding of the Mini-D_2 facility, in order to guarantee the level of radiation outside the experiment below the law limit of $5\mu Sv/h$. In the past, using the MCNP code (Monte Carlo N-Particles), a complete simulation was made of the geometry of the FRM-II reactor. Therefore, exact data on neutron and gamma flux energy distribution at the SR4 level are available. For instance [61], the magnitude of the thermal neutron flux closer to the cold-source is in the order of $\phi_{CS} \simeq 3.63 \cdot 10^{10}\ n/cm^2 s$. This data was used as input source for modelling the Mini-D_2 external shielding. To be congruent with the previous calculations, the same neutron transport code was used (MCNP Ver. 4B/C). Recent and repeated measurements (starting from July 2004) of the FRM-II nuclear parameters are in excellent agreement with the monte-carlo simulations.

6.1 Description of MCNP code

The remarkable enhancement of the computers performance and the corroboration of acquired data have improved the reliability of computer based codes. Nowadays simulations are essential tools also in experimental physic. Besides being relative not expensive, this kind of approach is extremely flexible and safe (important in nuclear applications). To perform simulations in phenomena like particles transport one could apply two techniques: the analytical method and the stochastic one (so-called monte-carlo). In general, the analytical approach is based on exact solution of specific transport equations and unfortunately could be applied only in simple realistic cases. As alternative, the monte-carlo methods could be applied. The basic idea is to use the converging properties of the statistical distributions (central limit theorem, CLT). Indeed, considering a sufficient number of events is possible to extract information on average quantities like intensity or energy distribution of a neutron flux.

The neutron code used in this project [15] is "state of the art" in terms of reliability: the Monte Carlo N-Particle (MCNP ver.4B/C). The code can be used for neutron, photon, electron transport and in the calculation of eigenvalues for criticality system. Basically the code is a random number generator supported by a rich library cross section (ENDF/series). This allows assigning interaction probabilities (scattering, absorption, etc.) in processes involving different particles.

6.1.1 Physics and mathematics behind the code

In this section are illustrated the basic mechanisms implemented in the calculator core of MCNP. The programming procedure adopted in writing the code takes advantage of a rich equations package available in nuclear and mathematic physics.

Performing general simulations, the MCNP-code plays a set of occurrences denoted as "stories", logically equivalent to particle tracks. At the beginning, each generated event

has a statistical weight (W). When an interaction occurs, this weight is accurately split (for example between two different neutrons in scattering phenomena). The integral at the vertex, of course, is conserved. As a result each story has a particular "statistical weight function" that could be linked to a particle track. The sampling method is based on the following consideration. The probability of a first collision for a particle between the path l and $l + dl$ is evidently given by

$$p(l)dl = e^{-\Sigma_t l}\Sigma_t dl \tag{6.1}$$

where Σ_t is the macroscopic total cross section of the medium. If χ is a generated random number in the range [0,1), results

$$\chi = \int_0^l e^{-\Sigma_t s}\Sigma_t ds = 1 - e^{-\Sigma_t l} \tag{6.2}$$

therefore

$$l = -\frac{1}{\Sigma_t} ln(1 - \chi) \tag{6.3}$$

The function $1 - \chi$ is distributed, a part a constant factor, as χ. In this context could be replaced by the same χ. An expression for the collision distance could be written as

$$l = -\frac{1}{\Sigma_t} ln(\chi) \tag{6.4}$$

Finally, we have a powerful method to extract information on a real parameter (l) by sampling a random variable (χ). Is significant to note how sampling generates a quantity called track length (T_l= transit time$*$velocity, cm unit).

Generally the different interactions are treated by applying a well known and accepted model. For example, let's consider the particles mostly contributing in dose rate estimation, for instance neutrons and photons (also as secondary emitted particles). Thermal motion of the atoms in neutrons collision is considered. At relative low energy ($E_n \leq 4eV$) the Bragg diffusion theory is applied. Corrections for elastic cross section at "zero-temperature" are also implemented. Nonelastic reaction cross section for neutron

capture is treated as temperature independent. In the elastic scattering process, the direction of the particle is sampled from proper angular distribution tables. The dynamic implies two-body kinematics as

$$E_{out} = E_{in}[\frac{1 + A^2 + 2A\mu_{cm}}{(1 + A)^2}] \tag{6.5}$$

Where E_{in} and E_{out} are respectively the incident neutron energy and the scattered one. Here A is the mass of collision nuclide in proper units and μ_{cm} is the "center of mass" cosine angle between incident and exiting directions. A rich package for fission events like in uranium or plutonium is available (Maxwell fission spectrum, evaporation spectrum, energy dependent Watt spectrum, etc.).

Photons interactions are differently treated according with the range of energy. For example the so-called DPT model (detailed physics treatment) includes also fluorescence. Incoherent (Compton) scattering is sampled including an appropriate factor modifying the well-known Klein-Nishina formula. The correction reduces the cross section in the forward direction (appropriate especially for low energy transfer and high Z material). The coherent (Thomson energy independent) scattering cross section is also modified. In this case the correction factor produces an enhancement in backward scattering for high energy events and low Z material. In the photoelectric effect the MCNP code considers absorption of the incoming photon and, according with the branching ratio, emission of secondary fluorescence photons or electrons (Auger effect). The pair production process consists of incoming high-energy photon, electron-positron production, annihilation and low-energy photons emission. The first emitted photon ($E_\gamma \simeq 0.511 MeV$) is sampled isotropically, the second one is produced in opposite direction.

6.1.2 Typical output quantities of MCNP

Using sampling procedure described in the previous section, the code provides a set of standard neutron and photon outputs (tallies) to extrapolate useful physical quantities from the track length information like surface flux (F2 card) or flux (F4 card). All tallies

are normalized to be per starting particle. For example, according with the definition of particle flux $\Phi(\overrightarrow{r}, E, t) = vN(\overrightarrow{r}, E, t)$ results in the time integrated flux

$$\int_V \int_t \int_E \Phi(\overrightarrow{r}, E, t) dt dE \frac{dV}{V} = \frac{Wvt}{V} = \frac{WT_l}{V} \tag{6.6}$$

For the particle density, as consequence of the normalization, it is valid that $N = W/V$ (particle weight over unit volume). Therefore F4 produces an output as particles per surface (for instance $1/cm^2$). Introducing apposite multiplication factor ($H(E)$, heating response) it is possible to evaluate also the energy deposition (MeV/gr) of particles passing through sample cells. This option could be used in heating estimation problems.

6.1.3 Error analysis

Errors analysis in MCNP, as well as in all monte-carlo methods, is a powerful cross checking tool. The code calculates several quantities that aid the user to control the wished quality of the confidence interval. Important parameters are true mean $E(x)$ and the associated sample mean $\overline{x}$ defined as

$$E(x) = \int x f(x) dx; \qquad \overline{x} = \frac{1}{N} \sum_{i=1}^{N} x_i; \tag{6.7}$$

The "Strong Law of the Large Numbers" states that if $E(x)$ is finite , $\overline{x}$ tends to the limit $E(x)$ as N (number of samples) approaches infinity. This allows to approximate, for a given population of x values, also the variance (and the associated standard deviation σ) with the so-called estimated variance resulting from the sampling. Indeed, is valid

$$\sigma^2 = \int (x - E(x))^2 f(x) dx \quad \simeq \quad S^2 = \frac{\sum_{i=1}^{N} (x_i - \overline{x}^2)}{N - 1} \tag{6.8}$$

Results also that the estimated variance of $\overline{x}$ is given by

$$S_{\overline{x}}^2 = \frac{S^2}{N} \quad \longrightarrow \quad S_{\overline{x}} \propto 1/\sqrt{N} \tag{6.9}$$

Therefore reducing for example $S_{\overline{x}}$ by a factor of 2 involves an enhancement in N by a factor of 4 with consequential improving of the computation time. To manage this aspect

the code supports the users with various techniques of "reduction of the variance". The definition of the confidence interval is derived from the CLT (central limit theorem) that states ($N \to \infty$)

$$Pr[\alpha S_{\overline{x}} < \frac{\overline{x} - E(x)}{\sigma\sqrt{N}} < \beta S_{\overline{x}}] \quad \sim \quad \frac{1}{\sqrt{2\pi}} \int_{\alpha}^{\beta} e^{-t^2/2} dt \tag{6.10}$$

where α, β are arbitrary value and $Pr[X]$ is the probability. Therefore, for identically distributed independent random variables x_i with finite mean and variance (first and second moment), the sampled distribution approach a normal distribution. For example a tally checking the mean of an intense neutron flux ($\overline{x}$) requires a normal distribution around $E(x)$ with the an associated (95%) confidence level interval as

$$\overline{x} - 2S_{\overline{x}} < E(x) < \overline{x} + 2S_{\overline{x}} \tag{6.11}$$

Where the percentage is in accord with the standard table of the normal distribution function. In synthesis MCNP has about 10 different checks (mainly related with higher order moments) controlling the congruence of the results within the statistical precision frame. Of course, as with all the others monte-carlo methods, could not estimate also the accuracy of the convergent results.

6.2 Model of the shield at SR4 beam channel

In the Fig.6.1 is shown the plan of FRM-II hall and emphasized the position of the Mini-D_2 facility with coupled the proposed radiation shield. Practically all the facility will be mounted on a rail system. When experiments are not in process is possible to partially remove the solid deuterium converter from the intense radiation source area with consequently heating reduction. This phenomena is important for UCN production and especially for saving coolant quantity. Because of the relative compact dimension of the system, special concrete (with hematite, granular iron, etc.) was chosen. The average density is about $4.7 g/cm^3$. This guarantees also the limit for the maximum superficial weight allowed at the FRM-II ground floor ($8t/m^2$) is not exceeded. The Mini-D_2 shield

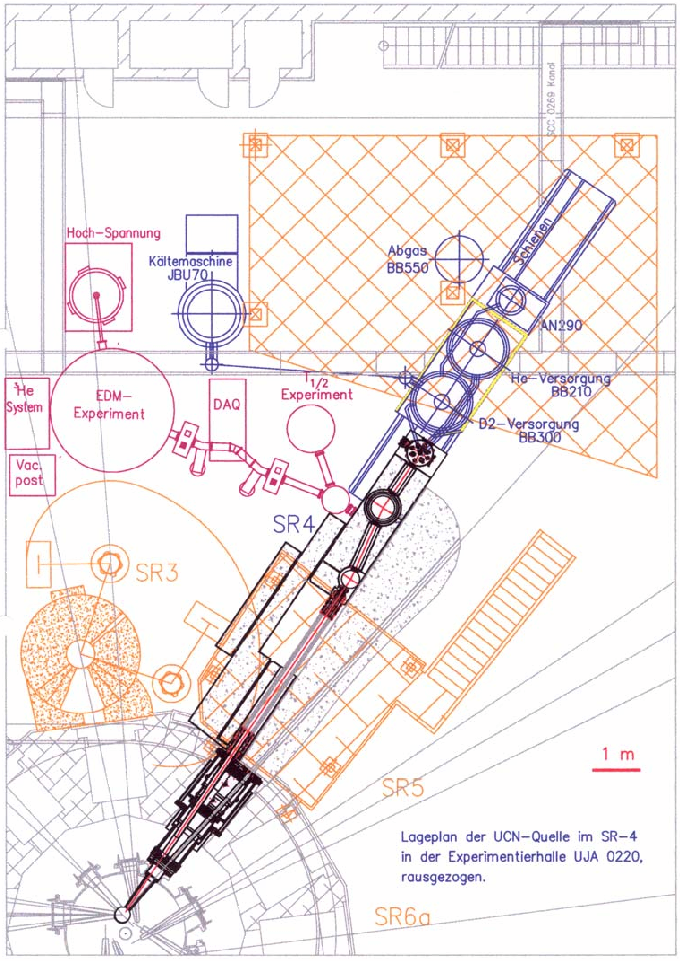

Figure 6.1: Reactor hall at FRM-II

is modular assembling of blocks of concrete embedded with a layer of normal iron. To prevent specials straight flees for the particles, the profile of each block was designed to have, after the mounting, a labyrinth configuration. With this technique the probability to have multi-scattering escape in such complex geometry is very low.

In the Fig.6.2 are shown in detail vertical and horizontal cut views of the UCN shield when no experiments are in process (maximum shift on the rail system of $1.8m$). This is obviously the worst case for the radiation estimation. With this special concrete an

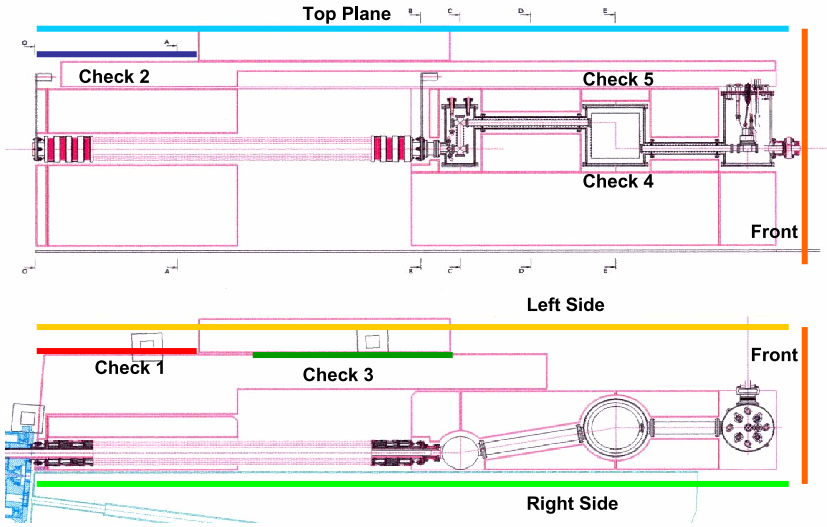

Figure 6.2: Vertical and horizontal cut view of the proposed shield

additional thin layer of $10cm$ involves an attenuation factor of 10. For improving the performance of the shielding, and because of the minute space available, the extraction guide has not a straight configuration (optimum for UCN transportation). For example, one can note a $40cm$ vertical step and a horizontal tilted tube ($\sim 35^o$). Therefore results a projection of an additional $1.2m$ concrete shield in the direction of the beam. The shield has two main components: the movable and the fixed part. The total length is $8m$. Generally the hight is $2.4m$, except in the void region generated by the shift of the movable shield. Here on the top is located an additional $40cm$ block. The total width is $1.4m$ with a supplementary $30cm$ in the deplete region. Because of the heavy total weight of the concrete ($\sim 100ton$, $\sim 20m^3$) and the tolerance during the manufacturing was included into the design a $1cm$ gap between the movable and the fixed part. For safety reasons (decoupling in earthquake event), an extra gap of $0.5cm$ was considered at the area connecting the UCN shield with the biological shield of the FRM-II. At this

level the profile was carefully shaped in order to have well fitting with the SR4 beam tube (and realistic easy assembling).

6.3 Implementation in the MCNP-code

As mentioned in the previous section, the code used in this estimation is MCNP ver.4C developed by the Los Alamos laboratory. The set of cross sections data become from the ENDF/B (Evaluated National Data Files, Brookhaven National Laboratory) libraries [15].

6.3.1 Main input parameters

In Fig.6.3 is plotted the neutron dose functions (ICRP-74, Conversion Coefficients for use in Radiological Protection Against External Radiation, [62, 63]) used to convert the particles flux (MeV) in appropriate dose units (Sv/s). The model of the neutron source is shown in picture 6.4. It's easy to distinguish a "Maxwellian spectrum" centered at $50K$. In fact this is reasonable considering the temperature of the liquid deuterium cold source. At this level the source yield is $\Phi_{CS} \simeq 5.23 \cdot 10^{12}\ n/s$. Neutrons give the main contribution on the global dose.

6.3.2 Virtual detectors technique and synthesis of the results

A set of grids of 5x5cm "virtual detectors" was implemented into the model and placed in strategic position along the UCN shield (Fig.6.2). In order to improve the statistic, a technique of "reduction of variance" was applied. More than 20 million events were played. The CPU time implicated during the run was about 70 days (200 particles per minute). Because of the difficulty to reach in relative short time very low level of statistical errors, the criteria assumed were to have an aim of the dose 5 times lower than the legal limit. A check grid of virtual detectors was sited at the left side of first unmovable block of concrete (Check1) close to the biological shield of the FRM-II. The results

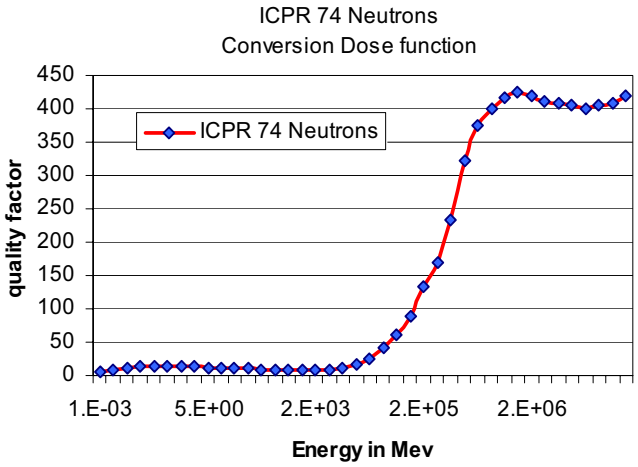

Figure 6.3: Standard quality factor function for neutrons

shown an average value of the dose of $0.55\mu Sv/h$ (statistical error $\sim 40\%$). Another set of detector placed at the top (Check2) of the same unmovable block gave an average value of $63\mu Sv/h$ (err. $\sim 30\%$), probably because of the $0.5cm$ earthquake gap. This means that in the final shield a layer of at least $10cm$ needs to be added in this region. To give an idea of the radiation source involved the value of the average dose inside the so-called buffer volume (Check4) is about 700 times the legal limit. On the left zone of the deplete region, between the normal bunker and the additional $30cm$ block of concrete (Fig.5, Check3), the average of the dose (mostly from neutron scattering) is only $0.66\mu Sv/h$ (err. $\sim 50\%$). Therefore this block could be removed in the real shield. A special grid of virtual detectors was implemented at the top of the buffer volume (Check5) but still inside the shield. The average of the dose in this region is $17\mu Sv/h$ (err. $\sim 27\%$), with a peak orders of magnitude higher. Finally, a complete "box" of virtual detectors (Front, Top-Plane, Left-side, Right-side) surrounded the full geometry of the shield was

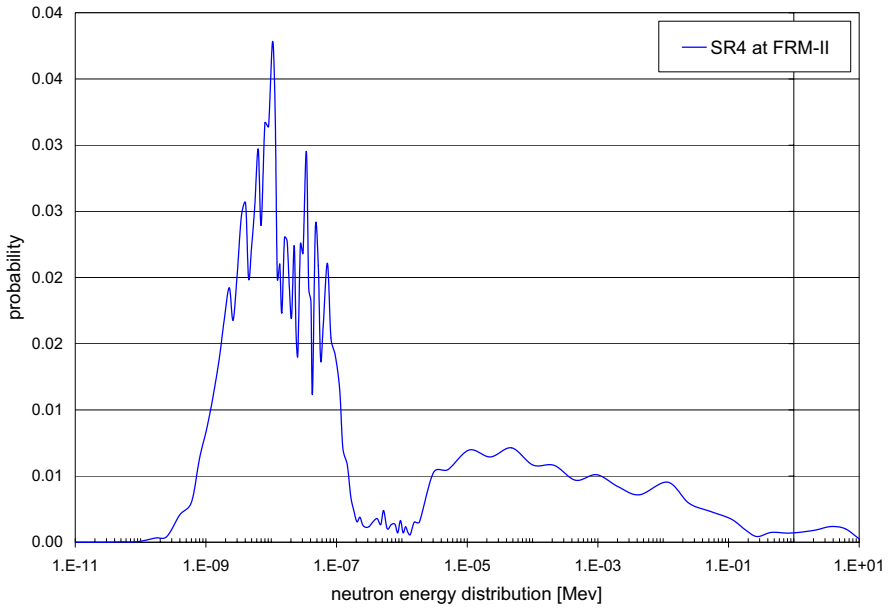

Figure 6.4: Neutron source at the entrance of the SR4 beam

applied. Paradoxically, because of the good quality of the shielding process, even with 20 millions of events, the statistic of these detectors is not fine (the statistical errors are about 55%). Nevertheless, on the front plane (Front) in the beam direction ($8m$ from the biological shield of FRM-II reactor) the neutron dose is only $0.085\mu Sv/h$ (err.$\sim$ 35%) and the gamma dose is 10 times lower (err.$\sim$ 27%).

6.3.3 Suggested modifications and conclusions

This concept of UCN shield allows to achieve the aim of low dose in almost all the regions outside the Mini-D_2. Unfortunately, some high dose problems still exist in the area between the UCN and the Tomography facility ($2cm$ width of void window). Indeed,

because of the divergence of the neutron beam in the "empty shifted zone" of the shield, the estimated dose is relatively high. To contain this phenomena, in the final design we planned to include borated flexibly panels in this zone. An additional liner of $1.4mm$ of cadmium applied on the external surface of the UCN long zircalloy tube will reduce practically to negligible amount the neutron dose originated by the divergence of the beam. Furthermore, it will reduce to $1cm$ the gap needed for the rail system. Another liner of $0.7mm$ of cadmium (associated with lead blocks) will be mounted at the upper surface of the buffer volume tank.

The monte-carlo simulation performed with the MCNP-code showed that is possible, modifying some small details, to guarantee the law limit of $5\mu Sv/h$ outside the Mini-D_2 facility. All calculations were made for the worst situation of "shifted" configuration of the system (limited in time). The estimation of the dose does not consider that in the authentic Mini-D_2 experiment there will be an additional protection of a double walled zircalloy tube. Last but not least, the energy of the neutrons should be much lower (ultra cold instead of cold neutrons).

6.4 Measurement of the dose rate

The Mini-D_2 facility shares with the tomography facility (Antares) the SR4 beam channel of the FRM-II reactor. Because there is only one common internal beam shutter, and because the schedule time of these two experiments is different, a temporary UCN shield was projected, simulated and manufactured. In this way is possible to disconnect the functionality of the two projects from separate opening of the SR4 beam channel. The estimation of the dose for the provisional shield was made using the same MCNP code. The main expensive part of this shield (the special shaped block connected with the biological shield of the reactor) could be in future re-used.

During the operation of the FRM-II at a reactor power of 250kW (6^{th} July 2004),

with the SR4 beam shutter opened, the authorities of radiation protection checked the dose close to the shield. Nearly all measurements showed values below $0.1\mu Sv/h$ for neutron and gamma radiation (within the natural background). Only at one point the dose was significantly higher than the background (but still within the law limit). Indeed, on the top of the gap between the Mini-D_2/Antares shields a gamma dose power peak of $0.3\mu Sv/h$ was detected (easily controllable with a small liner of additional lead). Additional measurements at FRM-II nominal thermal power (20MW) confirmed the low level of the dose.

Chapter 7

Summary and Outlook

This work was done in the framework of the Mini-D_2 project, an innovative source for ultra-cold neutrons (UCN) planned to be installed at the FRM-II reactor in Munich. An important component of this facility, the solid deuterium UCN converter, is the main subject of this work.

A multi-purpose device (Cube-D_2) was projected, assembled and successfully put in operation at the Mephisto position of the FRM-II. In different configurations, a UCN count rate up to $5s^{-1}$ was detected. During the long measuring period (more than a reactor cycle $70days$) many parameters associated with efficient UCN production/extraction were investigated (deuterium converter, extraction/storage system, neutron valves, DAQ, remote control system, etc..). In particularly was tested the so-called oxisorb converter unit, which allows a high concentration of ortho deuterium to be reached. The facility and the technique used (Raman spectroscopy) to extract the ortho-D_2 fraction in deuterium gas samples is briefly presented.

A relevant part of this work was dedicated to evaluate UCN guide properties. In this context, various experiments were performed at the ILL UCN-source in Grenoble. A new method to extract parameters such the UCN loss probability per wall collision (μ) or the

probability for diffuse scattering (f) was developed and tested.

A secondary but important topic of this work was dedicated in projecting, simulating and in partially realizing the UCN radiation shield for the Mini-D_2.

At the time of writing, the status of the Mini-D_2 project is in a promising advanced stage. Indeed, basic ideas or important components are already manufactured and tested. Nevertheless, further investigations are planned in order to optimize the UCN production.

Chapter 8

Own Contributions

I dedicated the first part of my thesis in the project and in the simulation of the UCN radiation shield for the Mini-D_2. I realized the implementation of the shield model using the Monte Carlo N-Particles code (MCNP Ver.4B/C).

In the experiments associated with the studies on UCN guide properties performed at the ILL, I contributed in the preparation of the samples, in the mounting in-situ of the set-up and in the data acquisition runs (shifts). Under the supervision of Dr.I.Altarev I did the related analysis of the results.

In the last one-and-half year of my thesis I was involved in the Cube-D_2 project. The basic idea, the scientific program and the realization of the complete set-up of the Cube-D_2 experiment was mainly done by myself and by A.R.Müller.

Beside the interface with the work-shop, I project the gas system and I implemented the temperature sensors. I also assembled, prepared and tested the freezing chambers. During the preliminary phase of the experiment at the E18-UCN labor, I investigated various deuterium freezing procedures as well as the safety concepts associated with the Cube-D_2.

At the Mephisto location of the FRM-II, I extensively contribute in the re-mounting of the set-up and in the realization of the radiation shield. The coordination of this specific part of the work was done by Dr.H.F.Wirth.

During the irradiation with neutrons (UCN production) I participated in the data acquisition process doing several shifts. I also contributed in up-dating the "to-do-list" when new physical questions rose up. Under the supervision of Dr.E.Gutsmiedl I did the subsequent analysis of the results. In this context I developed a first approximation method to extract information on "loss" cross sections respect to UCN production.

I prepared the deuterium gas samples for the ortho-deuterium measurements performed at the WMI and I did the associated data analysis.

Chapter 9

Acknowledgments

First of all I would like to thank Prof.Stephan Paul for giving me the opportunity to be dynamically involved in the "UCN-business" and for interacting in the analysis of the data providing important advices, comments and some useful critics.

I would like to thank my tutors Igor Altarev and Erwin Gutsmiedl, equally important for the development of my scientific skills. Thanks for the proficient advices, the patience and the friendly atmosphere in every single discussion!

I would like to thank all the people of the UCN group for the sociable environment I had the chance to experience. Many thanks to Prof.Oliver Zimmer for general advices and for the interesting lectures. Special regards to F.J.Hartmann for useful suggestions and for the translation of the "Zusammenfassung". Very thanks to Peter Amos for screening the thesis and removing part of my mistakes in English. Furthermore, thanks to the expert "bosses" of the workshop at the UCN labor, Thomas and Herbert. I learned more from them than in my text books of mechanical engineering! Thanks to all the working students participating in the various UCN sub-projects.

I also would like to thank the scientists I met during my experiments at ILL, PSI and

FRM-II where I learned that in research the appropriate word is not competition but synergy. In particular during my short visit at PSI were I had the chance to exchange information on "UCN subjects" in a very competent group.

Of course, I would like to thank all the others members of the E18 institute I had the chance to know over the years (COMPASS, PANDA and whatsoever groups). Especially "occhibelli" Rita De Masi, Michael Wiesmann, Boris Grube and Anna-Maria Dinkelbach for being enjoyable officemates.

Particular regards to Karin Frank who patiently helped me in all the troubles connected "mit deutscher Bürokratie".

I would like to thank all the friends working in the campus in Garching. Thanks for sharing with me hundreds of espressos discussing topics of physic... and especially non-physic. A big hug to Johnny, Christian, Laura, Ken, Leo, Chiara, Massi, Claudia, Paolo, Vasso, Cecilia and Marina.

A special thanks to my "Trauzeuge" Andreas Weiler for explaining me a bit of physic from a "theoretician" point of view... including the complicated theory of "many-bodies scattering" in the billiard context!

Finally, I would like to thank Prof.Stephan Paul and Dr.Roberto Rosa which indirectly (but essentially) contributed to the happiness in my private life... allowing me to come in Munich and let me know to Susanne, my lovely wife.

Bibliography

[1] W-M Yao et al., *J.Phys.G: Nucl.Part.Phys.,* **33***, (2006)*

[2] U.Trinks et al., Mini-D2: a source for UCN at FRM-II, *Nucl.Instr.Meth.,* **A440***, 666, (2000)*

[3] http://ucn.web.psi.ch

[4] http://lpsc.in2p3.fr

[5] http://lansce.lanl.gov

[6] R.Golub, D.J.Richardson and S.K.Lamoreaux, *Ultra-Cold Neutrons, Adam Hilger, Bristol, (1991)*

[7] W.Mampe et al., *Nucl.Instr.Meth.,* **A284***, 111, (1989)*

[8] V.K.Ignatovich, *The Physics of Ultracold Neutrons, Clarendon Press, Oxford, (1990)*

[9] A.Steyerl et al., *Phys.Lett.,* **A116***, 347, (1986)*

[10] http:/wwwnew.frm2.tum.de

[11] I.Altarev et al., Die UCN-Quelle am Forschungreaktor TRIGA Mainz, *Institut für Kernchemie, Annual Report, (2005)*

[12] O.Zimmer, MEPHISTO: a measuring facility for particle physics with cold neutrons, *contribution to the FRM-II Annual Report, (2002)*

[13] I.Altarev et al., A method for evaluating the trasmission properties of ultracold-neutron guides, *Nucl.Instr.Meth.,* **A570***, 101, (2007)*

[14] http://www.wmi.badw.de

[15] J.F.Briesmeister, MCNP: A General Monte Carlo N-Particle Transport Code Ver.4B, *Radiation Safety Information Computational Center (RSICC), Oak Ridge, (1977)*

[16] K.Gobrecht, E.Gutsmiedl and A.Scheuer, Status report on the cold neutron source of the Garching neutron research facility FRM-II *Physics of Condensed Matter,* **B311***, 148, (2002)*

[17] I.S.Altarev et al., Mini-D2: A source for ultracold neutrons at FRM-II, *internal report, TUM-E18, (2000)*

[18] R.Golub and K.Böning, *Z.Phys., Condensed Matter* **B 51***, 95, (1983)*

[19] O.Zimmer, Fundamental physics with slow neutrons, *Notes of a lecture at TUM, (2004)*

[20] M.Romalis, Limits on CP Violation from Searches for Electric Dipole Moments, *American Physical Society, Abstract 1A.005, (2002)*

[21] S.Abel et al., EDM Constraints in Supersymmetric Theories *Nucl.Phys.,* **B606***, 151, (2001)*

[22] N.F.Ramsey, *Rep.Progr.Phys.,* **45***, 95, (1982)*

[23] R.Golub and P.R.Huffman, Search for neutron electric dipole moment, *J.Res.Natl.Inst.Stand.Technol., May-June, (2005)*

[24] C.A.Baker et al., *Phys.Rev.Lett.,* **97***, 131801, (2006)*

[25] P.G.Harris et al., *Phys.Rev.Lett.,* **82***, 904, (1999)*

[26] I.S.Altarev et al., *Phys.At.Nucl.* **59***, 1152, (1996)*

[27] H.Abele et al., *Phys.Lett.B,* **407***, 212, (1979)*

[28] K.Hagiwara et al., *Particle Physics Booklet, AIP, (2002)*

[29] A.Serebrov et al., *Phys.Lett.B,* **605***, 72, (2005)*

[30] F.J.Hartmann et al., Proceeding of the 2002 Workshop on Quark-Mixing and CKM-Unitarity, *H.Abele and D.Mund eds., Heidelberg, (2002)*

[31] R.Picker et al., *J.Res.Natl.Inst.Stand.Technol., 110-4, (2005)*

[32] J.Bröcker, *Diploma thesis, TUM-E18, (2004)*

[33] R.Picker, *Diploma thesis, TUM-E18, (2004)*

[34] I.F.Silvera, *Rev.Mod.Phys.,* **52***, 393, (1980)*

[35] P.C.Souers, Hydrogen Properties for Fusion Energy, *University of California, Berkeley, (1986)*

[36] J.A.Young and J.U.Koppel, Slow Neutron Scattering by Molecular Hydrogen and Deuterium, *Phys.Review,* **135***, 603, (1964)*

[37] I.S.Altarev et al., *Phys.Lett.,* **A80***, 413, (1980)*

[38] V.V.Nesvizhevsky et al., *Nature,* **415***, 297, (2002)*

[39] A.Frei, *Diploma thesis, TUM-E18, (2002)*

[40] A.Gschrey, *Diploma thesis, TUM-E18, (2004)*

[41] D.Tortorella et al., Cube-D_2: a Device for the Investigation of Solid UCN Converters, *Maier-Leibnitz-Laboratorioum (MML), Annual Report, (2005)*

[42] OXISORB is registerd product of the Messer-Griesheim company, Germany

[43] G.F.Knoll, Radiation Detection and Measurements, *Wiley, New York, (1979)*,

[44] The Helium-3 neutron detector was manufactured at the JINR in Dubna.

[45] I.Altarev et al., Transmission properties of a novel ultra-cold neutron guide, *Test 930, ILL Annual Report, (2005)*

[46] F.Atchison et al., *Phys.Review.,* **B68***, 094114, (2003)*

[47] C.-Y.Liu et al., *Phys.Review,* **B62***, 3581, (2000)*

[48] J.L.Yarnell et al., *International Conference on Quantum Crystals, (1974)*

[49] E.Gutsmiedl, Private communication on the TRIGA-Mainz experiment, *(2006)*

[50] F.Atchison et al., *Phys.Rev.Lett.,* **95***, 182502, (2005)*

[51] K.Kirch et al., *Phys.Rev.,* **C71***, 054601, (2005)*

[52] A.Frei, *Ph.D. thesis, in progress*

[53] I.Altarev et al., Test of new stainless steel tubes as UCN guides, *Experimental report T-939, ILL-Grenoble, (2005)*

[54] I.V.Groshev et al., Experiments with ultracold neutrons, *Phys.Lett.,* **B34***, 293, (1971)*

[55] V. Ignatovich et al., Experiments on UCN Storage in Bottles in the Channel Mode, *Communication of JINR,* **P3-82-811***, Dubna, (1982)*

[56] W. Mampe et al., Ultra Cold Neutron Life Times in Glow Discharge Cleaned Bottles, *Z.Phys.,* **B45***, 1-14, (1981)*

[57] E.Korobkina et al., *Annual Report, ILL, (2004)*

[58] A.Honig et al., *Phys.Rev.Lett.,* **56***, 1866, (1986)*

[59] I.F.Silvera et al., *Phys.Rev.,* **B12***, 753, (1975)*

[60] http://einrichtungen.physik.tu-muenchen.de/antares

[61] W.Gaubatz, PhD Thesis, *Physik Department E21, Technische Universität München, (1999)*

[62] http://www.icrp.org International Commission on Radiological Protection

[63] http://www.iaea.org Databases and Information Services